

T. KARAYUMAK

**MODELING AND STABILIZATION CONTROL
OF A MAIN BATTLE TANK**

TÜRKER KARAYUMAK

METU

2011

SEPTEMBER 2011

MODELING AND STABILIZATION CONTROL OF A MAIN BATTLE TANK

**A THESIS SUBMITTED TO
THE GRADUATE SCHOOL OF NATURAL AND APPLIED SCIENCES
OF
MIDDLE EAST TECHNICAL UNIVERSITY**

BY

TÜRKER KARAYUMAK

**IN PARTIAL FULFILLMENT OF THE REQUIREMENTS
FOR
THE DEGREE OF DOCTOR OF PHILOSOPHY
IN
MECHANICAL ENGINEERING**

SEPTEMBER 2011

Approval of the thesis:

MODELING AND STABILIZATION CONTROL OF A MAIN BATTLE TANK

submitted by **TÜRKER KARAYUMAK** in partial fulfillment of the requirements for the degree of **Doctor of Philosophy in Mechanical Engineering Department, Middle East Technical University** by,

Prof. Dr. Canan ÖZGEN
Dean, Graduate School of **Natural and Applied Sciences**

Prof. Dr. Süha ORAL
Head of Department, **Mechanical Engineering**

Prof. Dr. Tuna BALKAN
Supervisor, **Mechanical Engineering Dept., METU**

Examining Committee Members

Prof. Dr. Y. Samim ÜNLÜSOY
Mechanical Engineering Dept., METU

Prof. Dr. Tuna BALKAN
Mechanical Engineering Dept., METU

Prof. Dr. Kemal LEBLEBİCİOĞLU
Electrical and Electronics Engineering Dept., METU

Asst. Prof. Dr. Yiğit YAZICIOĞLU
Mechanical Engineering Dept., METU

Asst. Prof. Dr. K. Bilge ARIKAN
Mechatronics Engineering Dept., Atılım University

Date:

11.09.2011

I hereby declare that all information in this document has been obtained and presented in accordance with academic rules and ethical conduct. I also declare that, as required by these rules and conduct, I have fully cited and referenced all material and results that are not original to this work.

Name, Last Name : Türker KARAYUMAK

Signature :

ABSTRACT

MODELING AND STABILIZATION CONTROL OF A MAIN BATTLE TANK

KARAYUMAK, Türker

Ph.D., Department of Mechanical Engineering

Supervisor: Prof. Dr. Tuna BALKAN

September 2011, 126 Pages

In this study, a parametric model for a main battle tank electric gun turret drive system stabilization controller has been developed. Main scope was the study of the muzzle deviation due to barrel flexibility. Traverse and elevation dynamics has been modeled to include the drive-line and barrel flexibilities. Order of the models has been kept large enough to cover the frequencies dominant in the interest scope but at the same time low enough to create a parametric model which can be used in real-time fire control computers. Therefore a 5-dof elevation and a 7-dof traverse models have been implemented. These models have been used to design a classical feedback and feedforward controllers which performed good enough to meet 0.5mrad stabilization accuracies.

After satisfactory results have been obtained from the stabilization controller, a special coincidence algorithm has been implemented by time-series analysis of the disturbance signal which is constantly being measured by the feedforward gyro. Necessity of predicting the future muzzle angular orientation due to the latency in fire is discussed and by using autoregressive modeling of the disturbance signal, future values of the disturbance signal has been entered into the observer model. The prediction horizon has been set to the time delay value between the trigger is pulled by the gunner and the ammunition exit from the muzzle.

By checking the future coincidence within a very narrow windowing (0.05mrad) a 100% first round hit probability in theory has been achieved. This is assured since the coincidence inhibited the fire signals which were to miss the aiming point with a large error.

Keywords: Fire Control System, Gun Stabilization, Disturbance Compensation, Main Battle Tank Modeling and Control, Fire Coincidence Algorithm, Electrical Gun Turret Drive and Stabilization System

ÖZ

ANA MUHAREBE TANKININ MODELLENMESİ VE STABİLİZASYON KONTROLÜ

KARAYUMAK, Türker

Doktora, Makina Mühendisliği Ana Bilim Dalı

Tez Yöneticisi: Prof. Dr. Tuna BALKAN

Eylül 2011, 126 Sayfa

Bu çalışmada, elektrik takatli tank kule namlu takat sisteminin parametric modeli oluşturularak stabilizasyon denetleci geliştirilmiştir. Ana ilgi alanı namlu ucunun namlu esnekliği sebebiyle deplasmanları olmuştur. Yan ve yükseliş eksenli takat sistemi dinamiği, aktarma organları esneklikleri ve namlu esnekliklerini içerecek biçimde modellenmiştir. Parametrik modelleme derecesi, kontrol ve stabilizasyon probleminin ilgi dahilinde olacak kadar yüksek, ancak aynı zamanda da herhangi bir atış kontrol bilgisayarında gerçek zamanlı koşturulabilecek kadar da düşük seviyelerde tutulmaya çalışılmıştır. Bu sebeple, yan eksen modeli 7 serbestlik dereceli, yükseliş eksenli ise 5 serbestlik dereceli olarak modellenmiştir. Bu modeller, klasik geri-besleme, ileri-besleme denetleç tasarımıyla sistem olarak kullanılmış ve tasarlanan denetleç 0.5mrad stabilizasyon hassasiyetini fazlasıyla karşılamıştır.

Başarılı bir stabilizasyon denetleci tasarlandıktan sonra, ileri-besleme jiroskobu ile ölçülmekte olan bozucu etkinin zaman serisi analizi yapılarak özel bir çakıştırma algoritması geliştirilmiştir. Tetik sinyali üretildiği an ile mühimmatın namlu ucundan çıktığı an arasındaki gecikme ve bu aralıkta namlu ucunun farklı konuma kayması sebebiyle, bozucu etki sinyalinin tam bu gecikme kadar sonraki değerinin otoregresyon yöntemi ile modellenmesi ve

gözlem modeline girdi oluşturması gerekliliği anlatılmıştır. Gözlem modeli namlu ucu açısal pozisyonu üzerinde çok dar bir çakıştırma penceresi (0.05mrad) oluşturulmuş, ve atışa bu çakıştırma algoritmasının karar vermesi sağlanmıştır. Bu sayede hedef noktası üzerinden sapacak olan tüm atışlar kesilmiş, teoride %100 ilk atımda vuruş ihtimali elde edilmiştir.

Anahtar Kelime: Atış Kontrol Sistemi, Namlu Stabilizasyonu, Bozucu Giriş Düzeltme, Ana Muharebe Tankı Modelleme ve Kontrolü, Çakıştırma Algoritması, Elektrikli Kule Namlu Takat ve Stabilizasyon Sistemi

to my son, and to all brilliant children of this country.....

ACKNOWLEDGEMENTS

I express my sincere appreciation to my thesis supervisor Prof. Dr. Tuna BALKAN for his supervision, support and helpful critics throughout the progress of my thesis study.

I would like to thank to Serdar GÖRGÜÇ and Mustafa BAKIRCI for their grateful support and valuable commands.

Finally, many thanks to all of my colleagues at present and in the past for sharing the same excitement and giving endless support in battle tank fire control design business.

TABLE OF CONTENTS

PLAGIARISM.....	III
ABSTRACT.....	IV
ÖZ.....	VI
ACKNOWLEDGEMENTS.....	IX
TABLE OF CONTENTS.....	X
LIST OF FIGURES.....	XII
CHAPTER	
1 INTRODUCTION.....	1
2 AIM AND SCOPE OF THE STUDY.....	6
2.1 Modeling the Main Battle Tank.....	6
2.1.1 Hull and Suspension.....	6
2.1.2 Turret Servo Dynamics Model.....	7
2.1.3 Gun Servo Dynamics Model.....	8
2.2 Disturbance Modeling.....	9
2.2.1 APG Course Modeling.....	9
2.2.2 Sinuous Course Modeling.....	11
2.2.3 Other Sources of Disturbances.....	11
2.3 Stabilization Controller Design.....	12
2.3.1 Elevation Stabilization Control.....	12
2.3.2 Azimuth Stabilization Control.....	14
2.4 Simulations.....	15
2.4.1 Stationary Tank Servo Feedback Controller Design.....	15
2.4.2 APG Course and Sinuous Path Crossing Tank Stabilization Controller Design.....	15
2.4.3 APG Course Crossing and Firing Tank Stabilization and Coincidence Simulation.....	15
2.5 Contribution of the Study to the Literature.....	15
3 MODELING SERVO DYNAMICS.....	16
3.1 7-DOF Traverse Axis Servo Dynamics Model.....	16
3.2 5-DOF Elevation Axis Servo Dynamics Model.....	25
4 DISTURBANCE MODELING.....	34

4.1 APG Course Definition.....	34
4.2 Sinuous Course Definition.....	36
4.3 Other Disturbances.....	36
4.4 Experimental Data.....	36
4.5 Simulations.....	41
5 STABILIZATION CONTROLLER DESIGN.....	46
5.1 Elevation Controller Design.....	46
5.1.1 Elevation Feedback Controller Design.....	46
5.1.2 Elevation Feedforward Controller Design.....	50
5.2 Azimuth Controller Design.....	57
5.2.1 Azimuth Feedback Controller Design.....	58
5.2.2 Azimuth Feedforward Controller Design.....	61
6 COINCIDENCE FIRING DESIGN.....	68
6.1 Coincidence Algorithm Necessity.....	68
6.2 Coincidence Algorithm Design.....	69
6.3 Three Dimensional Visual Simulation Design.....	80
7 MUZZLE RATE OBSERVABILITY AND MUZZLE RATE STABILIZATION.....	82
7.1 Observability.....	82
7.2 Muzzle Rate Observability.....	83
7.3 Luenberger Observer and Muzzle Rate Stabilization.....	86
7.3.1 Muzzle Accelerometer Consideration.....	88
7.3.2 Muzzle Rate Stabilization.....	94
8 CONCLUSION AND FUTURE WORK.....	99
REFERENCES.....	101
APPENDICES.....	107
VITA.....	126

LIST OF FIGURES

1.1 Effect of Stabilization.....	1
1.2 Basic Servo Stabilization.....	2
1.3 Feedforward (Second Generation) Stabilization Systems.....	3
1.4 A View of Gyro Stabilized Head Mirror on the Tank and the Gunner's Periscope Alone...4	
1.5 Director-Type Stabilization System.....	5
2.1 Disturbance Measurement.....	6
2.2 3-DOF Turret Servo Dynamics Model.....	7
2.3 Turret Azimuth Drive.....	8
2.4 Elevation Drive.....	8
2.5 Gun Servo Dynamics Model.....	9
2.6 Tank Crossing an APG Course, Bump Dimensions.....	10
2.7 APG Course Disturbances in Gun Elevation.....	10
2.8 Sinuous Course.....	11
2.9 Effect of Flexibility of the Barrel.....	12
2.10 The Components of Gun Jump.....	13
3.1 7-DOF Turret Servo Dynamics Model.....	16
3.2 5-DOF Elevation Servo Dynamics Model.....	25
3.3 Elevation Drive Line Linearization.....	26
4.1 Tank Crossing an APG Course, Bump Dimensions.....	34
4.2 APG Course Disturbances in Gun Elevation.....	35
4.3 Sinuous Course Disturbances in Turret Yaw Axis.....	36
4.4 A General View on Leopard1A1 Tank Data Acquisition Setup.....	37
4.5 APG Course Elevation Disturbance.....	37
4.6 APG Course Azimuth Disturbance.....	38
4.7 APG Course Elevation Disturbance PSD.....	38
4.8. APG Course Azimuth Disturbance PSD.....	39
4.9 Sinuous Course Elevation Disturbance.....	39
4.10 Sinuous Course Azimuth Disturbance.....	40
4.11 Sinuous Course Elevation Disturbance PSD.....	40
4.12 Sinuous Course Azimuth Disturbance PSD.....	41
4.13 Simulink Model for Disturbance Response w/o Controller.....	41

4.14 APG Response of the Muzzle w/o Controller.....	42
4.15 APG Angular Position Response of the Muzzle w/o Controller.....	42
4.16 Sinuous Response of the Muzzle w/o Controller.....	43
4.17 Sinuous Angular Position Response of the Muzzle w/o Controller.....	43
4.18 Position Difference Between Gun Muzzle and Trunnion for APG w/o Controller.....	44
4.19 Position Difference Between Gun Muzzle and Trunnion for Sinuous w/o Controller.....	44
5.1 Simulink Model for Elevation Feedback Controller Design.....	47
5.2 Dual PI Controller.....	47
5.3 Output Constraints and Response Optimization.....	48
5.4 Elevation Feedback Controller Step Response with the Optimized Gains.....	49
5.5 Elevation Feedback Controller Stabilization Performance and Muzzle Deviation.....	49
5.6 Feedback System with Disturbance Feedforward.....	51
5.7 Bode Plot of Improper Gff.....	52
5.8 Bode Plot of Gff2, LP Filter is Added to Gff.....	53
5.9 HSVD Plot for Gff2.....	54
5.10 HSVD Plot for Gff2s (Stable Part of Gff2)	56
5.11 Feedforward Controller Simulation.....	57
5.12 Simulink Model for Elevation Feedback Controller Design.....	58
5.13 Dual PI Controller Block (Azimuth)	59
5.14 Output Constraints and Response Optimization (Azimuth)	59
5.15 Azimuth Feedback Controller Stabilization Performance and Muzzle Deviation.....	60
5.16 Bode Plot of Improper Gff (Azimuth)	63
5.17 Bode Plot of Gff2, LP Filter is Added to Gff.....	64
5.18 HSVD Plot for Gff2.....	65
5.19 HSVD Plot for Gff2s (Stable Part of Gff2)	66
5.20 Feedforward Controller Simulation.....	67
6.1. Effect of Flexibility of the Barrel.....	68
6.2 Fixed Firing Delay Between the Trigger and the Muzzle.....	69
6.3 Coincidence Algorithm.....	70
6.4 Graphical Representation of Coincidence Algorithm.....	71
6.5 Stochastic Process Time Series Representation.....	72
6.6 AR-Prediction Sub-system.....	74
6.7 Coincidence Simulation Model.....	76

6.8 Fire Demand (red), Coincidence Check Result (green), Muzzle Orientation (blue) , Coincidence Window (black-dashed)	77
6.9 Two Axes Coincidence Simulation Model.....	78
6.10 Fire Demand (red), Coincidence Check Result (green), Muzzle Orientation (Traverse: blue, Elevation: red), Coincidence Window(black-dashed)	79
6.11 Simulink Model for Creating OpenGL Animation Data	80
6.12 A View From Animation Code and The Compiled Application Window....	81
7.1 General State Estimation.....	82
7.2 General Form of the Luenberger Observer.....	86
7.3 Muzzle Rate Stabilization Scheme.....	87
7.4 Muzzle Rate Estimation Scheme.....	88
7.5 Performance and Cost of Different MEMS accelerometer.....	90
7.6 Modified Analog Devices ADXL203 MEMS Accelerometer Behavioral Model.....	94
7.7 Muzzle Rate Stabilization Scheme.....	95
7.8. Physical System Block (Azimuth).....	95
7.9 Constraint Equations Block.....	96
7.10 Detrend Block.....	96
7.11 Muzzle Rate Estimator Block.....	97
7.12 Muzzle Rate Estimator Constraint Equations Block.....	97

CHAPTER 1

INTRODUCTION

Demands on increasing the battlefield mobility, that is, the ability of tanks to move when in actual or imminent contact with enemy forces, inevitably lead to the requirement of firing on the move, instead of having to stop every time they engage a target. This requirement call, in turn, for gun control systems which minimize the effects of vehicle motion on the main armament of tanks and in particular its ability to hit targets [1, 2].

The effects of vehicle motion on the armament of the tank can be minimized by gun stabilization systems that are designed to maintain the spatial orientation of guns. Figure 1.1 represent the effect of stabilization in gun elevation and turret azimuth [5]. Systems to accomplish this are basically closed loop servo systems which control the orientation of the guns relative to the inertial space by employing gyroscopes to sense the motion of the guns relative to it and using position or velocity feedback signals provided by them [4].

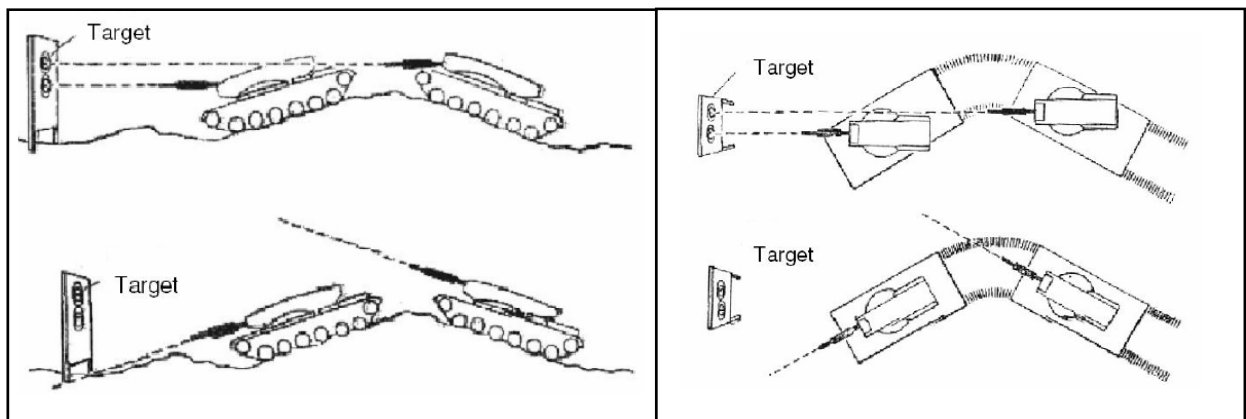


Figure 1.1. Effect of Stabilization

Basic systems involve two individual closed-loop servo systems for azimuth and elevation. Angular velocities of the axes with respect to the inertial frame are sensed by the gyroscopes and the error is compensated by servo loop (Figure 1.2) [1].

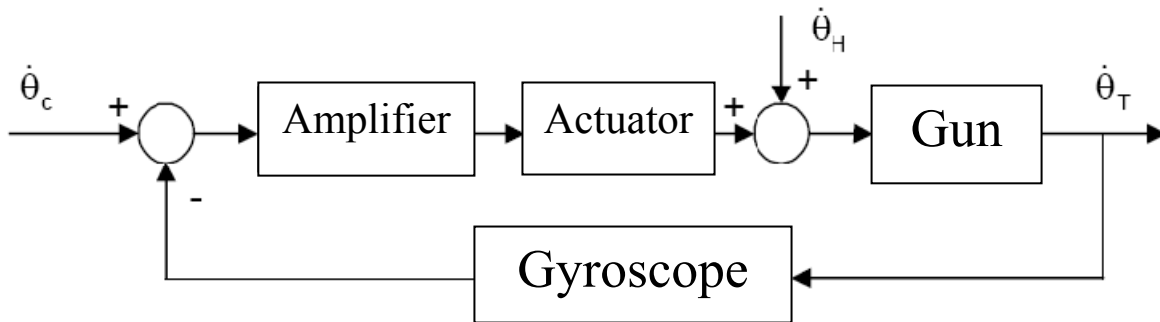


Figure 1.2. Basic Servo Stabilization

The basic two gyro control systems have proved reasonably effective and even if they do not always make it possible for gunners to aim accurately on the move, they can at least aim roughly, so that only relatively small adjustments have to be made when their tanks stop to fire. However, in the nature of things, the response of the basic systems is not sufficiently low level when tanks move at speed over rough ground. In consequence, more elaborate systems began to be developed in 1960s. These "second generation" systems incorporate two additional gyros in feedforward open loops which respond to angular velocities of the vehicle and provide anticipatory commands to the azimuth and elevation drives, thereby approximately stabilizing the gun. Thus, one additional gyro is mounted in the hull to sense the angular rotation of the hull in plane of the rotation of the turret, and generate feedforward commands to the traverse drive (Figure 1.3). The second of the additional gyros is mounted in the turret to sense the angular rotation of the turret in the elevation plane of the gun, and to generate feedforward commands to the elevation drive. As a result, the demand on the two gun mounted gyros is reduced to correcting the errors of the feedforward loops and the stabilization of the gun is considerably improved [4].

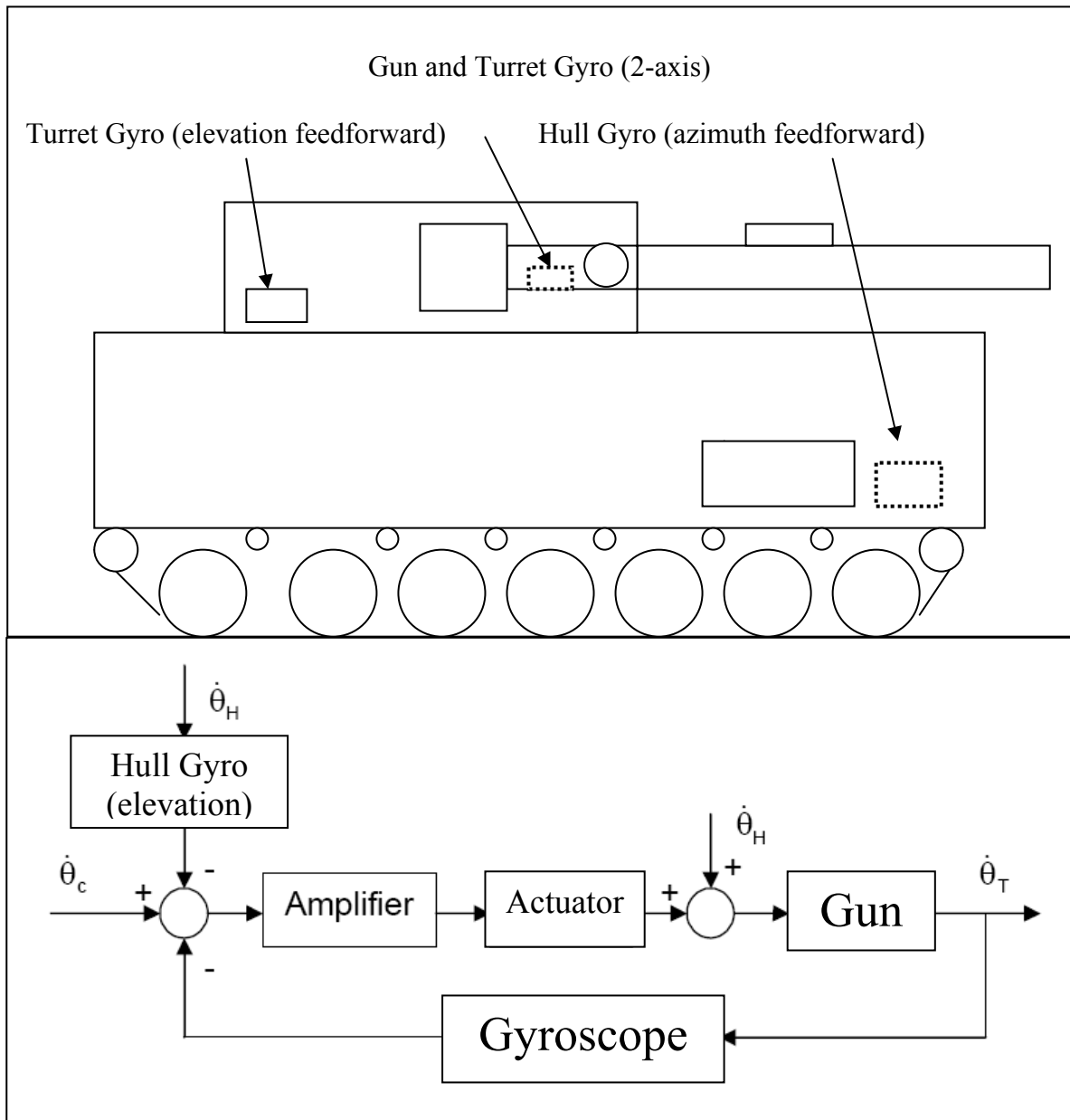


Figure 1.3. Feedforward (Second Generation) Stabilization Systems

The outcome of all refinements incorporated in the second-generation systems has been to reduce considerably gun-pointing errors and consequently to increase further the probability of hitting targets on the move. However, second-generation systems still only maintain the position of the tank guns in space and they do not provide gunners with all the aids which are possible. In particular, the gunners still have to track targets or, in other words, close the overall weapon-target loop by visual feedback [1,4].

In modern tanks, there is an independently stabilized gunner's periscope. These periscopes have thermal imaging and day TV CCD imaging cameras over which a very accurately gyro stabilized head mirrors (Figure 1.4). Stabilization accuracies of these head mirrors are typically at least 4 or 5 times accurate than the stabilization of the tank turret & gun itself (≤ 0.15 mrad stabilized mirror accuracy). Detailed information on stabilized head mirrors and gunner's periscopes can be found in [6].

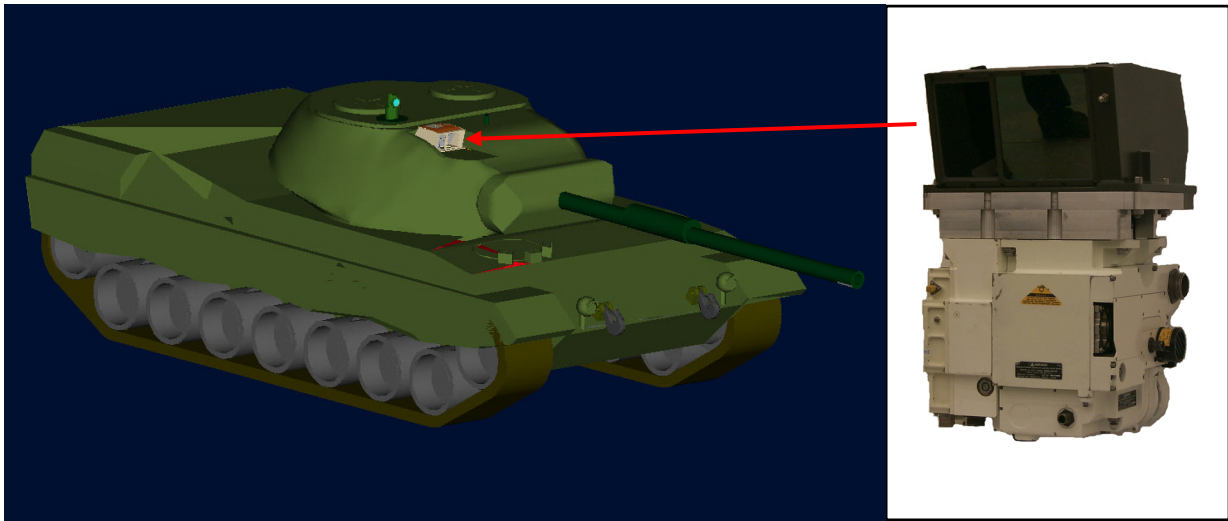


Figure 1.4. A View of Gyro Stabilized Head Mirror on the Tank and the Gunner's Periscope Alone

The high degree of line-of-sight stabilization achieved with independently stabilized sights raises the quality of the images which are provided by them and this, in turn, gives gunners more chance to detect targets quickly and at longer ranges. The accuracy with which the line of sight is stabilized makes it possible to use it as an inertial reference for the gun and the turret. In fact, this is done whenever an independently stabilized sight is used and the gun and the turret are then slaved to the sight, which results in a director-type fire control system [1,4].

In [4], "Director-Type Stabilization System" is explained as a single position loop for the gun. In fact there are two cascaded closed loops. One is the velocity feedback and hull disturbance feedforward inner loop and the other is the outer position loop in which the gun is slave to the sight position (Figure 1.5).

CHAPTER 2

AIM AND SCOPE OF THE STUDY

In this chapter, the thesis work is to be explained. Thesis structure will be presented and the proposed solutions to the subject and the methods to be followed will be explained to a certain extend.

2.1 Modeling the Main Battle Tank

2.1.1 Hull and Suspension

A certain experimental data that is measured from a main battle tank turret on the move. This data is measured by the hull and turret feedforward gyros of the tank itself (Figure 2.1). Hull feedforward gyro will measure the azimuth disturbance and the turret feedforward gyro will measure the elevation disturbance. Instead of modeling the tank suspension, this measured data at different forward velocities during APG course crossing will be used.

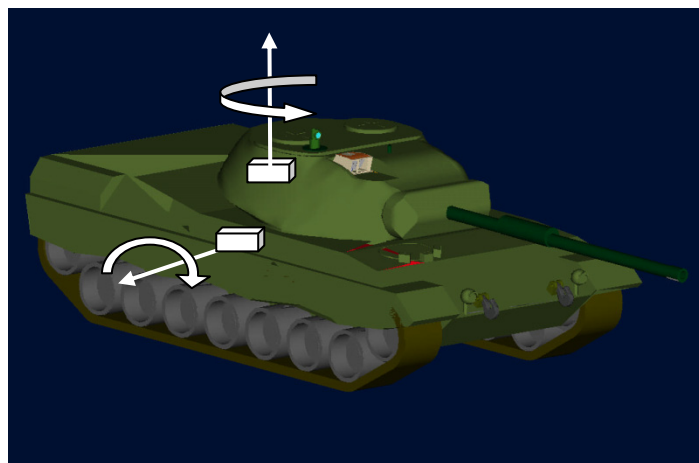


Figure 2.1. Disturbance Measurement

2.1.2 Turret Servo Dynamics Model

The turret will be designed as a 7-dof system (Figure 2.2).

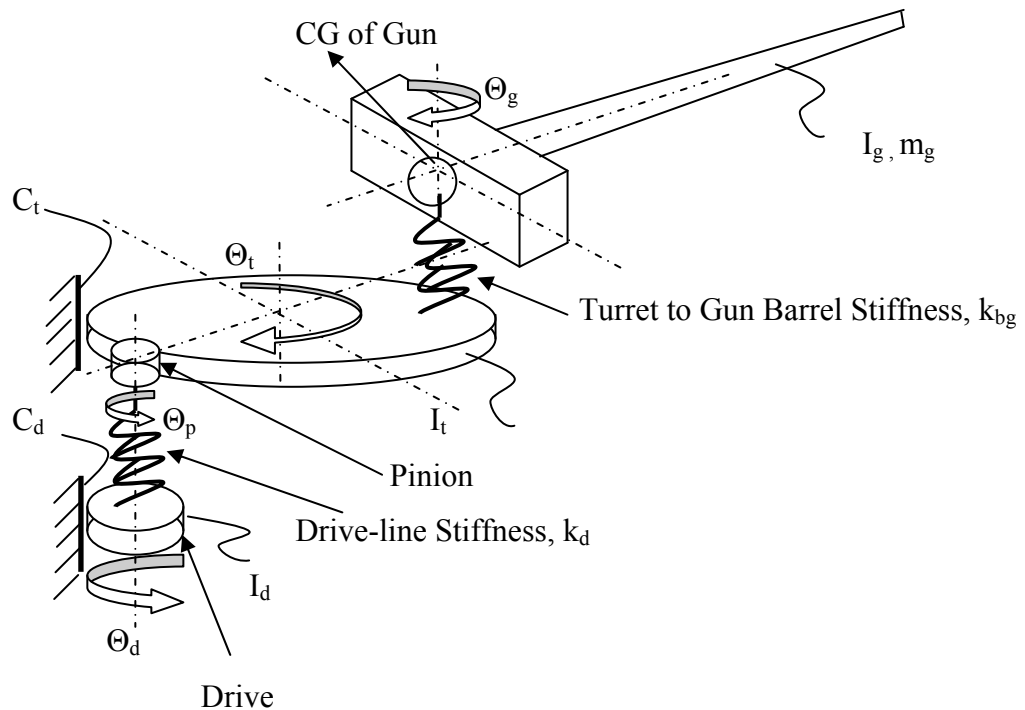


Figure 2.2. 3-DOF Turret Servo Dynamics Model

State Variables: $\Theta_d, \Theta_t, \Theta_g$

Gun will be modeled as flexible in the turret model. Azimuth controller is going to be developed using this model. Azimuth drive will be an electric-drive configuration (Figure 2.3). Main components are an electric motor being powered by a power amplifier, a planetary gearbox, a drive pinion at the exit shaft and the turret ring gear fixed to the turret.

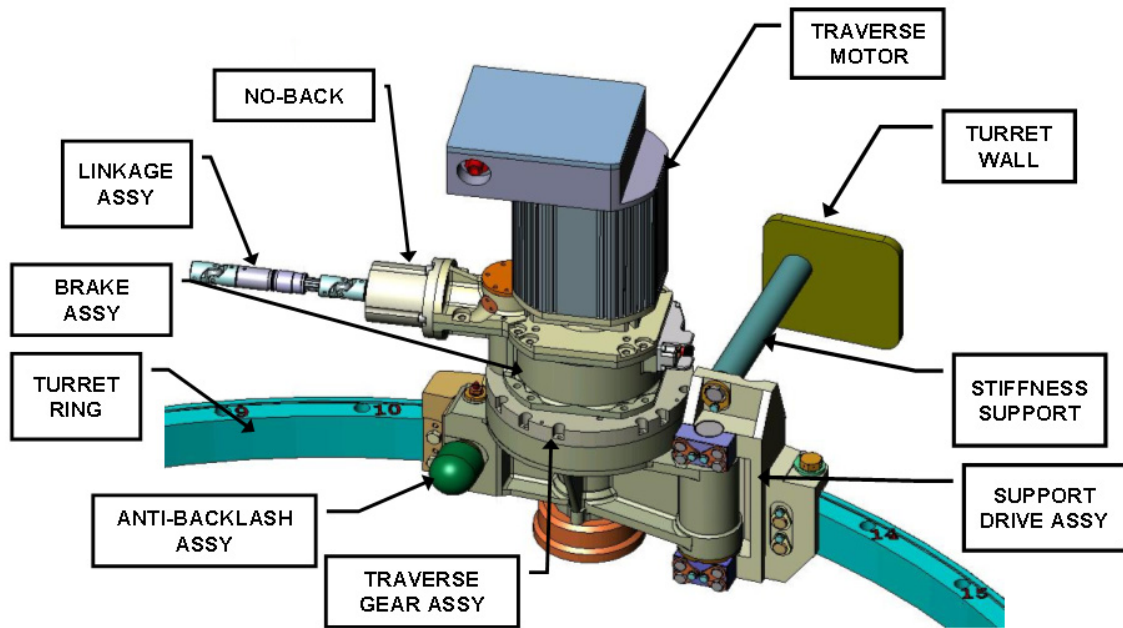


Figure 2.3. Turret Azimuth Drive

2.1.3 Gun Servo Dynamics Model

Elevation drive will be an electric-drive configuration (Figure 2.4). Main components are an electric motor being powered by a power amplifier, and a ball-screw spindle gearbox.

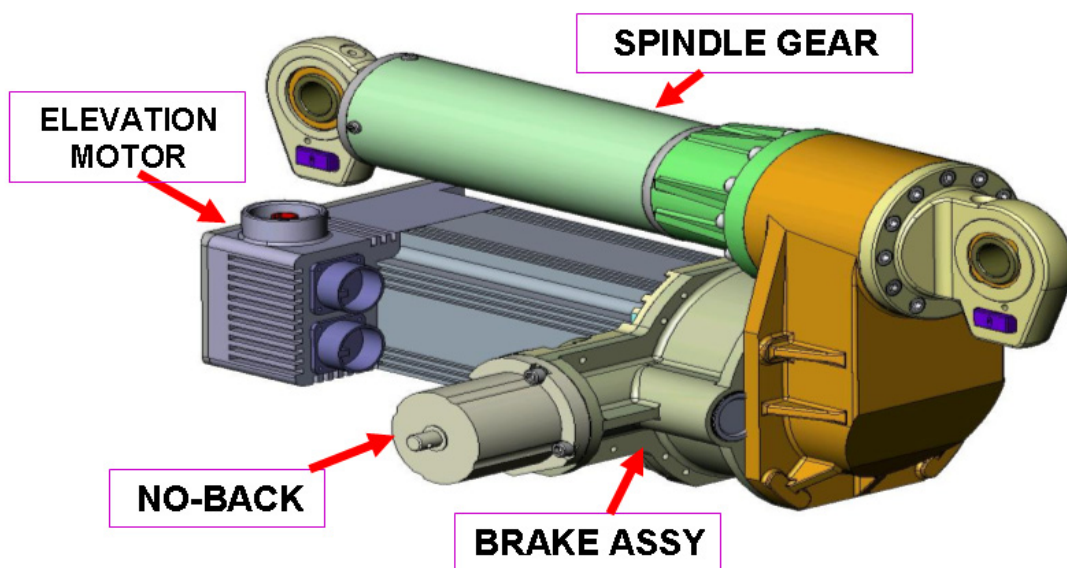


Figure 2.4. Elevation Drive

In the elevation model, gun will be modeled as flexible. The model will also include the drive viscous friction (c_d), drive-line linear stiffness (k_d), nonlinear trunnion (elevation axis revolute joint and barrel guide part) friction (c_t), cradle sleeve bearing friction (c_s) (Figure 2.5).

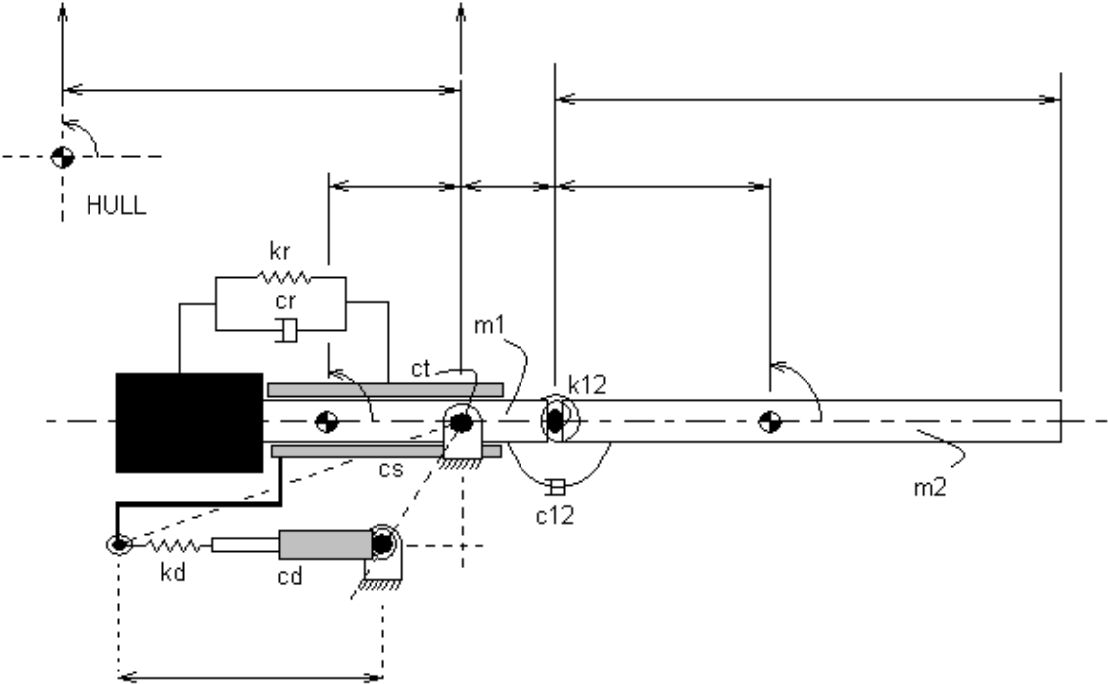


Figure 2.5. Gun Servo Dynamics Model

2.2 Disturbance Modeling

2.2.1 APG Course Modeling

The APG (Aberdeen Proven Ground) course is composed of a certain number of bumps separated with certain distances (Figure 2.6). Tank is driven through this standard course and the stabilization accuracy of the elevation axis is checked. For first round hit probability tests, again this course is used. Tank fires to a stationary or moving target while passing through the APG course.

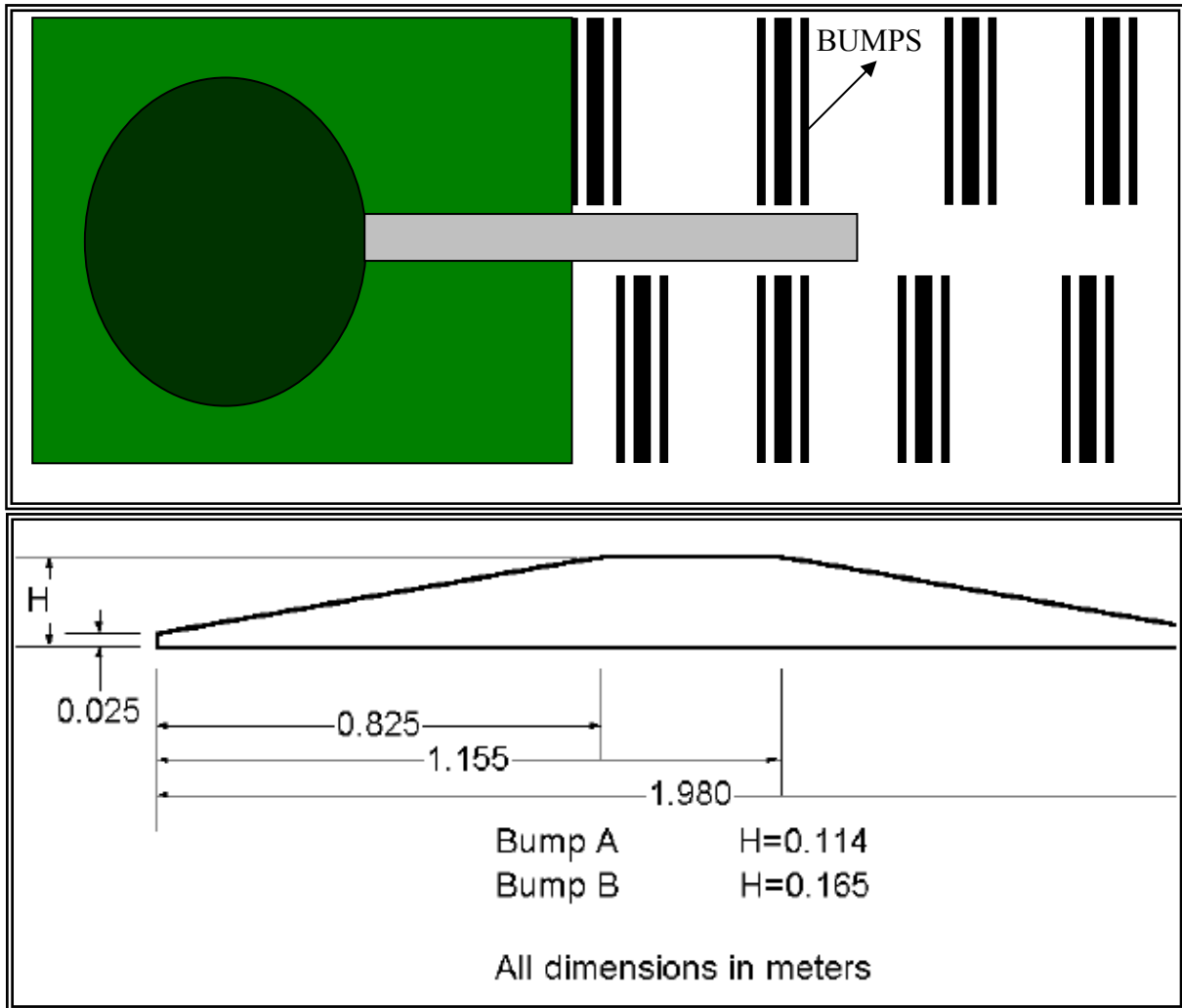


Figure 2.6. Tank Crossing an APG Course, Bump Dimensions

APG course creates disturbances mainly in hull body pitch and bounce directions. These are low frequency disturbances (0-5 Hz) due to bump geometry and a wide vibration spectrum (0 - 300 Hz) due to track and tank engine disturbing the gun elevation stabilization (Figure 2.7).

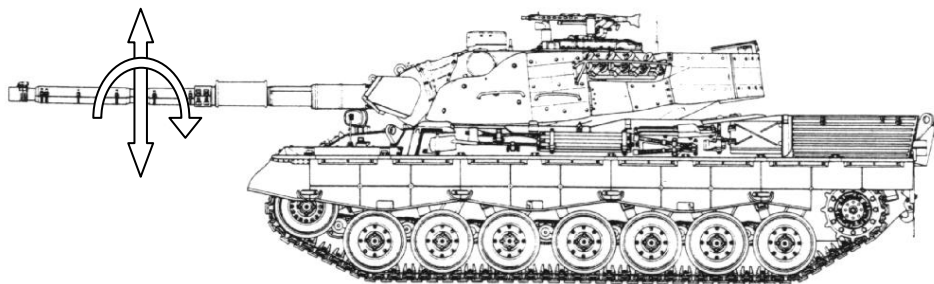


Figure 2.7. APG Course Disturbances in Gun Elevation

Body bounce linear accelerations turns into torque disturbance if there is an unbalance in the elevation axes. There is always unbalance in real life since it is not possible to have a perfectly balanced gun assembly practically. Ammunition itself is an unbalance mass (typically 15~20 kg) being loaded and fired during operation.

2.2.2 Sinuous Course Modeling

Sinuuous course is the turret azimuth stabilization test course. It is an S-curved road without bumps like in APG course Figure 2.8. This course is used to produce hull body yaw motion.

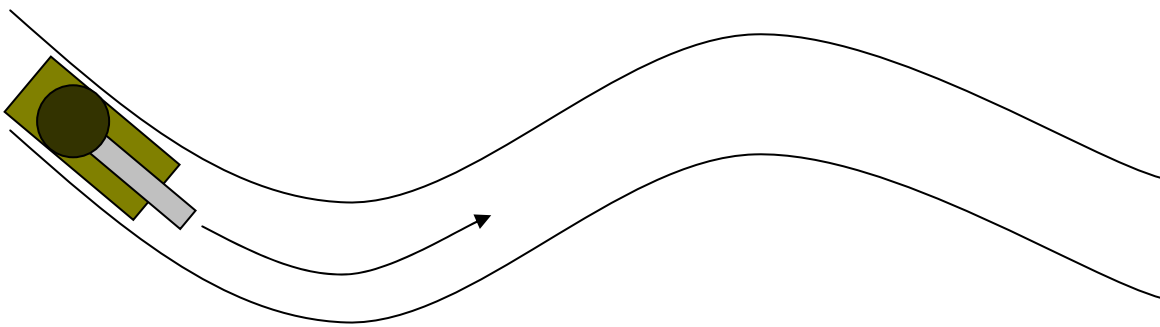


Figure 2.8. Sinuous Course

2.2.3 Other Sources of Disturbances

A battle tank is a massive vehicle (~60 ton) propelling with its tracks. A very powerful engine powers these tracks. This creates a very vibratory environment for the vehicle. The engine itself creates a considerable amount of vibration. Tracks are not like smooth car wheels. As the tank moves, tracks create harsh vibrations in both axes of control concern. These vibrations are very complex to model [28]. Instead of modeling the track vibrations, some experimental test data, covering all kind of disturbance sources from the ground to the turret, is going to be used to model these high frequency disturbances [27].

While the tank fire, a shock-wave propagates and the barrel recoils through the trunnion sleeve bearing (See Figure 2.4). Though internal ballistics and barrel axis offsets creates considerable amount of disturbances and cause "*gun jump*", modeling the ballistics is

beyond the scope of this study and the ammunition explosion will only be modeled as a disturbing impulse exciting the gun elevation and the azimuth.

2.3 Stabilization Controller Design

2.3.1 Elevation Stabilization Control

Stabilization controller in the elevation is the second generation director-type stabilization with disturbance feed forward as presented in Chapter 1 (See Figure 1.5). A very detailed analysis will be conducted and a controller in this form is to be optimized.

Difference from the existing controllers to be studied in this thesis is the muzzle stabilization during fire. Classical coincidence algorithms being used checks the coincidence of the director sight reference position and the gun position. However, gun position is measured from the optical encoder mounted at the elevation revolution axis of the gun. In fact, gun holding part, trunnion block, is stabilized instead of the gun muzzle. Flexibility of the gun is discarded (Figure 2.9).

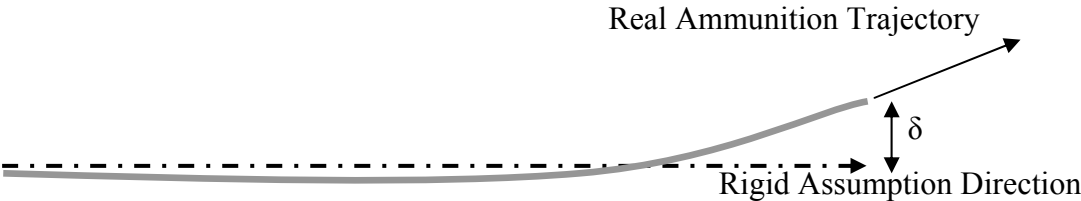
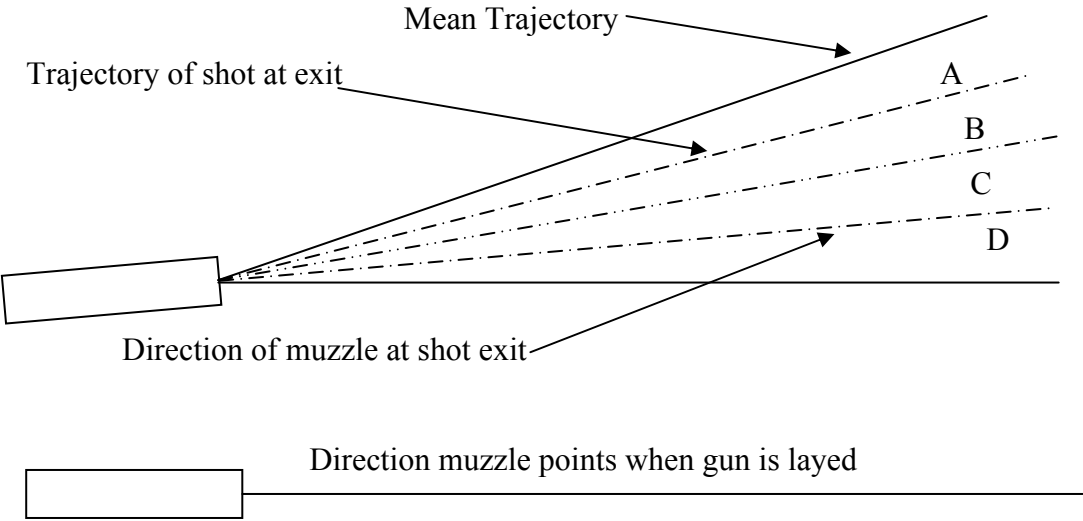


Figure 2.9. Effect of Flexibility of the Barrel

The levels of displacement vary considerably from gun to gun. Typically, the muzzle displacement will be of the order of 0.5 mm at shot elder but can be considerably larger after that time [3].

For a 105 mm barrel used in Leopard1 tank, the barrel length is 4235 mm. Taking muzzle deviation δ as 1 mm, muzzle deviation is calculated as $\tan^{-1}(1/4235) = 0.236$ mrad. Comparing the stabilization accuracy of the gun (0.5 mrad) to this value, almost half of the accuracy is lost due to the muzzle deviation. 0.236 mrad error results in 23.6 cm deviation from the target at 1000 m. Taking the effective target distance of a main battle tank as 4,000 meters, this deviation comes up to be $23.6\text{cm} * 4 = 94.4$ cm. In other words, for a perfectly stabilized gun, ammunition may hit the aimed target point placed at 4,000 m of distance, at a point deviating ± 1 m of the target point itself. It is a dramatic reduction for the "First Round Hit Probability" value of the fire control system, which is one of the main performance criteria of a main battle tank.

Flexing of the barrel is not the only source of muzzle deviation. During shot on fire, a combination of effects due to internal ballistics adds on to the gun flexure. The total deviation of muzzle is called "gun jump". An illustration is adopted from [8], Figure 2.10.



Components of gun jump:

D - Muzzle angle C- Muzzle Transverse Velocity B - Transverse Velocity of shot

Barrel Jump = D + C

Shot Jump = D + B + C

Gun Jump = A + B + C + D

Figure 2.10. The Components of Gun Jump

Mechanisms producing "shot jump" are off-axis masses, barrel curvature, barrel expansion, off-axis forces, shot interaction with barrel bore and shot tip-off [8].

In this thesis, a new control strategy that will compensate for the gun muzzle flexibility during fire is to be developed. The system will be modeled as multi-dof parametric model and a complex coincidence technique will be implemented. With this control strategy, no matter what source is the muzzle deviation, firing will be activated if the deviation conforms to the coincidence algorithm check. Advantages and shortcomings in real application will be discussed and solutions will be suggested for the hardware implementations. Gun flexibility is especially important for battle tanks having longer barrels. Nowadays, interest in longer barrels is increased due to the need for increased kill power against more effective armor technologies. Therefore a number of battle tanks under development or already in service use 120mm bore diameter L55 barrels, which means a barrel length of $55 * 120\text{mm} = 6,600\text{mm}$. This means a 2.3 meters longer cantilever barrel tube than the Leopard1 tank's 105mm barrel. Indeed there are readily available devices to compensate for the muzzle deviation, like “*dynamic muzzle reference systems*” but, in this thesis, it is proposed that the use of the dynamic muzzle reference systems, which are costly and bulky, can be eliminated by proper modeling and control.

2.3.2 Azimuth Stabilization Control

Stabilization controller in the azimuth is again the second generation director-type stabilization with disturbance feedforward as presented in Chapter 1 (See Figure 1.5). A very detailed analysis for the azimuth stabilization will be conducted too, and a controller in this form is to be optimized. The only difference this time is the absence of the coincidence algorithm. But there is no practical limitation to implement the similar coincidence algorithm for the azimuth controller in real life as long as the hardware resources running the controller software is sufficient.

2.4 Simulations

2.4.1 Stationary Tank Servo Feedback Controller Design

In these simulations, tank will be stationary. There will be no disturbances. It will be the first stage before the stabilization controller design and the aim is to tune the servo

feedback controller for a servo demand input. Azimuth and elevation axes will be simulated independently. For both axes, deviation of the muzzle will be monitored.

2.4.2 APG Course and Sinuous Path Crossing Tank Stabilization Controller Design

In these simulations, a standard APG course crossing tank will be simulated for the elevation and sinuous path crossing tank will be simulated for the azimuth, to design the stabilization feedback and feedforward controllers. The disturbances are hull motion in pitch and yaw axes respectively. Vehicle forward velocity is 40 kph.

2.4.3 APG Course Crossing and Firing Tank Stabilization and Coincidence Simulation

In this simulation, a standard APG course crossing tank will be simulated for the elevation to design the coincidence algorithm.. The disturbance is hull motion in pitch axis. Vehicle forward velocity is 40 kph.

2.5 Contribution of the Study to the Literature

Ultimate performance criteria for a main battle tank is the “First Round Hit Probability (FRHP)” figure, no matter how good is the gun and turret stabilization performance is. The final decision maker to enable or inhibit a fire trigger request made by a tank gunner is the coincidence algorithm. The performance of the coincidence algorithm directly influences the FRHP figure. Major contribution of this thesis to the literature is the complex coincidence algorithm design, which is absent in most of the fire control systems in use and in literature as well. Existing coincidence algorithms only monitor the stabilization error signal measured with the feedback gyro mounted on the trunnion and permits fire if this error signal is within a pre-defined range. These conventional coincidence algorithms do not consider the muzzle deflection due to barrel flexure and the time elapsed by the ammunition from being fired in the breech until exit from the muzzle. Proposed complex coincidence algorithm by this study takes the barrel flexure and the time delay into account and predicts the future orientation of the muzzle to permit or inhibit the fire trigger request by the gunner. By the use of this proposed technique, a 100% FRHP level can be achieved in theory.

CHAPTER 3

MODELING SERVO DYNAMICS

3.1 7-DOF Traverse Axis Servo Dynamics Model

In traverse axis, servo dynamics is modeled having 7-DOF. Gun is modeled as a five element lumped parameter flexible gun. Actuator servo stiffness and trunnion (turret to gun barrel) joint stiffness are the remaining two degrees of freedom.

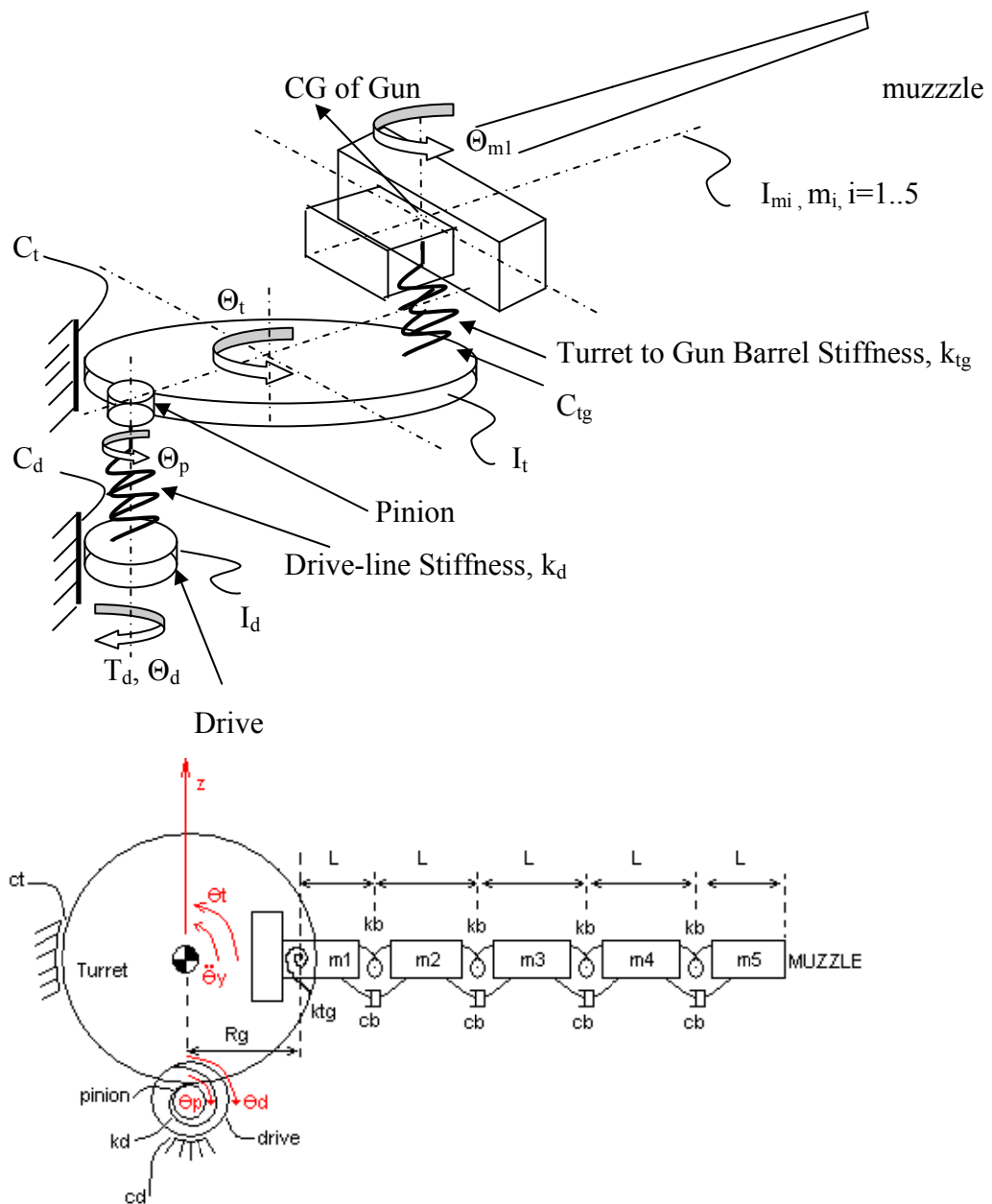


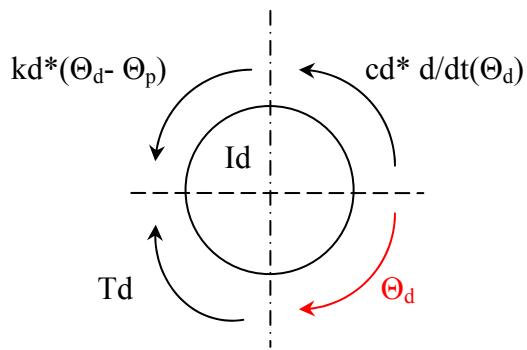
Figure 3.1. 7-DOF Turret Servo Dynamics Model

In this model, actuator torque T_d is the control input. Disturbance input in this axis is the angular acceleration and rate of hull yaw ($d^2/dt^2(\Theta_y)$, $d/dt(\Theta_y)$). It is assumed that the rotation center of hull is coincident with the rotation center of turret. It is also assumed that there is no unbalance in the azimuth axis so that the disturbance in hull sway (linear acceleration) does not act into the system [30, 31, 32, 33]. Descriptions of the system parameters and the free body diagrams (FBD) of each part are as follows;

Θ_t : Turret rotation w.r.t ground fixed frame (rad)
 Θ_y : Hull rotation w.r.t ground fixed frame (rad)
 R_p : Pinion pitch circle radius (m)
 R_t : Turret pitch circle radius (m)
 R_g : Turret rotation center to gun rotation center (trunnion joint center) (m)
 I_d : Drive Inertia ($kg \cdot m^2$)
 I_t : Turret inertia ($kg \cdot m^2$)
 I_a : Total inertia in azimuth ($kg \cdot m^2$)
 c_d : Drive viscous friction ($N \cdot m \cdot s / rad$)
 k_d : Drive-line stiffness ($N \cdot m / rad$)
 c_t : Turret ring gear total viscous friction ($N \cdot m \cdot s / rad$)
 k_{tg} : Turret to gun barrel stiffness
 k_b : Barrel part structural connection stiffness ($N \cdot m / rad$)
 c_b : Barrel part structural connection viscous damping ($N \cdot m \cdot s / rad$)
 m_1 : Mass of gun part 1 (includes gun breech) (kg)
 m_2 : Mass of gun part 2 (kg)
 m_3 : Mass of gun part 3 (kg)
 m_4 : Mass of gun part 4 (kg)
 m_5 : Mass of gun part 5 (includes any equipment mounted at muzzle) (kg)
 I_1 : Inertia of gun part 1 ($kg \cdot m^2$)
 I_2 : Inertia of gun part 2 ($kg \cdot m^2$)
 I_3 : Inertia of gun part 3 ($kg \cdot m^2$)
 I_4 : Inertia of gun part 4 ($kg \cdot m^2$)
 I_5 : Inertia of gun part 5 ($kg \cdot m^2$)
 Θ_d : Drive rotation w.r.t ground fixed frame (rad)
 Θ_p : Pinion rotation w.r.t ground fixed frame (rad)
 Θ_t : Turret rotation w.r.t ground fixed frame (rad)
 Θ_{m_1} : m_1 rotation w.r.t ground fixed frame (rad)
 Θ_{m_2} : m_2 rotation w.r.t ground fixed frame (rad)
 Θ_{m_3} : m_3 rotation w.r.t ground fixed frame (rad)
 Θ_{m_4} : m_4 rotation w.r.t ground fixed frame (rad)
 Θ_{m_5} : m_5 rotation w.r.t ground fixed frame (rad)
 T_d : Drive actuator torque ($N \cdot m$)
 f_d : Pinion to turret ring gear force (N)
 z : Linear degree of freedom in sway axis (m)
 L : Length of each lumped barrel part (m)
 η_1 : Distance from gun rotation center to m_1 center of gravity (m)

$$\Theta_t > \Theta_{m_1} > \Theta_{m_2} > \Theta_{m_3} > \Theta_{m_4} > \Theta_{m_5}$$

FBD of Drive:

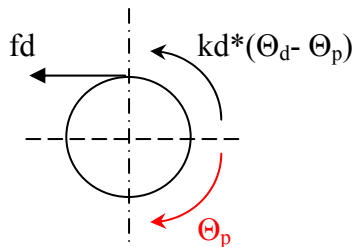


$$I_d \cdot \theta_{dd} = T_d - c_d \cdot \dot{\theta}_d - k_d(\theta_d - \theta_p) \quad (3.1)$$

Note that subscript d refers the first derivative and dd refers the second derivative w.r.t time.

⊕ represents the center of gravity.

FBD of Pinion:



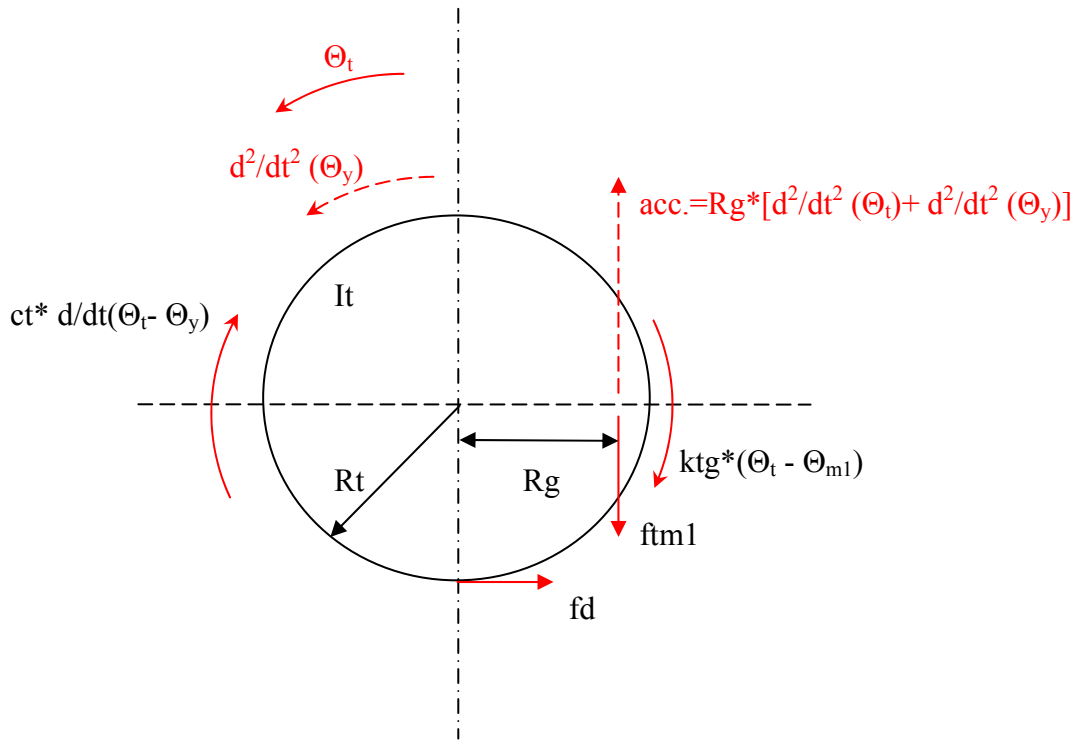
$$k_d \cdot (\theta_d - \theta_p) - f_d \cdot R_p = 0$$

$$R_p \cdot \theta_p = R_t \cdot \theta_t$$

$$\Rightarrow \theta_p = - (R_t / R_p) * \theta_t$$

$$(3.2)$$

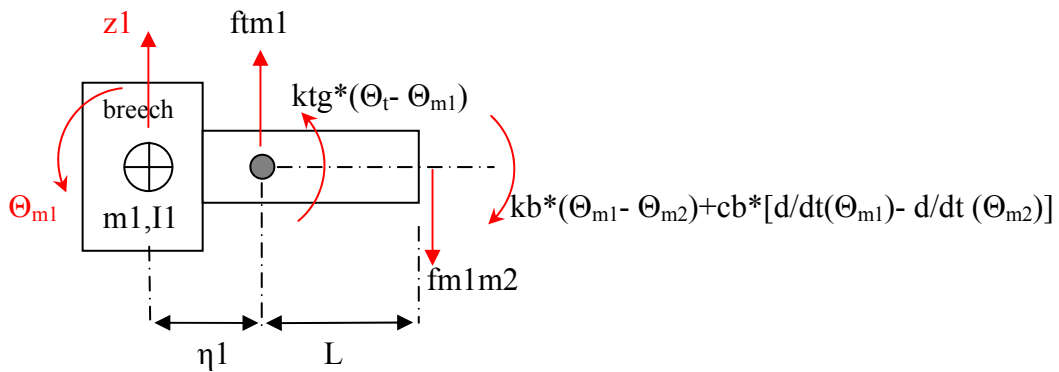
FBD of Turret:



$$I_t \cdot \theta_{tdd} = I_a \cdot \theta_{ydd} + f_d \cdot R_t - f_{tm1} \cdot R_g - k_{tg} \cdot (\theta_t - \theta_{m1}) - c_t \cdot (\theta_{td} - \theta_{yd}) \quad (3.3)$$

Note that yaw disturbance enters into dynamics as $[I_a \cdot d^2/dt^2(\theta_y)]$ and $[c_t \cdot d/dt(\theta_y)]$.

FBD of m1:

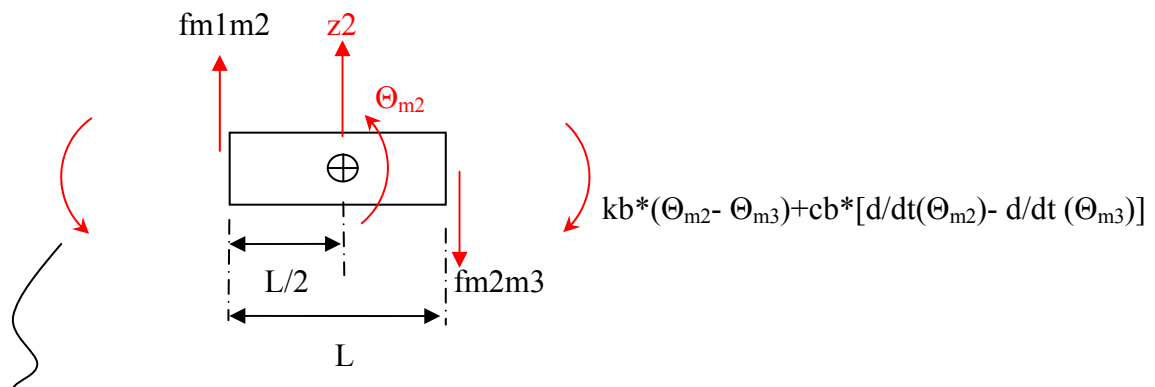


$$m1 \cdot z1_{dd} = f_{tm1} - f_{m1m2}$$

$$I1 \cdot \theta_{m1dd} = k_{tg} \cdot (\theta_t - \theta_{m1}) + f_{tm1} \cdot \eta_1 - k_b \cdot (\theta_{m1} - \theta_{m2}) - c_b \cdot (\theta_{m1d} - \theta_{m2d}) - f_{m1m2}(\eta_1 + L)$$

$$(3.4)$$

FBD of m2:



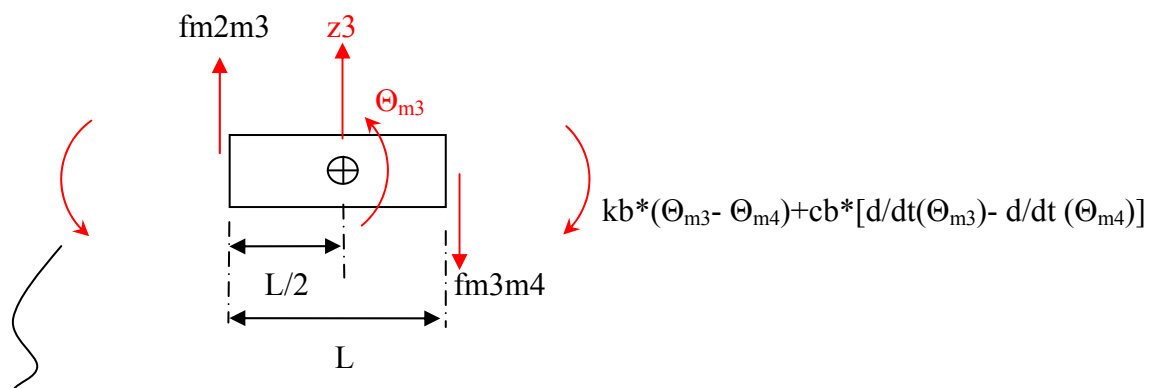
$$kb*(\Theta_{m1} - \Theta_{m2}) + cb*[d/dt(\Theta_{m1}) - d/dt(\Theta_{m2})]$$

$$m_2 \cdot z_{2dd} = f_{m1m2} - f_{m2m3}$$

$$I_2 \cdot \theta_{2dd} = kb \cdot (\theta_{m1} - \theta_{m2}) + cb \cdot (\theta_{m1d} - \theta_{m2d}) - kb \cdot (\theta_{m2} - \theta_{m3}) - cb \cdot (\theta_{m2d} - \theta_{m3d}) - \frac{1}{2} \cdot L \cdot (f_{m1m2} + f_{m2m3})$$

(3.5)

FBD of m3:



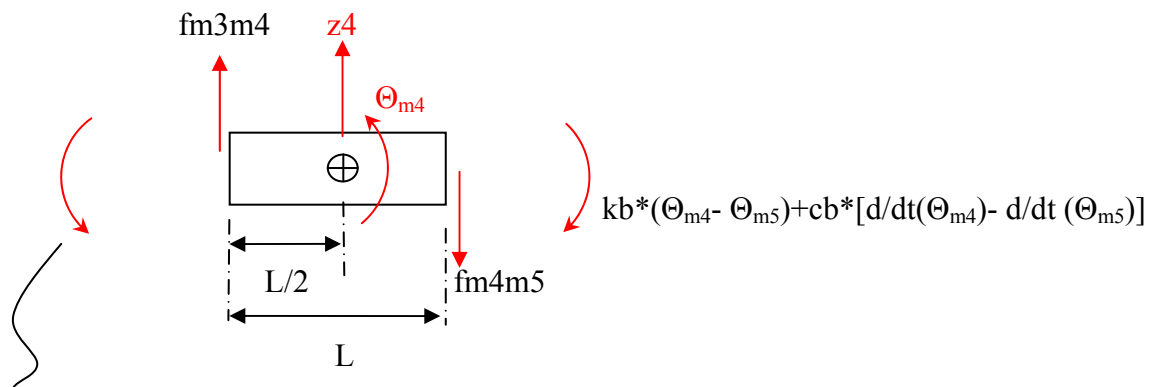
$$kb*(\Theta_{m2} - \Theta_{m3}) + cb*[d/dt(\Theta_{m2}) - d/dt(\Theta_{m3})]$$

$$m_3 \cdot z_{3dd} = f_{m2m3} - f_{m3m4}$$

$$I_3 \cdot \theta_{3dd} = kb \cdot (\theta_{m2} - \theta_{m3}) + cb \cdot (\theta_{m2d} - \theta_{m3d}) - kb \cdot (\theta_{m3} - \theta_{m4}) - cb \cdot (\theta_{m3d} - \theta_{m4d}) - \frac{1}{2} \cdot L \cdot (f_{m2m3} + f_{m3m4})$$

(3.6)

FBD of m4:

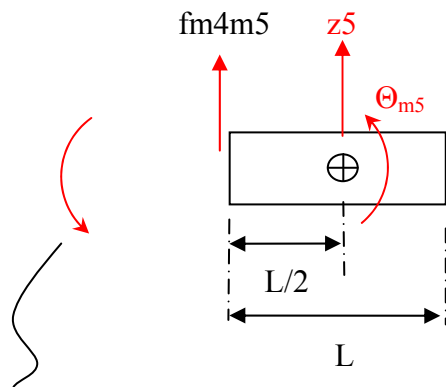


$$kb \cdot (\Theta_{m3} - \Theta_{m4}) + cb \cdot [d/dt(\Theta_{m3}) - d/dt(\Theta_{m4})]$$

$$m_4 z_{4dd} = f_{m3m4} - f_{m4m5}$$

$$I_4 \cdot \Theta_{4dd} = kb \cdot (\theta_{m3} - \theta_{m4}) + cb \cdot (\theta_{m3d} - \theta_{m4d}) - kb \cdot (\theta_{m4} - \theta_{m5}) - cb \cdot (\theta_{m4d} - \theta_{m5d}) - \frac{1}{2} \cdot L \cdot (f_{m3m4} + f_{m4m5}) \quad (3.7)$$

FBD of m5:



$$kb \cdot (\Theta_{m4} - \Theta_{m5}) + cb \cdot [d/dt(\Theta_{m4}) - d/dt(\Theta_{m5})]$$

$$m_5 \cdot z_{5dd} = f_{m4m5}$$

$$I_5 \cdot \Theta_{5dd} = kb \cdot (\theta_{m4} - \theta_{m5}) + cb \cdot (\theta_{m4d} - \theta_{m5d}) - \frac{1}{2} \cdot L \cdot f_{m4m5}$$

$$(3.8)$$

Constraint Equations:

$$z1 = Rg \cdot (\theta t + \theta y) - \eta 1 \cdot \sin(\theta m1)$$

$$Rg \cdot (\theta t + \theta y) + L \cdot \sin(\theta m1) = z2 - \frac{1}{2} \cdot L \cdot \sin(\theta m2)$$

$$z2 + \frac{1}{2} L \cdot \sin(\theta m2) = z3 - \frac{1}{2} \cdot L \cdot \sin(\theta m3)$$

$$z3 + \frac{1}{2} L \cdot \sin(\theta m3) = z4 - \frac{1}{2} \cdot L \cdot \sin(\theta m4)$$

$$z4 + \frac{1}{2} L \cdot \sin(\theta m4) = z5 - \frac{1}{2} \cdot L \cdot \sin(\theta m5)$$

(3.9)

Integrating twice assuming small Θ ;

$$z1_{dd} = Rg \cdot (\theta t_{dd} + \theta y_{dd}) - \eta 1 \cdot (\theta m1_{dd})$$

$$Rg \cdot (\theta t_{dd} + \theta y_{dd}) + L \cdot (\theta m1_{dd}) = z2_{dd} - \frac{1}{2} \cdot L \cdot (\theta m2_{dd})$$

$$z2_{dd} + \frac{1}{2} L \cdot (\theta m2_{dd}) = z3_{dd} - \frac{1}{2} \cdot L \cdot (\theta m2_{dd} - \theta m3_{dd})$$

$$z3_{dd} + \frac{1}{2} L \cdot (\theta m3_{dd}) = z4_{dd} - \frac{1}{2} \cdot L \cdot (\theta m4_{dd})$$

$$z4_{dd} + \frac{1}{2} L \cdot (\theta m4_{dd}) = z5_{dd} - \frac{1}{2} \cdot L \cdot (\theta m5_{dd})$$

(3.10)

Solving for linear accelerations $z1_{dd}$ to $z5_{dd}$;

$$z1_{dd} = Rg \cdot \theta t_{dd} + Rg \cdot \theta y_{dd} - \frac{1}{2} \cdot \theta m1_{dd}$$

$$z2_{dd} = Rg \cdot \theta t_{dd} + Rg \cdot \theta y_{dd} + L \cdot \theta m1_{dd} + \frac{1}{2} \cdot L \cdot \theta m2_{dd}$$

$$z3_{dd} = Rg \cdot \theta t_{dd} + Rg \cdot \theta y_{dd} + L \cdot \theta m1_{dd} + \frac{3}{2} \cdot L \cdot \theta m2_{dd} - \frac{1}{2} \cdot L \cdot \theta m3_{dd}$$

$$z4_{dd} = Rg \cdot \theta t_{dd} + Rg \cdot \theta y_{dd} + L \cdot \theta m1_{dd} + \frac{3}{2} \cdot L \cdot \theta m2_{dd} + \frac{1}{2} \cdot L \cdot \theta m4_{dd}$$

$$z5_{dd} = Rg \cdot \theta t_{dd} + Rg \cdot \theta y_{dd} + L \cdot \theta m1_{dd} + \frac{3}{2} \cdot L \cdot \theta m2_{dd} + L \cdot \theta m4_{dd} + \frac{1}{2} \cdot L \cdot \theta m5_{dd}$$

(3.11)

Linear accelerations $z1_{dd}$ to $z5_{dd}$ in the FBD equations are eliminated and the equations of motion for the system are reduced to the following form;

$$[M_1]_{7 \times 7} [\ddot{\theta}]_{7 \times 1} + [C_1]_{7 \times 7} [\dot{\theta}]_{7 \times 1} + [K_1]_{7 \times 7} [\theta]_{7 \times 1} = [I_1]_{7 \times 3} [u]_{3 \times 1}$$

where

$$[\theta] = [\theta_d \quad \theta_t \quad \theta_{m1} \quad \theta_{m2} \quad \theta_{m3} \quad \theta_{m4} \quad \theta_{m5}]^T$$

$$[u] = [T_d \quad \ddot{\theta}_y \quad \dot{\theta}_y]^T$$

(3.12)

Derivation of the equations are in Appendix A1. Results are following;

$$\mathbf{M1} = \begin{bmatrix} 0 & , & 2*L*Rg*m5 & , & 2*L^2*m5 & , & 3*L^2*m5 & , & 0 & , & 2*L^2*m5 & , & 4*I5+L^2*m5 ; \\ 0 & , & -2*L*Rg*(m4+2*m5) & , & -2*L^2*(m4+2*m5) & , & -3*L^2*(m4+2*m5) & , & 0 & , & -L^2*(m4+4*m5) & -4*I4 & , & -2*L^2*m5 ; \\ 0 & , & -2*L*Rg*(m3+2*m4+2*m5) & , & -2*L^2*(m3+2*m4+2*m5) & , & -3*L^2*(m3+2*m4+2*m5) & , & -4*I3+m3*L^2 & , & -2*L^2*(m4+2*m5) & , & -2*L^2*m5 ; \\ 0 & , & -2*L*Rg*(2*m3+m2+2*m5+2*m4) & , & -2*L^2*(m2+2*m3+2*m4+2*m5) & , & -4*I2-L^2*(m2+6*m3+6*m4+6*m5) & , & 2*m3*L^2 & , & -2*L^2*(m4+2*m5) & , & -2*L^2*m5 ; \\ 0 & , & -2*Rg*(L*(m3+m2+m5+m4)-m1*eta) & , & -2*(I1+L^2*(m2+m3+m4+m5))-eta*m1 & , & -L^2*(m2+3*m3+3*m4+3*m5) & , & m3*L^2 & , & -L^2*(m4+2*m5) & , & -L^2*m5 ; \\ 0 & , & -2*Rp*(Rg^2*(m3+m2+m1+m4+m5)+It) & , & -2*Rg*Rp*L*(m2+m3+m4+m5)+Rg*Rp*m1 & , & -Rg*Rp*L*(m2+3*m3+3*m4+3*m5) & , & Rg*Rp*m3*L & , & -Rg*Rp*L*(m4+2*m5) & , & -Rg*Rp*L*m5 ; \\ Id*Rp & , & 0 & , & 0 & , & 0 & , & 0 & , & 0 & , & 0 &]$$

$$\mathbf{C1} = \begin{bmatrix} 0 & , & 0 & , & 0 & , & 0 & , & 0 & , & -4*cb & , & 4*cb & ; \\ 0 & , & 0 & , & 0 & , & 0 & , & 4*cb & , & -8*cb & , & 4*cb & ; \\ 0 & , & 0 & , & 0 & , & 4*cb & , & -8*cb & , & 4*cb & , & 0 & ; \\ 0 & , & 0 & , & 4*cb & , & -8*cb & , & 4*cb & , & 0 & , & 0 & ; \\ 0 & , & 0 & , & -2*cb & , & 2*cb & , & 0 & , & 0 & , & 0 & ; \\ 0 & , & -2*ct*Rp & , & 0 & , & 0 & , & 0 & , & 0 & , & 0 & ; \\ cd*Rp & , & 0 & , & 0 & , & 0 & , & 0 & , & 0 & , & 0 &]$$

$$\mathbf{K1} = \begin{bmatrix} 0 & , & 0 & , & 0 & , & 0 & , & 0 & , & -4*kb & , & 4*kb ; \\ 0 & , & 0 & , & 0 & , & 0 & , & 0 & , & 4*kb & , & -8*kb & , & 4*kb ; \\ 0 & , & 0 & , & 0 & , & 0 & , & 4*kb & , & -8*kb & , & 4*kb & , & 0 ; \\ 0 & , & 0 & , & 4*kb & , & -8*kb & , & 4*kb & , & 0 & , & 0 & , & 0 ; \\ 0 & , & 2*ktg & , & -2*(ktg+kb) & , & 2*kb & , & 0 & , & 0 & , & 0 & , & 0 ; \\ 2*kd*Rt & , & -2*(ktg*Rp+kd*(Rt^2/Rp)) & , & 2*ktg*Rp & , & 0 & , & 0 & , & 0 & , & 0 & , & 0 ; \\ kd*Rp & , & kd*Rt & , & 0 & , & 0 & , & 0 & , & 0 & , & 0 & , & 0]$$

$$\mathbf{I1} = \begin{bmatrix} 0 & , & -2*L*Rg*m5 & , & 0 & , & ; \\ 0 & , & 2*L*Rg*(m4+2*m5) & , & 0 & , & ; \\ 0 & , & 2*L*Rg*(m3+2*m4+2*m5) & , & 0 & , & ; \\ 0 & , & 2*L*Rg*(m2+2*m3+2*m4+2*m5) & , & 0 & , & ; \\ 0 & , & 2*Rg*(m2*L+m3*L+m4*L+m5*L-eta*m1) & , & 0 & , & ; \\ 0 & , & 2*Rp*(Rg^2*(m1+m2+m3+m4+m5)-Ia) & , & -2*ct*Rp & , & ; \\ Rp & , & 0 & , & 0 & , &]$$

In state-space form;

$$\begin{aligned}\dot{x} &= Ax + Bu \\ y &= Cx + Du\end{aligned}\tag{3.13}$$

where

$$\begin{aligned}A &= \begin{bmatrix} \{0\}_{7 \times 7} & \{I\}_{7 \times 7} \\ -\{M_1\}^{-1}\{K_1\} & -\{M_1\}^{-1}\{C_1\} \end{bmatrix} \\ B &= \begin{bmatrix} \{0\} \\ -\{M_1\}^{-1}\{I_1\} \end{bmatrix} \\ C &= [\{I\}_{14 \times 14}] \\ D &= [\{0\}_{14 \times 3}]\end{aligned}\tag{3.14}$$

System parameters are inserted into the parametric equations for modeling. These parameters are roughly obtained from various battle tanks and are subject to change.

```

Id=25;           Azimuth Drive Inertia (kg.m^2)
It=45000;       Turret Inertia (kg.m^2)
m1=2500;        Mass of Gun Part 1 (kg) (Includes Gun Breech)
m2=125;         Mass of Gun Part 2 (kg)
m3=150;         Mass of Gun Part 3 (kg)
m4=125;         Mass of Gun Part 4 (kg)
m5=100;         Mass of Gun Part 5 (kg) (This is the Gun Muzzle)
L=1;           Length of each gun part except Part 1 (m)
I1=1000;        Inertia of Gun Part 1 (kg.m^2)
I2=9.5;         Inertia of Gun Part 2 (kg.m^2)
I3=9.5;         Inertia of Gun Part 3 (kg.m^2)
I4=9.5;         Inertia of Gun Part 4 (kg.m^2)
I5=9.5;         Inertia of Gun Part 5 (kg.m^2)
cd=150;         Drive viscous friction (N*m*s/rad)
ct=9e4;         Turret viscous friction (N*m*s/rad)
ctg=1e4;        Turret to gun(m1) viscous friction (N*m*s/rad)
ktg=4.5e8;      Turret to gun(m1) stiffness (N*m/rad)
kd=2e6;         Drive stiffness (N*m/rad)
cb=2e3;         Gun parts joint viscous friction (N*m*s/rad) (Between m1,m2,m3,m4,m5)
kb=4e6;         Gun parts joint stiffnesses (N*m/rad) (Between m1,m2,m3,m4,m5)
Rp=0.08;        Pinion Pitch Circle Radius (m)
Rg=0.9;         Turret rotation center to Turret-Gun_m1 Joint Distance
Rt=1.1;         Turret Ring Gear Pitch Circle Radius (m)
Ia=It+(m1+m2+m3+m4+m5)*Rg^2;  Total azimuth inertia (turret + gun) (kg.m^2)
eta=0.5;        Trunnion to CG of breech (m1) part (m)

```

For this data set, a Matlab® m-file is written to calculate the natural frequencies and unit step response. Complete code of this m-file is in Appendix A2. Natural frequencies (in Hz) are calculated as follows;

$$\text{natural_frequencies} = [1/(2*\pi)]*\text{sqrt}[\text{eigenvalues}[\{M1\}^{-1} * \{K1\}]]$$

Output of the m-file given in Appendix A2 is as follows;

```
naturalfrequencies_sorted =
1.0e+002 *
0 + 0.0000i
0.0662
0.2976
0.4263
0.8386
0.9323
2.1056
```

3.2 5-DOF Elevation Axis Servo Dynamics Model

In elevation axis, servo dynamics is modeled having 5-DOF. Gun is modeled as a five element lumped parameter flexible gun. Actuator servo stiffness is also modeled.

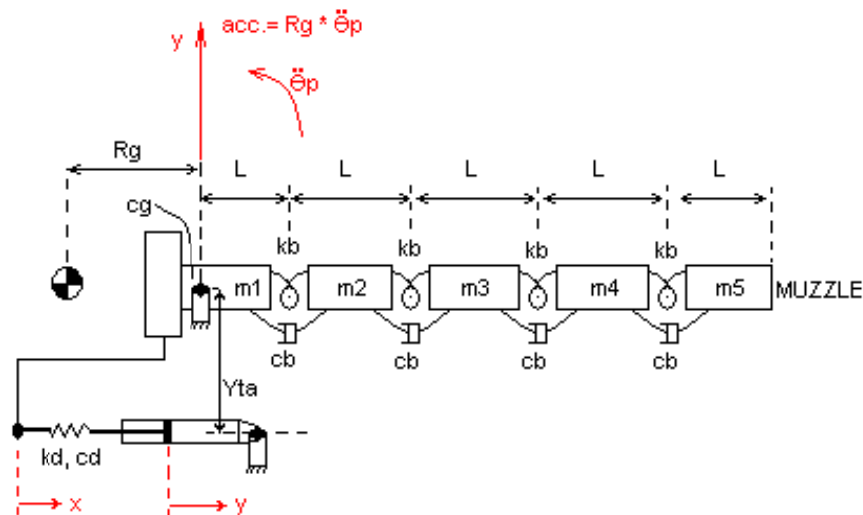


Figure 3.2. 5-DOF Elevation Servo Dynamics Model

Elevation drive-line is linearized around level gun position.

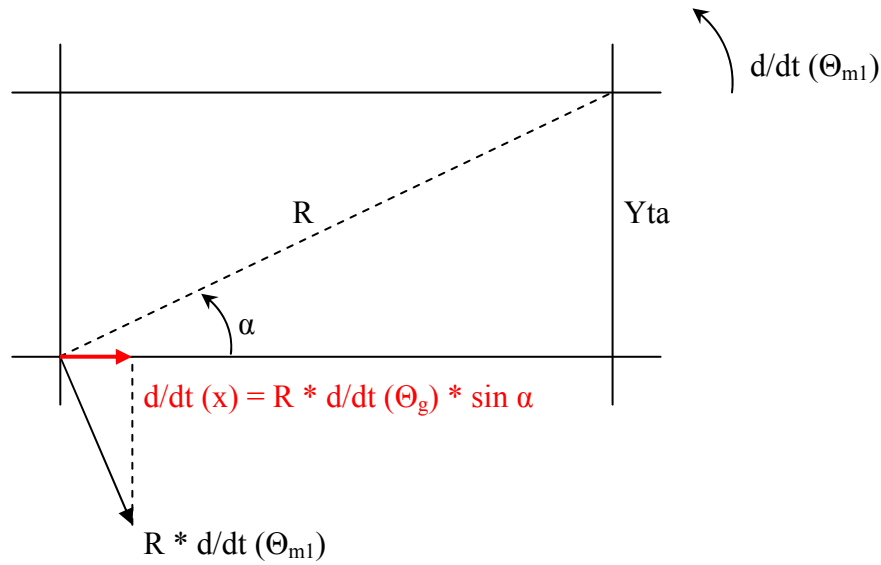


Figure 3.3. Elevation Drive Line Linearization

$$\dot{x} = R\dot{\theta}_{m1}\sin\alpha$$

$$\dot{x} = R\dot{\theta}_{m1} \frac{Y_{ta}}{R}$$

$$dx = Y_{ta}d\theta_{m1}$$

(3.15)

In this model, actuator position y is the control input. Disturbance input in this axis is the angular acceleration and rate of hull reduced to the elevation plane ($d^2/dt^2(\Theta_p)$, $d/dt(\Theta_p)$). It is assumed that the rotation center of disturbance is coincident with the rotation center of turret. It is also assumed that there is no unbalance in the elevation axis so that the disturbance in hull heave direction (linear acceleration) does not act into the system. Descriptions of the system parameters and the free body diagrams (FBD) of each part are as follows;

Θ_p : Hull pitch rotation reduced to elevation plane w.r.t ground fixed frame (rad)

R_g : Turret rotation center to gun rotation center (trunnion joint center) (m)

Y_{ta} : Trunnion joint (gun elevation joint) to linear actuator line (m)

I_g : Total gun inertia ($kg \cdot m^2$)

k_d : Drive-line stiffness (N/m)

c_g : Trunnion joint (gun elevation joint) viscous friction ($N \cdot m \cdot s / rad$)

k_b : Barrel part structural connection stiffness ($N \cdot m / rad$)

c_b : Barrel part structural connection viscous damping ($N \cdot m \cdot s / rad$)

m_1 : Mass of gun part 1 (includes gun breech) (kg)

m_2 : Mass of gun part 2 (kg)

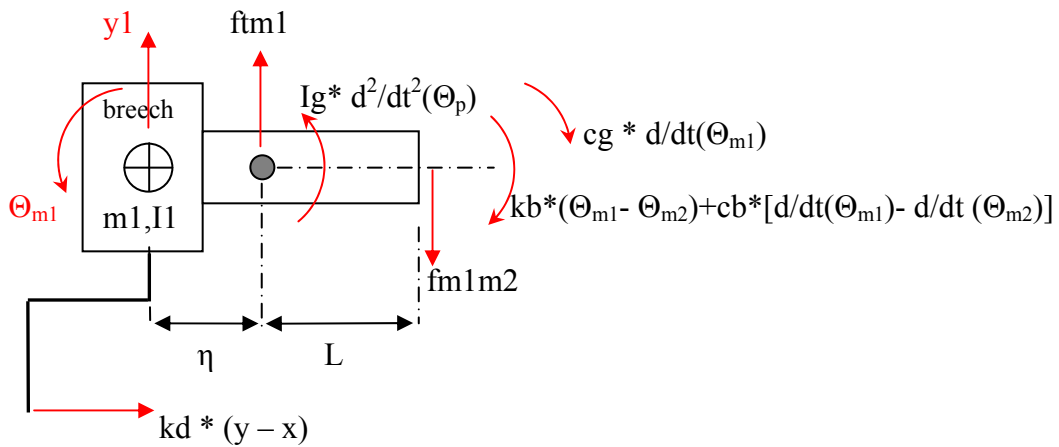
m_3 : Mass of gun part 3 (kg)

- m4 : Mass of gun part 4 (kg)
- m5 : Mass of gun part 5 (includes any equipment mounted at muzzle) (kg)
- I1 : Inertia of gun part 1 (kg*m²)
- I2 : Inertia of gun part 2 (kg*m²)
- I3 : Inertia of gun part 3 (kg*m²)
- I4 : Inertia of gun part 4 (kg*m²)
- I5 : Inertia of gun part 5 (kg*m²)
- y : Actuator linear position (m)
- Θ_{m1} : m1 rotation w.r.t ground fixed frame (rad)
- Θ_{m2} : m2 rotation w.r.t ground fixed frame (rad)
- Θ_{m3} : m3 rotation w.r.t ground fixed frame (rad)
- Θ_{m4} : m4 rotation w.r.t ground fixed frame (rad)
- Θ_{m5} : m5 rotation w.r.t ground fixed frame (rad)
- y_i : Linear degree of freedom in heave axis, i=1..5 (m)
- L : Length of each lumped barrel part (m)
- η : Distance from gun rotation center to m1 center of gravity (m)

$$\Theta_{m1} > \Theta_{m2} > \Theta_{m3} > \Theta_{m4} > \Theta_{m5}$$

$$y > x$$

FBD of m1:



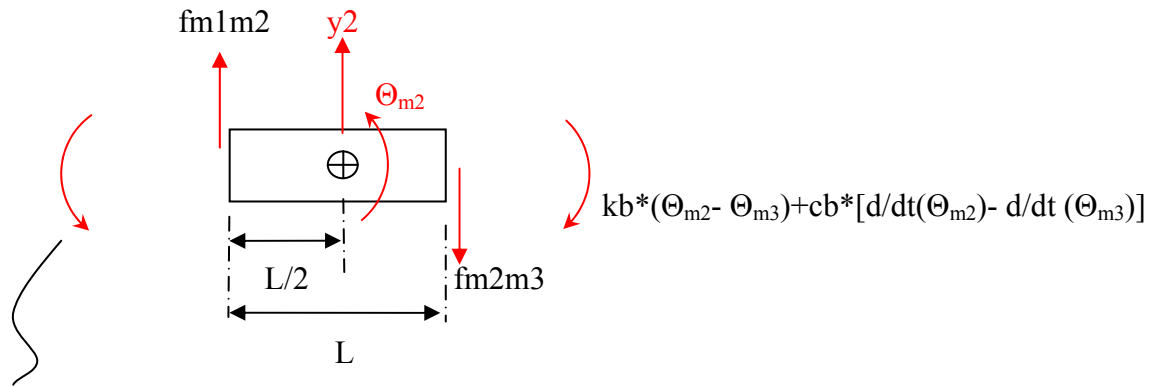
Note that pitch disturbance enters into dynamics as $[Ig * d^2/dt^2 (\Theta_p)]$ and $[cg * d/dt (\Theta_p)]$.

$$m1 \cdot y1_{dd} = ftm1 - fm1m2$$

$$I1 \cdot \Theta_{m1}_{dd} = Ig \cdot \Theta_{p_{dd}} - cg \cdot (\Theta_{m1}_{d} - \Theta_{p_d}) - kd \cdot Yta^2 \cdot \Theta_{m1} + kd \cdot Yta \cdot y - kb \cdot (\Theta_{m1} - \Theta_{m2}) - cb \cdot (\Theta_{m1_d} - \Theta_{m2_d}) - fm1m2(\eta + L) + ftm1 \cdot \eta$$

$$(3.16)$$

FBD of m2:

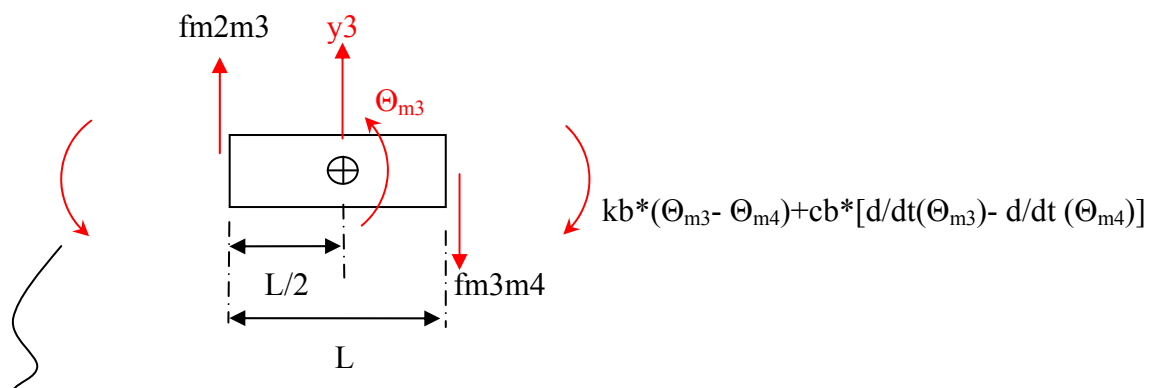


$$kb \cdot (\Theta_{m1} - \Theta_{m2}) + cb \cdot [d/dt(\Theta_{m1}) - d/dt(\Theta_{m2})]$$

$$m_2 \cdot y_{2dd} = f_{m1m2} - f_{m2m3}$$

$$I_2 \cdot \Theta_{2dd} = kb \cdot (\theta_{m1} - \theta_{m2}) + cb \cdot (\theta_{m1d} - \theta_{m2d}) - kb \cdot (\theta_{m2} - \theta_{m3}) - cb \cdot (\theta_{m2d} - \theta_{m3d}) - \frac{1}{2} \cdot L \cdot (f_{m1m2} + f_{m2m3}) \quad (3.17)$$

FBD of m3:

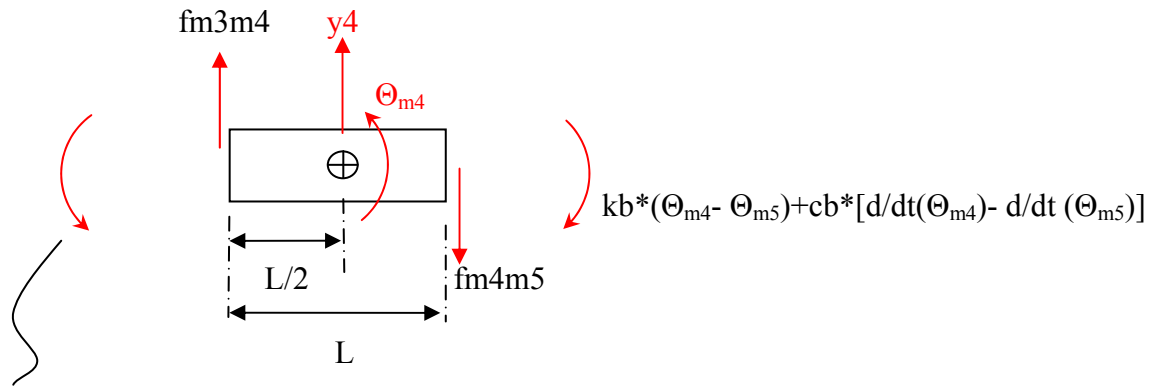


$$kb \cdot (\Theta_{m2} - \Theta_{m3}) + cb \cdot [d/dt(\Theta_{m2}) - d/dt(\Theta_{m3})]$$

$$m_3 \cdot y_{3dd} = f_{m2m3} - f_{m3m4}$$

$$I_3 \cdot \Theta_{3dd} = kb \cdot (\theta_{m2} - \theta_{m3}) + cb \cdot (\theta_{m2d} - \theta_{m3d}) - kb \cdot (\theta_{m3} - \theta_{m4}) - cb \cdot (\theta_{m3d} - \theta_{m4d}) - \frac{1}{2} \cdot L \cdot (f_{m2m3} + f_{m3m4})$$

FBD of m4:

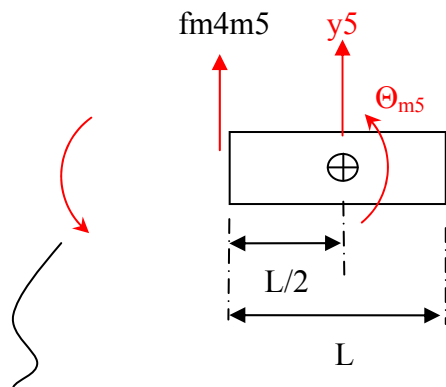


$$kb \cdot (\Theta_{m3} - \Theta_{m4}) + cb \cdot [d/dt(\Theta_{m3}) - d/dt(\Theta_{m4})]$$

$$m_4 y_{4dd} = f_{m3m4} - f_{m4m5}$$

$$I_4 \cdot \Theta_{4dd} = kb \cdot (\theta_{m3} - \theta_{m4}) + cb \cdot (\theta_{m3d} - \theta_{m4d}) - kb \cdot (\theta_{m4} - \theta_{m5}) - cb \cdot (\theta_{m4d} - \theta_{m5d}) - \frac{1}{2} \cdot L \cdot (f_{m3m4} + f_{m4m5}) \quad (3.18)$$

FBD of m5:



$$kb \cdot (\Theta_{m4} - \Theta_{m5}) + cb \cdot [d/dt(\Theta_{m4}) - d/dt(\Theta_{m5})]$$

$$m_5 \cdot y_{5dd} = f_{m4m5}$$

$$I_5 \cdot \Theta_{5dd} = kb \cdot (\theta_{m4} - \theta_{m5}) + cb \cdot (\theta_{m4d} - \theta_{m5d}) - \frac{1}{2} \cdot L \cdot f_{m4m5}$$

(3.19)

Constraint Equations;

$$y1 = Rg \cdot \theta p - \eta \cdot \sin(\theta m1)$$

$$Rg \cdot \theta p + L \cdot \sin(\theta m1) = y2 - \frac{1}{2} \cdot L \cdot \sin(\theta m2)$$

$$y2 + \frac{1}{2} L \cdot \sin(\theta m2) = y3 - \frac{1}{2} \cdot L \cdot \sin(\theta m3)$$

$$y3 + \frac{1}{2} L \cdot \sin(\theta m3) = y4 - \frac{1}{2} \cdot L \cdot \sin(\theta m4)$$

$$y4 + \frac{1}{2} L \cdot \sin(\theta m4) = y5 - \frac{1}{2} \cdot L \cdot \sin(\theta m5)$$

(3.20)

Integrating twice assuming small Θ ;

$$y1_{dd} = Rg \cdot \theta p_{dd} - \eta \cdot \theta m1_{dd}$$

$$Rg \cdot \theta p_{dd} + L \cdot (\theta m1_{dd}) = y2_{dd} - \frac{1}{2} \cdot L \cdot (\theta m2_{dd})$$

$$y2_{dd} + \frac{1}{2} L \cdot (\theta m2_{dd}) = y3_{dd} - \frac{1}{2} \cdot L \cdot (\theta m3_{dd})$$

$$y3_{dd} + \frac{1}{2} L \cdot (\theta m3_{dd}) = y4_{dd} - \frac{1}{2} \cdot L \cdot (\theta m4_{dd})$$

$$y4_{dd} + \frac{1}{2} L \cdot (\theta m4_{dd}) = y5_{dd} - \frac{1}{2} \cdot L \cdot (\theta m5_{dd})$$

(3.21)

Solving for linear accelerations $y1_{dd}$ to $y5_{dd}$;

$$y1_{dd} = Rg \cdot \theta p_{dd} - \eta \cdot \theta m1_{dd}$$

$$y2_{dd} = Rg \cdot \theta p_{dd} + L \cdot \theta m1_{dd} + \frac{1}{2} \cdot L \cdot \theta m2_{dd}$$

$$y3_{dd} = Rg \cdot \theta p_{dd} + L \cdot \theta m1_{dd} + L \cdot \theta m2_{dd} + \frac{1}{2} \cdot L \cdot \theta m3_{dd}$$

$$y4_{dd} = Rg \cdot \theta p_{dd} + L \cdot \theta m1_{dd} + L \cdot \theta m2_{dd} + L \cdot \theta m3_{dd} + \frac{1}{2} \cdot L \cdot \theta m4_{dd}$$

$$y5_{dd} = Rg \cdot \theta p_{dd} + L \cdot \theta m1_{dd} + L \cdot \theta m2_{dd} + L \cdot \theta m3_{dd} + L \cdot \theta m4_{dd} + \frac{1}{2} \cdot L \cdot \theta m5_{dd}$$

(3.22)

Linear accelerations y_{1dd} to y_{5dd} in the FBD equations are eliminated and the equations of motion for the system are reduced to the following form;

$$[M_1]_{5 \times 5} [\ddot{\theta}]_{5 \times 1} + [C_1]_{5 \times 5} [\dot{\theta}]_{5 \times 1} + [K_1]_{5 \times 5} [\theta]_{5 \times 1} = [I_1]_{5 \times 3} [u]_{3 \times 1}$$

where

$$[\theta] = [\theta_{m1} \quad \theta_{m2} \quad \theta_{m3} \quad \theta_{m4} \quad \theta_{m5}]^T$$

$$[u] = [y \quad \ddot{\theta}_p \quad \dot{\theta}_p]^T$$

(3.23)

Derivation of the equations are in Appendix A3. Results are following;

$$\mathbf{M1} = \begin{bmatrix} -2*L^2*m5 & , & -2*L^2*m5 & , & -2*L^2*m5 & , & -2*L^2*m5 & , & -(4*I5+ L^2*m5) ; \\ 2*m4*L^2+4*m5*L^2 & , & 2*m4*L^2+4*m5*L^2 & , & 2*m4*L^2+4*m5*L^2 & , & 4*m5*L^2+4*I4+m4*L^2 & , & 2*m5*L^2 ; \\ 2*m3*L^2+4*m4*L^2+4*m5*L^2 & , & 2*m3*L^2+4*m4*L^2+4*m5*L^2 & , & m3*L^2+4*I3+4*m4*L^2+4*m5*L^2 & , & 2*m4*L^2+4*m5*L^2 & , & 2*m5*L^2 ; \\ 2*m2*L^2+4*m3*L^2+4*m4*L^2+4*m5*L^2 & , & m2*L^2+4*I2+4*m3*L^2+4*m4*L^2+4*m5*L^2 & , & 2*m3*L^2+4*m4*L^2+4*m5*L^2 & , & 2*m4*L^2+4*m5*L^2 & , & 2*m5*L^2 ; \\ 2*m2*L^2+2*m4*L^2+2*m5*L^2+2*m3*L^2+2*m1*eta^2+2*I1 & , & m2*L^2+2*m4*L^2+2*m5*L^2+2*m3*L^2 & , & 2*m4*L^2+2*m5*L^2+m3*L^2 & , & 2*m5*L^2+m4*L^2 & , & m5*L^2 \end{bmatrix}$$

$$\mathbf{C1} = \begin{bmatrix} 0 & , & 0 & , & 0 & , & 4*cb & , & -4*cb ; \\ 0 & , & 0 & , & -4*cb & , & 8*cb & , & -4*cb ; \\ 0 & , & -4*cb & , & 8*cb & , & -4*cb & , & 0 ; \\ -4*cb & , & 8*cb & , & -4*cb & , & 0 & , & 0 ; \\ 2*cb+2*cg & , & -2*cb & , & 0 & , & 0 & , & 0 \end{bmatrix}$$

$$\mathbf{K1} = \begin{bmatrix} 0 & , & 0 & , & 0 & , & 4*kb & , & -4*kb ; \\ 0 & , & 0 & , & -4*kb & , & 8*kb & , & -4*kb ; \\ 0 & , & -4*kb & , & 8*kb & , & -4*kb & , & 0 ; \\ -4*kb & , & 8*kb & , & -4*kb & , & 0 & , & 0 ; \\ 2*kd*Yta^2+2*kb & , & -2*kb & , & 0 & , & 0 & , & 0 \end{bmatrix}$$

$$\mathbf{I1} = \begin{bmatrix} 0 & , & 2*L*m5*Rg & , & 0 & ; \\ 0 & , & -2*L*Rg*(m4+2*m5) & , & 0 & ; \\ 0 & , & -2*L*Rg*(m3+2*m4+2*m5) & , & 0 & ; \\ 0 & , & -2*L*Rg*(m2+2*m3+2*m4+2*m5) & , & 0 & ; \\ 2*kd*Yta & , & -2*(m2*Rg*L+m3*Rg*L+m4*Rg*L+m5*Rg*L-Ig-eta*m1*Rg) & , & 2*cg & \end{bmatrix}$$

In state-space form;

$$\begin{aligned}\dot{x} &= Ax + Bu \\ y &= Cx + Du\end{aligned}\tag{3.24}$$

where

$$\begin{aligned}A &= \begin{bmatrix} \{0\}_{5 \times 5} & \{I\}_{5 \times 5} \\ -\{M_1\}^{-1}\{K_1\} & -\{M_1\}^{-1}\{C_1\} \end{bmatrix} \\ B &= \begin{bmatrix} \{0\} \\ -\{M_1\}^{-1}\{I_1\} \end{bmatrix} \\ C &= [\{I\}_{10 \times 10}] \\ D &= [\{0\}_{10 \times 3}]\end{aligned}\tag{3.25}$$

System parameters are inserted into the parametric equations for modeling. These parameters are roughly obtained from various battle tanks and are subject to change.

```
m1=2500;    Mass of Gun Part 1 (kg) (Includes Gun Breech)
m2=125;    Mass of Gun Part 2 (kg)
m3=150;    Mass of Gun Part 3 (kg)
m4=125;    Mass of Gun Part 4 (kg)
m5=100;    Mass of Gun Part 5 (kg) (This is the Gun Muzzle)
L=1;      Length of each gun part except Part 1 (m)
eta=0.5;   Trunnion to CG of Gun Part 1 (m)
I1=1000;   Inertia of Gun Part 1 (kg.m^2)
I2=9.5;    Inertia of Gun Part 2 (kg.m^2)
I3=9.5;    Inertia of Gun Part 3 (kg.m^2)
I4=9.5;    Inertia of Gun Part 4 (kg.m^2)
I5=9.5;    Inertia of Gun Part 5 (kg.m^2)
Ig=7000;   Total Inertia of Gun (kg.m^2)
cd=10;     Drive viscous friction (N*m*s/rad)
cg=9e4;    Trunnion viscous friction (N*m*s/rad)
ctg=1e4;   Turret to gun(m1) viscous friction (N*m*s/rad)
kd=5.3e6;  Drive stiffness (N*m/rad)
cb=2e3;    Gun parts joint viscous friction (N*m*s/rad) (Between m1,m2,m3,m4,m5)
kb=4e6;    Gun parts joint stiffnesses (N*m/rad) (Between m1,m2,m3,m4,m5)
Rg=0.9;    Turret rotation center to Turret-Gun_m1 (trunnion) Joint Distance
Yta=0.5;   Trunnion to elevation drive distance (m)
```

For this data set, a Matlab® ® m-file is written to calculate the natural frequencies and unit step response. Complete code of this m-file is in Appendix A4. Natural frequencies (in Hz) are calculated as follows;

```
natural_frequencies = [1/(2*pi)]*sqrt[eigenvalues[{M1}^-1 * {K1}]
```

Output of the m-file given in Appendix A4 is as follows;

```
naturalfrequencies_sorted =
```

```
2.1423  
10.3184  
34.1585  
93.0921  
170.3659
```


CHAPTER 4

DISTURBANCE MODELING

4.1 APG Course Definition

The APG (Aberdeen Proven Ground) course is composed of a certain number of bumps separated with certain distances in compliance with the NATO standards (Figure 2.6). Tank is driven through this standard course and the stabilization accuracy of the elevation axis is checked. In shooting accuracy tests, again this course is used. Tank fires to a stationary or moving target while passing through the APG course.

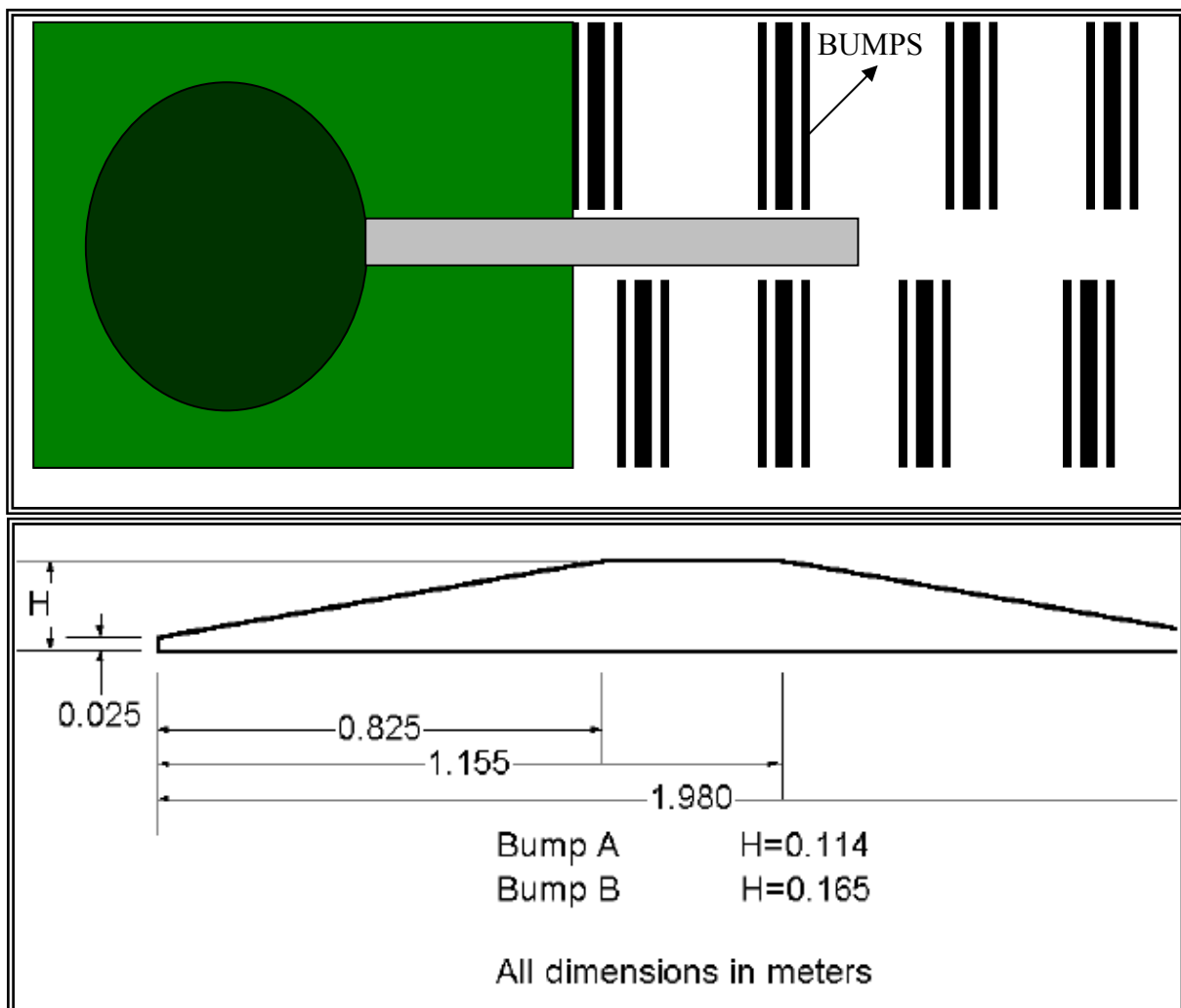


Figure 4.1. Tank Crossing an APG Course, Bump Dimensions

APG course creates disturbances mainly in hull body pitch and bounce directions. These are low frequency disturbances (0-5 Hz) due to bump geometry and the suspension response. Suspension pitch natural frequency is typically around 1.5 Hz depending on the suspension type. Conventional torsion bar type suspensions have these typical values, whereas active/semi active/passive in arm suspension unit (ISU) types has slightly lower values. Suspension design has another important effect in this course; if the suspension limits are reached either in re-bounce and jounce and the suspension hits the bumps, there arise a considerable amount of shock, which is an impulse to the stabilization system which is hard for the controller to regulate. Therefore any suspension design should take this into consideration as design criteria.

A wide vibration spectrum (0 - 300 Hz) due to track and tank engine disturbing the gun elevation stabilization exists and those require much regulation effort for any stabilization controller, especially when the typical gun stabilization bandwidths are around 10Hz (Figure 2.7).

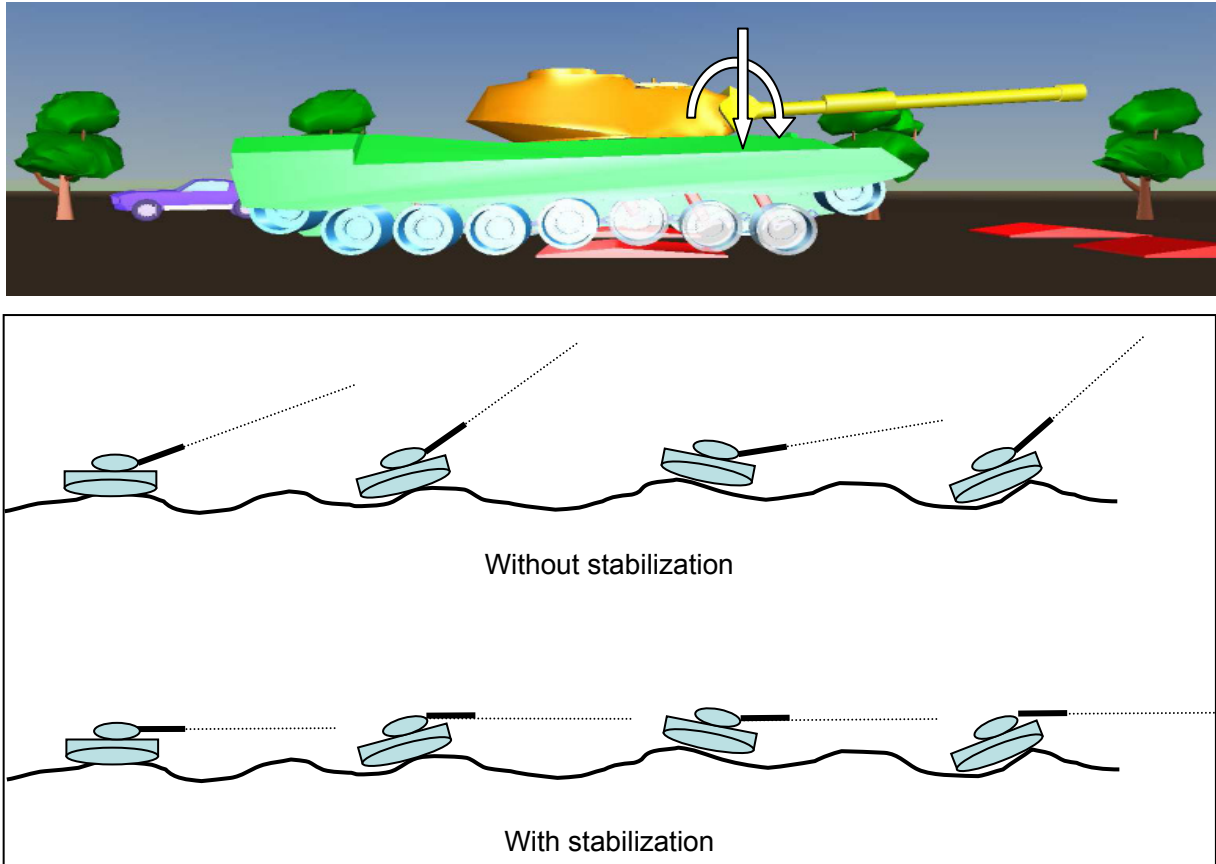


Figure 4.2. APG Course Disturbances in Gun Elevation

4.2 Sinuous Course Definition

The sinuous course is an eight-figured loop for the turret yaw stabilization test. High frequency disturbances mentioned for APG track still exist naturally in sinuous course, since the tank is on the move.

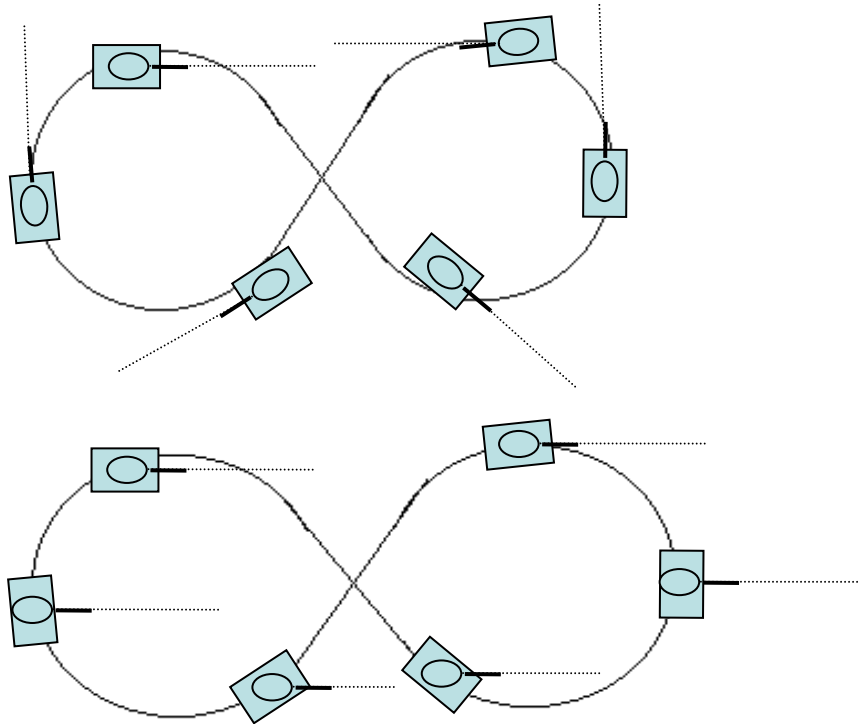


Figure 4.3. Sinuous Course Disturbances in Turret Yaw Axis

4.3 Other Disturbances

The remaining disturbance sources are due to the rotating components on tank, mainly the engine, transmission components and the vibration coming from the tracks due to ground interaction and the motion of the track elements. These disturbances have a wide spectrum.

4.4 Experimental Data

Instead of modeling a complex hull and suspension model, a set of experimentally measured disturbance data will be used. Disturbance data acquisition is made using feedforward gyros of an APG and sinuous course crossing Leopard1A1 tank. Data acquisition is made using a PC equipped with a "National Instruments 6035 DAQ board" and the sampling frequency is 500 Hz. This tank is originally an old design battle tank which has poor suspension characteristics. Therefore, compared to modern battle tanks like Leopard2, the acquired disturbances are significantly harsh. Considering this effect, any successful

stabilization controller design study using these data will be much effective for modern battle tanks.



Figure 4.4. A General View on Leopard1A1 Tank Data Acquisition Setup

During APG course test, tank has been brought to its maximum forward velocity 40 kph from stationary and then to a sudden stop. Therefore a very wide range of the high frequency disturbances created by engine and track vibration characteristics has been covered. Disturbances measured in elevation and azimuth axes during this course are plot in Figure 2.5 and Figure 2.6.

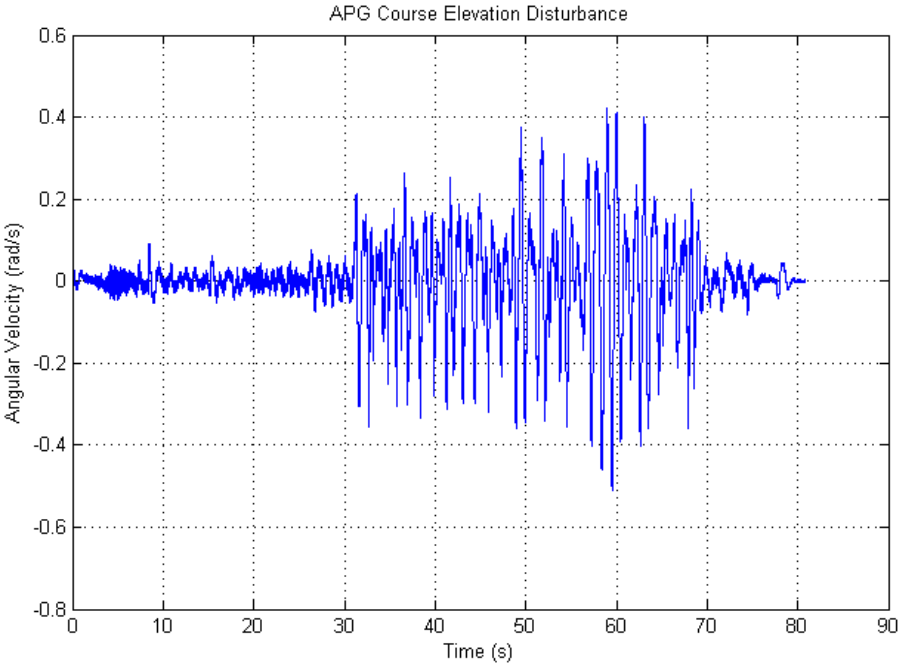


Figure 4.5. APG Course Elevation Disturbance

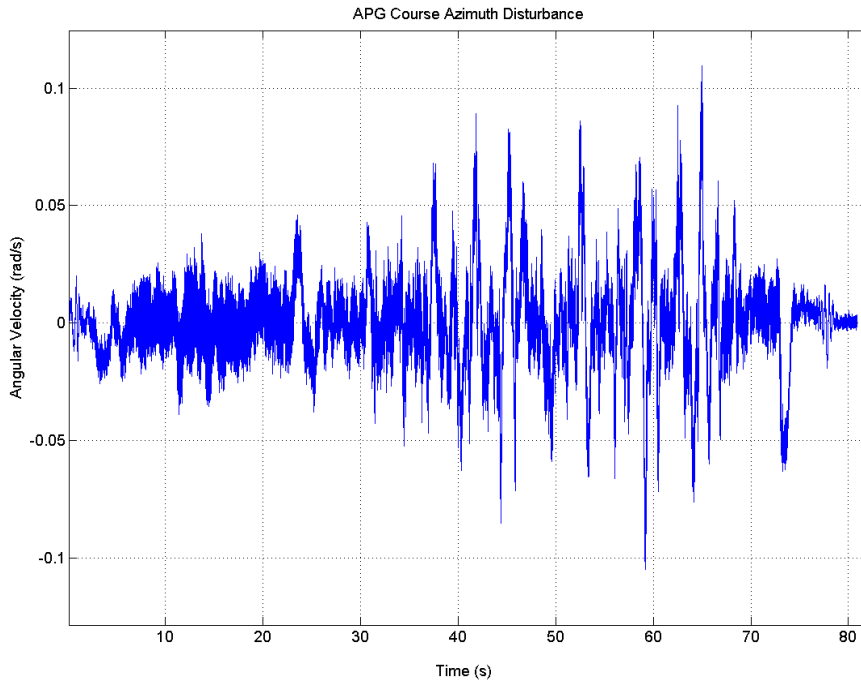


Figure 4.6. APG Course Azimuth Disturbance

Examining the time domain data, elevation disturbances are higher than the azimuth disturbances in terms of magnitude. From the start to the $t=31$ s, tank is approaching the bumps. Bump crossing is finished at $t=69$ s. Looking into the azimuth data, the effect of bump crossing is also apparent between $t=31$ to 69 s.

APG course data are further examined in frequency domain. To obtain the PSD (Power Spectral Density), Welch power spectral density estimation with Hamming window is used in MATLAB[®].

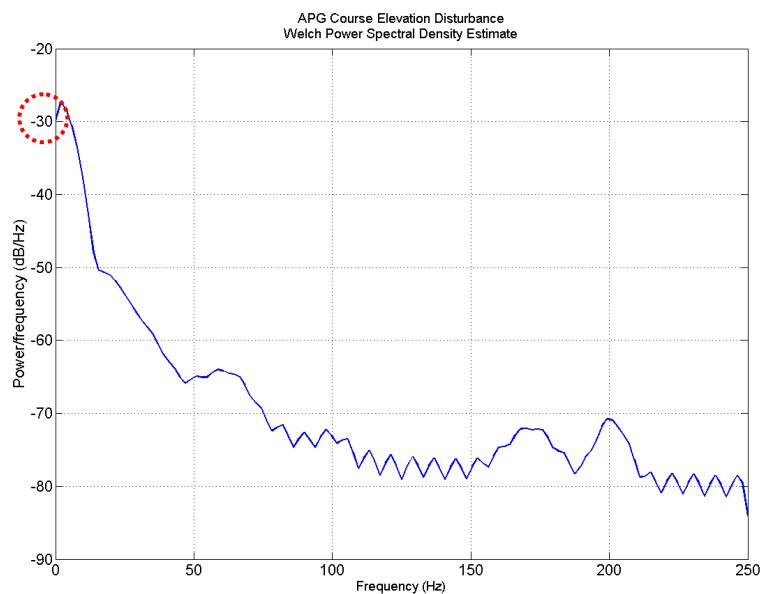


Figure 4.7. APG Course Elevation Disturbance PSD

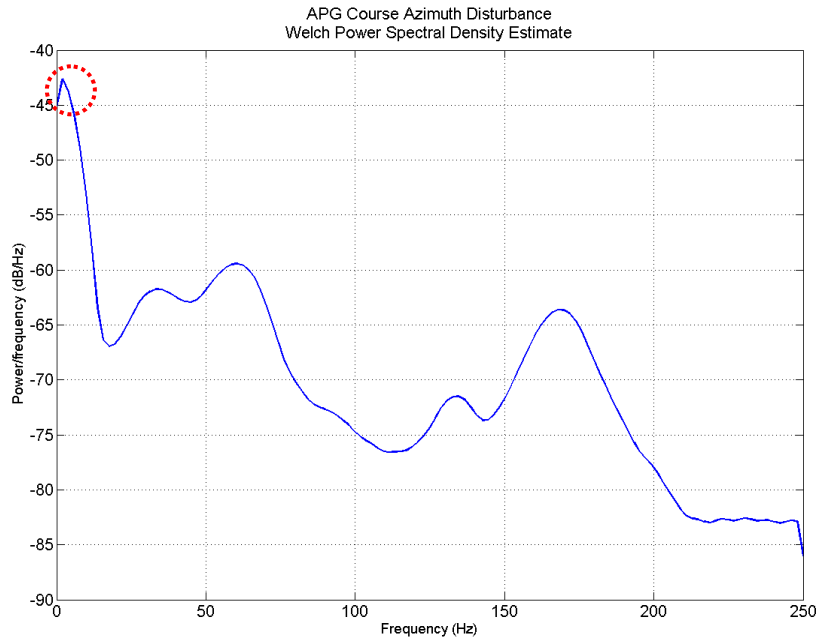


Figure 4.8. APG Course Azimuth Disturbance PSD

Examining the PSD's of the APG data, characteristics of hull suspension is apparent for both elevation and the azimuth (circled in with dotted line). Remaining are the high frequency disturbance characteristics.

During sinuous course test, data is started to be acquired when tank has been brought to its maximum forward velocity 40 kph and taking the eight curved course. Disturbances measured in elevation and azimuth axes during this course are plot in Figure 2.9 and Figure 2.10.

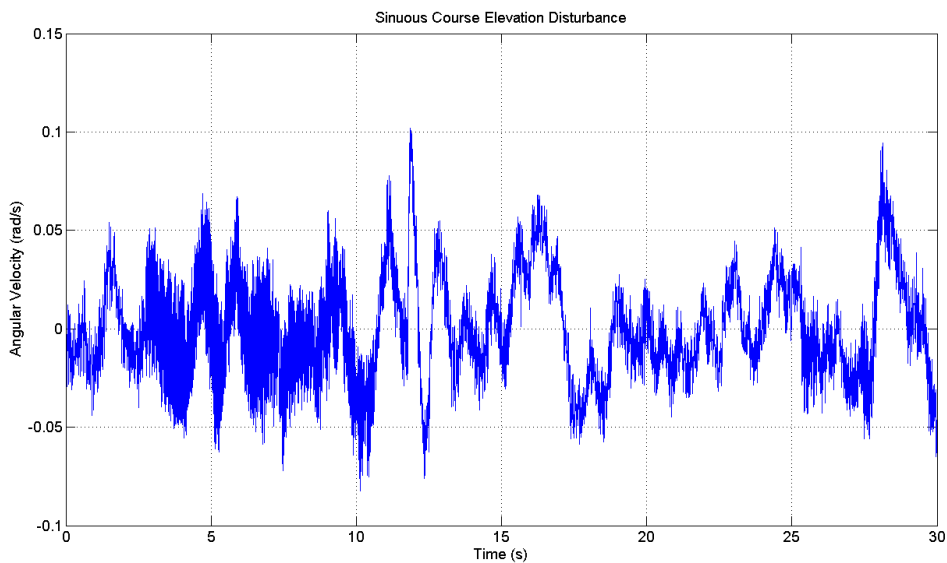


Figure 4.9. Sinuous Course Elevation Disturbance

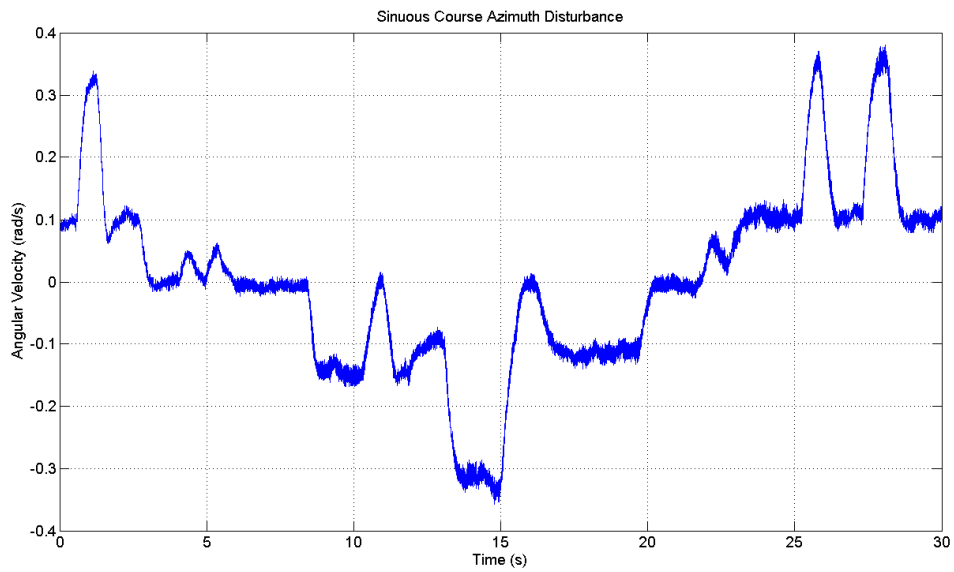


Figure 4.10. Sinuous Course Azimuth Disturbance

Examining the time domain data, azimuth disturbances are higher than the elevation disturbances in terms of magnitude. The effect of eight curved path can be seen clearly in the azimuth data (Figure 2.10).

Sinuous course data are further examined in frequency domain. To obtain the PSD (Power Spectral Density), Welch power spectral density estimation with Hamming window is used in MATLAB[®].

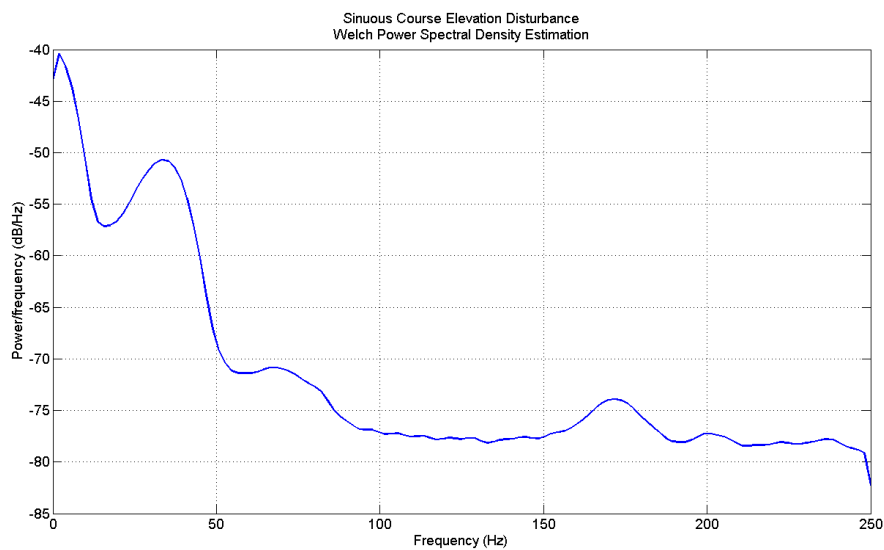


Figure 4.11. Sinuous Course Elevation Disturbance PSD

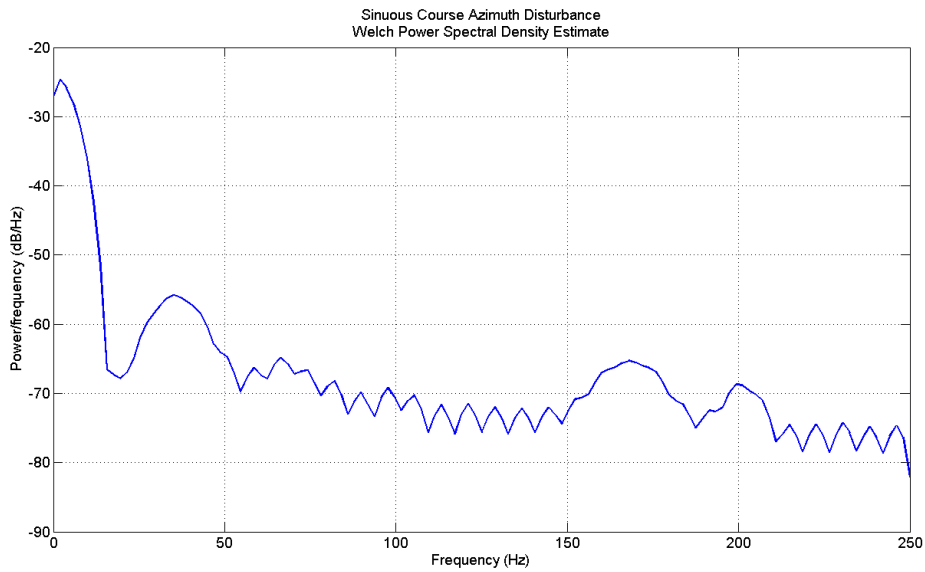


Figure 4.12. Sinuous Course Azimuth Disturbance PSD

4.5 Simulations

In this section, disturbance data will be given to the system model. All controller inputs will be zero. There will be no controller, so the disturbance rejection without controller will be observed. A Simulink model is prepared for the simulation. Response of the muzzle (m5) is plot for both axes.

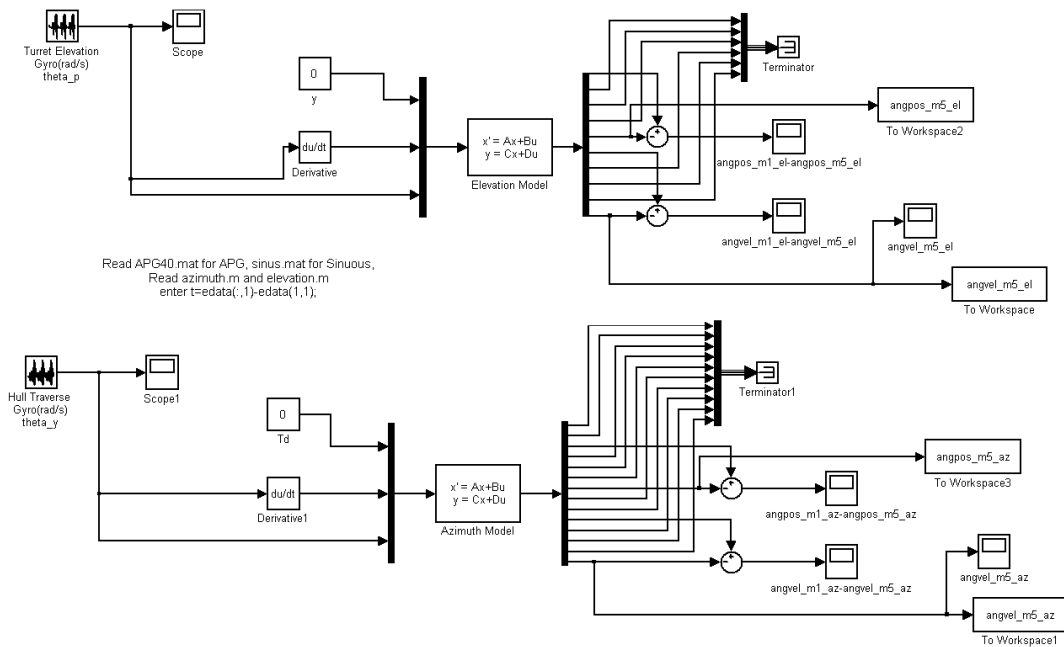


Figure 4.13. Simulink Model for Disturbance Response w/o Controller

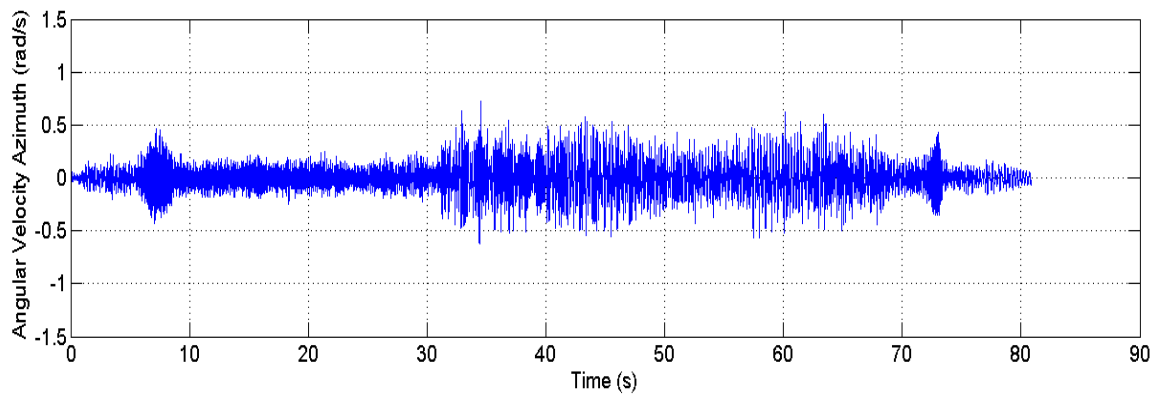
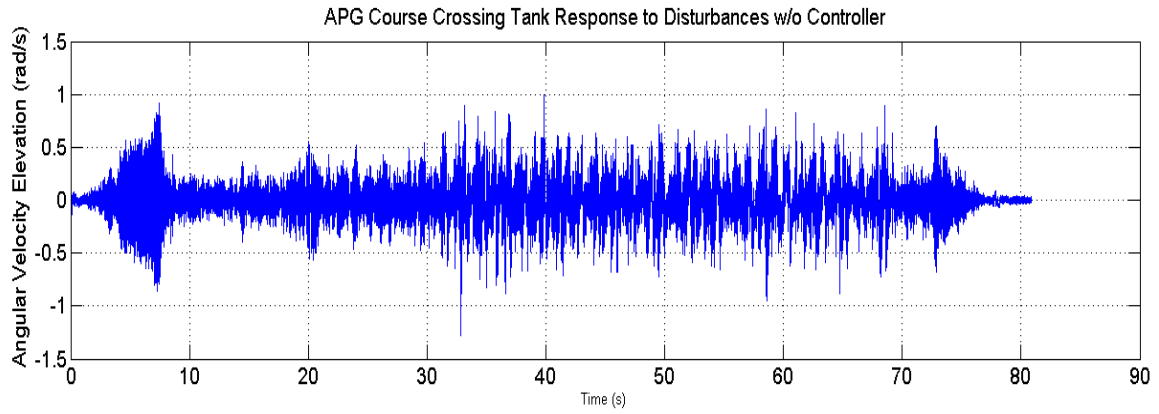


Figure 4.14. APG Response of the Muzzle w/o Controller

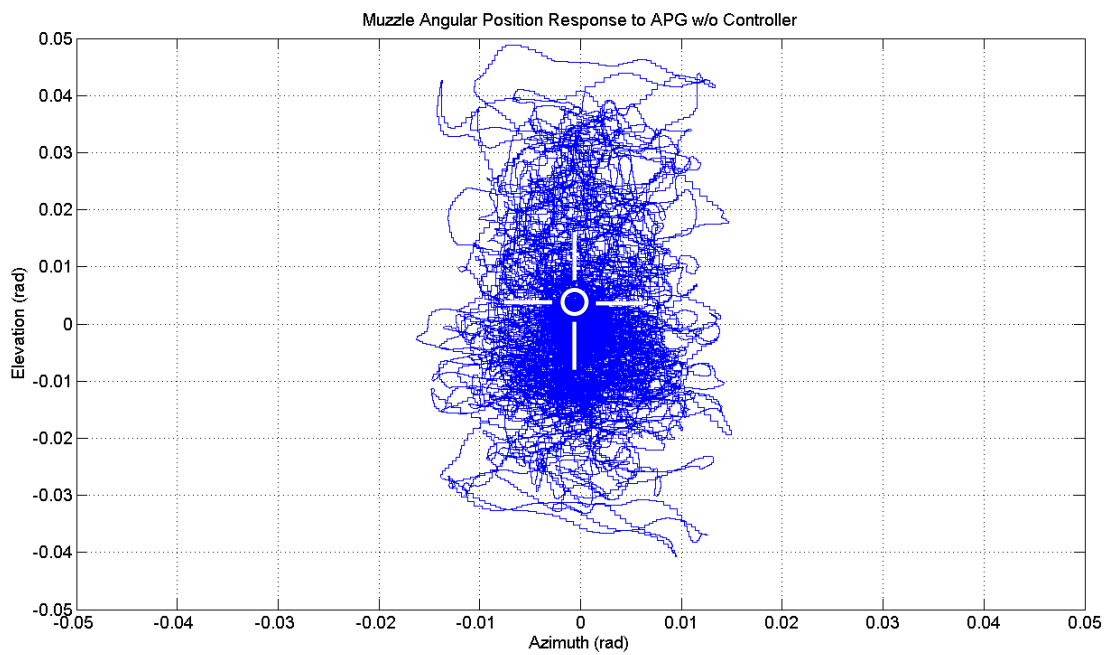


Figure 4.15. APG Angular Position Response of the Muzzle w/o Controller

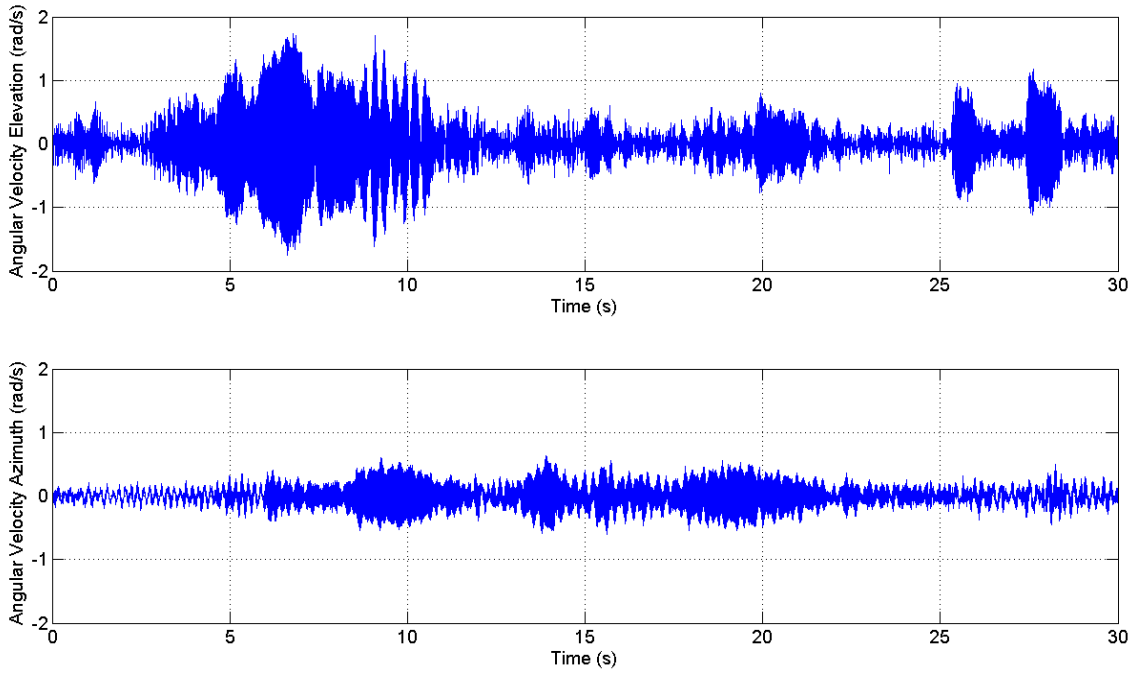


Figure 4.16. Sinuous Response of the Muzzle w/o Controller

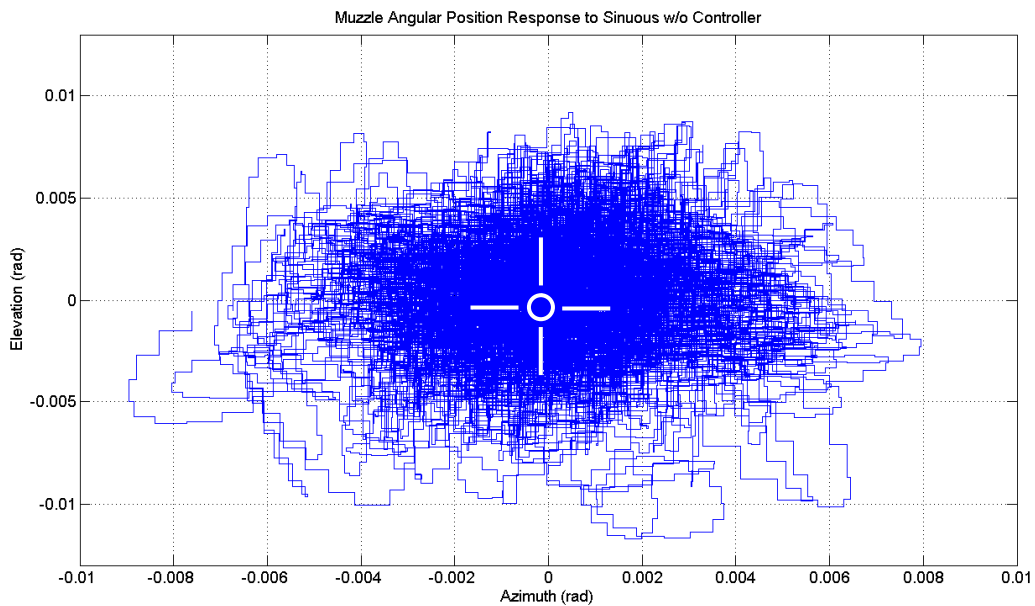


Figure 4.17. Sinuous Angular Position Response of the Muzzle w/o Controller

Further analysis will be made for the deflection between the gun trunnion (m1) and the gun muzzle (m5). This will emphasize the need for muzzle control instead of conventional rigid gun assumption trunnion stabilization. Difference between the position response of the muzzle (m5) and the trunnion (m1) will be plot for both APG and Sinuous course.

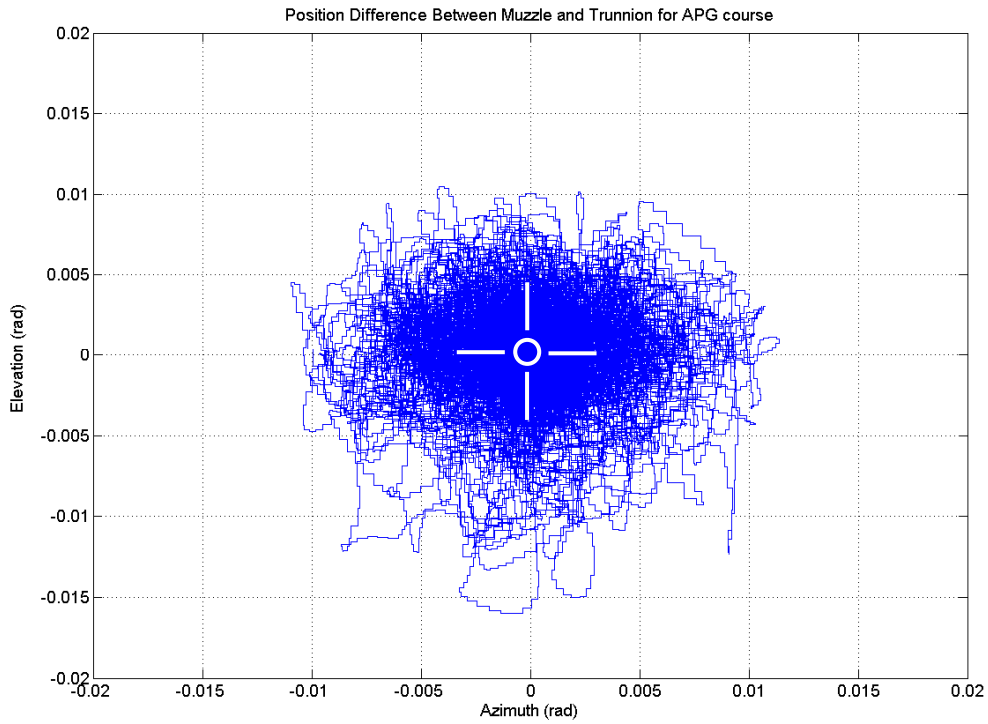


Figure 4.18. Position Difference Between Gun Muzzle and Trunnion for APG w/o Controller

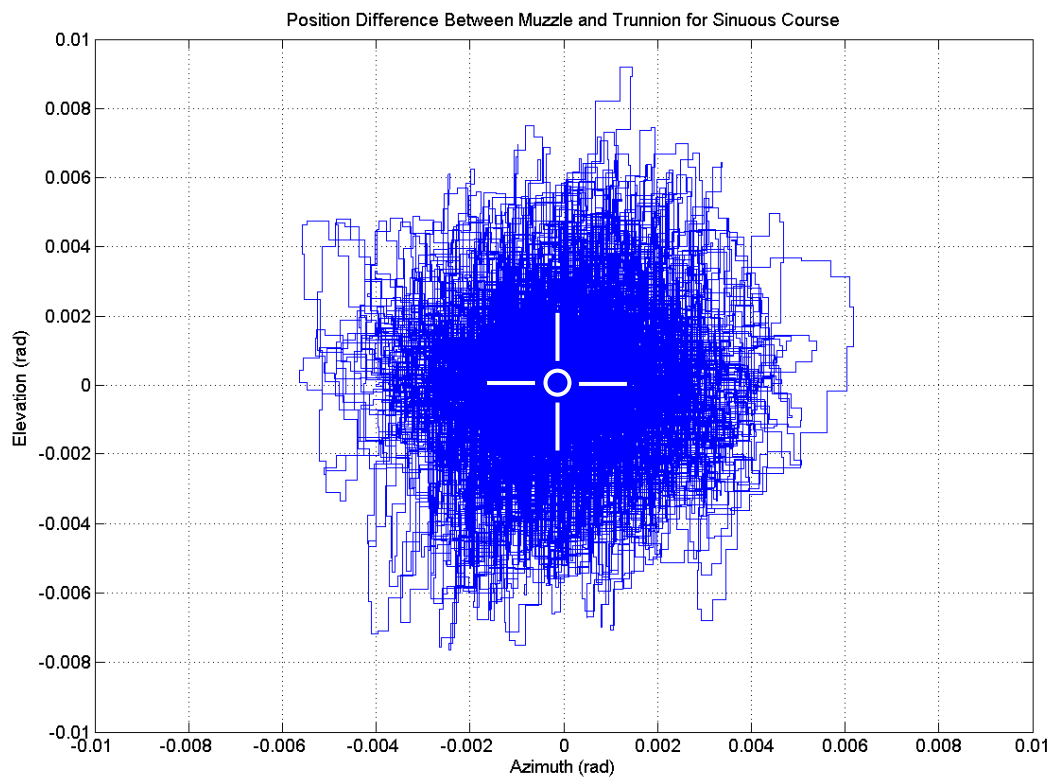


Figure 4.19. Position Difference Between Gun Muzzle and Trunnion for Sinuous w/o Controller

From Figure 2.18 and Figure 2.19, it can be seen that there is an appreciable amount of deflection between the gun muzzle and the trunnion. This deflection is a result of the gun flexibility.

CHAPTER 5

STABILIZATION CONTROLLER DESIGN

5.1 Elevation Controller Design

In this section, elevation controller schematics will be defined and a relevant controller will be developed using the 5-DOF state-space elevation model. The feedback controller will be designed by servo step response. The feedforward controller will be designed afterwards analyzing the disturbance rejectance characteristics. Aim and scope of this controller design effort will be kept at the level of a pre-determined stabilization performance and step response criteria satisfaction. The controller satisfying those criteria will be accepted and no further optimization will be studied. Aim of this thesis is to study mainly the effects of the flexibilities between the muzzle and the trunnion. At every step, the muzzle deviation will be monitored with respect to the trunnion where the feedback gyro is positioned.

5.1.1 Elevation Feedback Controller Design

5-DOF state-space elevation model is driven by a step input having 10 deg/s amplitude and the disturbance inputs are set to zero (Figure 5.1). Trunnion angular velocity output of the model is monitored as the response. This output is then filtered with the gyro transfer function and fed back into a dual PI controller (Figure 5.2). The gyro transfer function is obtained from the vendor of a dynamically tuned rate gyro, being used in similar fire control systems.

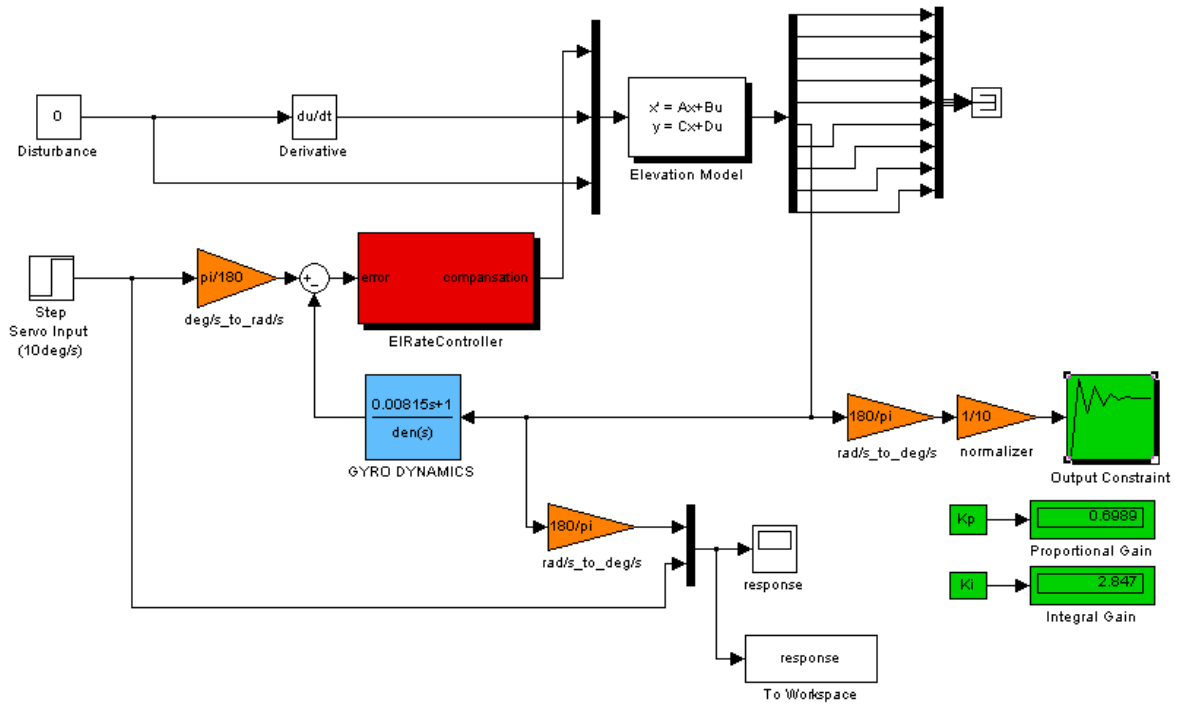


Figure 5.1 Simulink Model for Elevation Feedback Controller Design

Using a dual PI control scheme provides better disturbance characteristics especially in the low frequency region. PID scheme is not used since the derivative term has significant noise amplifying effects.

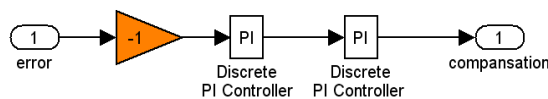


Figure 5.2 Dual PI Controller

PI controller gains (K_p , K_i) are entered as parametric variables into the controller model, and the “Simulink Response Optimization Toolbox” is used to obtain the values satisfying the desired response of the system to the step input. An “Output Constraint” block is used to limit the response in time domain (Figure 5.3).

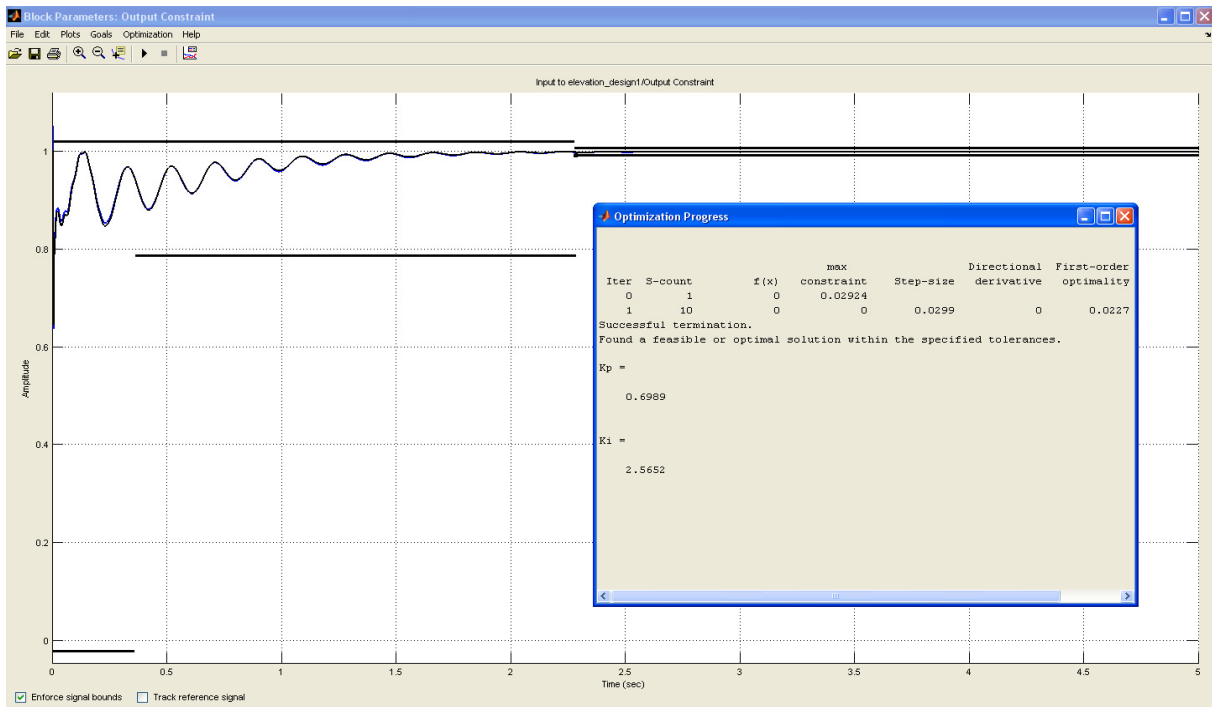


Figure 5.3 Output Constraints and Response Optimization

In tank control systems, servo response is required to have a very low level of overshoot to the step input. Therefore the overshoot constraint is set to 2%. Settling time is set to 2 seconds. When the optimization procedure is run, the proportional and the integral gains satisfying the response constraints are obtained as; $K_p = 0.6989$ and $K_i = 2.5652$. Rounding off to single significant digit after zero, the gains are used having values of “ $K_p = 0.7$ ” and “ $K_i = 2.6$ ”. Response to the step input is then simulated in the main model with these parameters (Figure 5.4).

Before designing the feedforward controller, the disturbance data will be entered into the model and the stabilization performance will be measured. Normally, the way of measuring the stabilization performance is done by integrating the gyro output once to have the inertial position and measure the RMS value in a time period. But the position output is already in hand from the state-space model. Therefore, the trunnion position is entered into a discrete RMS model and the simulation is run (Figure 5.5).

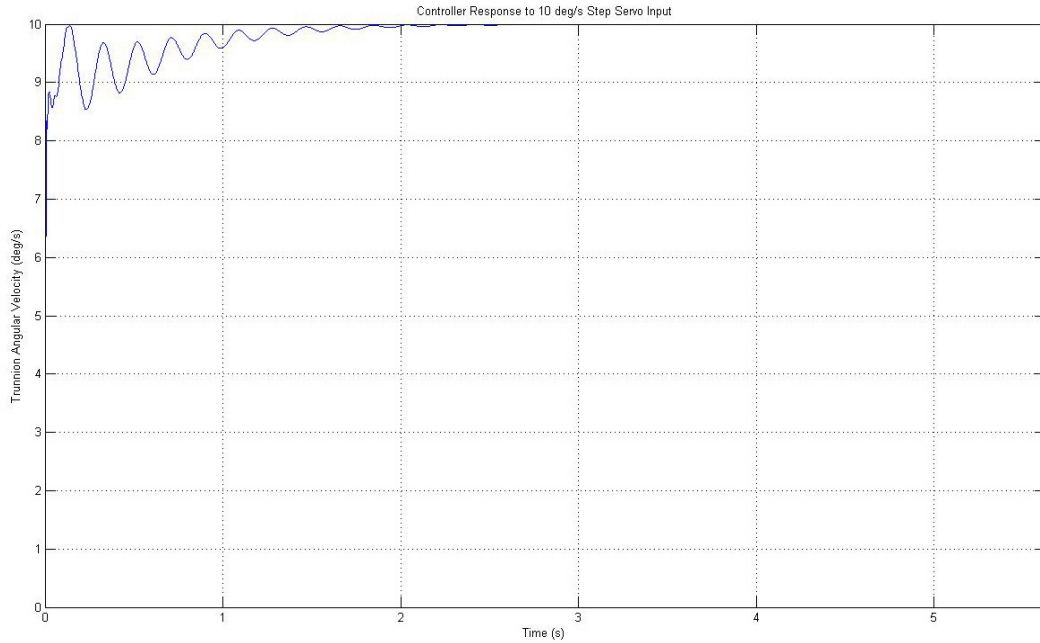


Figure 5.4 Elevation Feedback Controller Step Response with the Optimized Gains

At the same time, the muzzle deviation from the trunnion is monitored by taking the RMS value of the inertial position difference between the muzzle and the trunnion, and also the RMS value of muzzle inertial position (muzzle stabilization accuracy) is monitored.

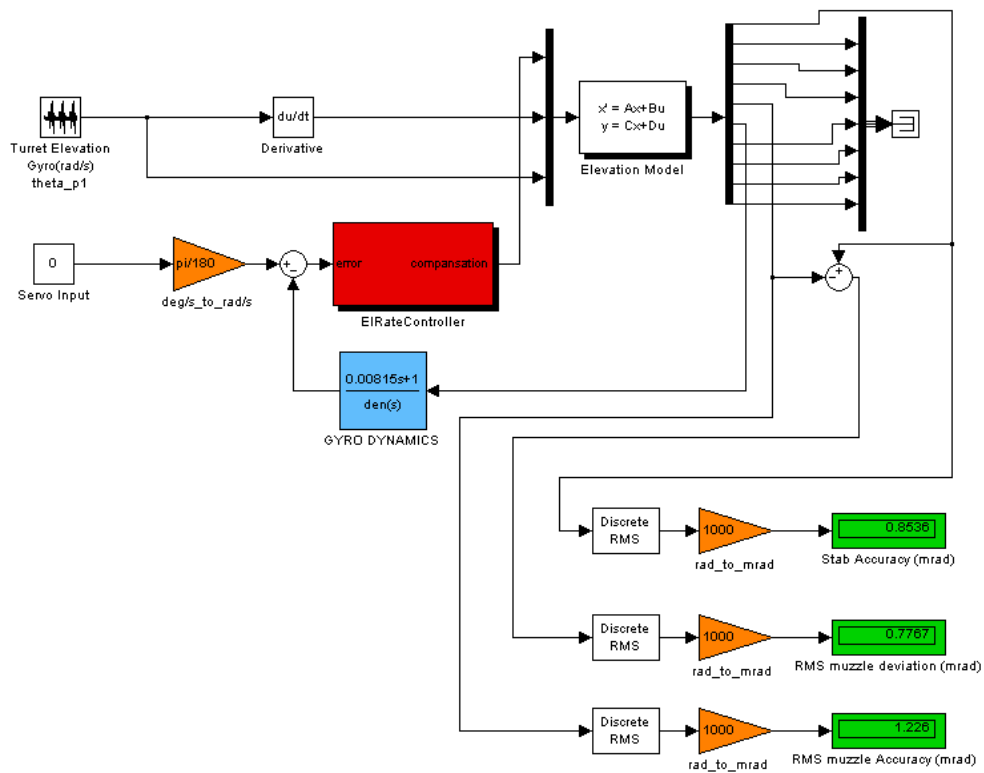


Figure 5.5 Elevation Feedback Controller Stabilization Performance and Muzzle Deviation

Simulation has given the stabilization accuracy as 0.854 mrad, RMS muzzle deviation as 0.777 mrad and RMS muzzle stabilization accuracy of 1.226 mrad. This means that, if the fire control system would measure the stabilization error signal (from the trunnion gyro like in every existing fire control systems) and allow firing at a certain coincidence window by comparing the absolute value of the error signal with the limits of the window (typically 0.5 mrad, meaning the absolute value of the error signal is less than 0.5 mrad) the real line of fire would not be within the coincidence window because of the muzzle deviation.

It is not practical to install any feedback device to the gun muzzle because of the extreme shocks during gun fire. But the muzzle deviation can be calculated using the state-space model and this signal can be used for the coincidence during fire.

It is also impractical to try to stabilize the muzzle itself by using the model, since this time the trunnion would be in the wrong inertial position. When the gunner's sight is slaved to the gun either mechanically or electronically, the extra error in the trunnion would be added to the sight inertial angular position and line of sight stabilization accuracy would get worse.

5.1.2 Elevation Feedforward Controller Design

In this part, a feedforward controller is to be developed and the stabilization accuracies will be compared to the feedback controller only case. First, the feedforward controller is to be reviewed in general.

Effect of the disturbance on the output of the controller system can be reduced by measuring this disturbance and using a feedforward controller. the feed forward transfer function, G_{ff} , should be the inversion of the ratio of the disturbance transfer function and the nominal plant transfer function. It should be remembered that the G_{ff} must be stable since it acts in open loop (Figure5.6) [5].

$$G_{ff} = -\frac{G_d}{G_u} \tag{5.1}$$

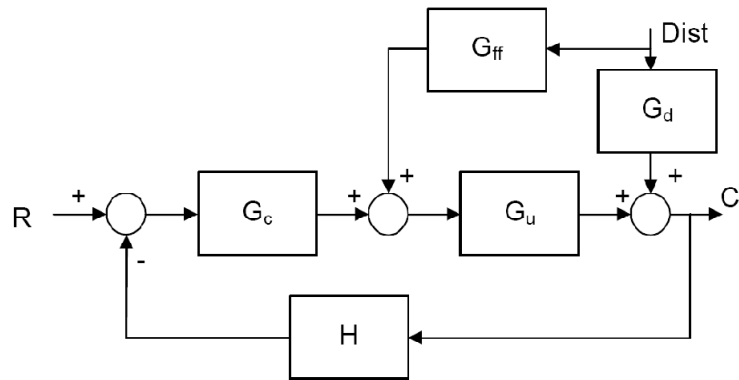


Figure 5.6 Feedback System with Disturbance Feedforward

R: Reference signal

G_c : Feedback controller

G_{ff} : Feedforward controller

G_u : Plant

G_d : Disturbance transfer function

H : Feedback gyro transfer function

To form G_{ff} , first G_d and G_u are to be obtained from the relevant input/output channels of the state-space elevation model. G_u is the transfer function of the model between the first input and the sixth output. G_d is the sum of the transfer functions of the model between the second and third input and the sixth output. The sixth output is the trunnion elevation angular velocity, where the feedback gyro is mounted. First input is the servo reference signal input, and the second and third inputs are the disturbances in elevation.

Following Matlab® commands are entered to obtain G_{ff} ;

```
[NUM1, DEN]=ss2tf(Ae1, Be1, Ce1, De1, 1);
Gu=tf(NUM1(6, :), DEN);
[NUM2, DEN]=ss2tf(Ae1, Be1, Ce1, De1, 2);
[NUM3, DEN]=ss2tf(Ae1, Be1, Ce1, De1, 3);
DER = tf([1 0], 1);
Gd1= DER * tf(NUM2(6, :), DEN);
```

```
f=logspace(-1,2.5,5000);
w=2*pi*f;

Gd2= tf(NUM3(6,:),DEN);
Gd = Gd1 + Gd2;
Gff = -Gd/Gu
bodemag(Gff,w); % Figure 5.7
grid;
```

Matlab[®] output for Gff;

```
-4.877 s30 - 1.178e004 s29 - 3.398e007 s28 - 4.967e010 s27 - 7.645e013 s26 - 7.593e016 s25 - 7.763e019 s24
- 5.474e022 s23 - 4.004e025 s22 - 2.03e028 s21 - 1.092e031 s20 - 3.937e033 s19 - 1.565e036 s18
- 3.915e038 s17 - 1.143e041 s16 - 2.014e043 s15 - 4.233e045 s14 - 5.231e047 s13 - 7.442e049 s12
- 6.2e051 s11 - 5.133e053 s10 - 2.695e055 s9 - 1.338e057 s8 - 4.345e058 s7 - 1.295e060 s6
- 2.723e061 s5 - 4.434e062 s4 - 5.067e063 s3 - 3.845e064 s2 - 1.767e065 s - 1.75e054

-----

1597 s29 + 3.84e006 s28 + 1.109e010 s27 + 1.616e013 s26 + 2.489e016 s25 + 2.464e019 s24 + 2.522e022 s23
+ 1.771e025 s22 + 1.297e028 s21 + 6.538e030 s20 + 3.525e033 s19 + 1.26e036 s18 + 5.028e038 s17
+ 1.24e041 s16 + 3.652e043 s15 + 6.29e045 s14 + 1.341e048 s13 + 1.6e050 s12 + 2.321e052 s11
+ 1.831e054 s10 + 1.541e056 s9 + 7.52e057 s8 + 3.822e059 s7 + 1.107e061 s6 + 3.442e062 s5
+ 5.93e063 s4 + 9.329e064 s3 + 7.379e065 s2 + 5.202e066 s + 6.981e053
```

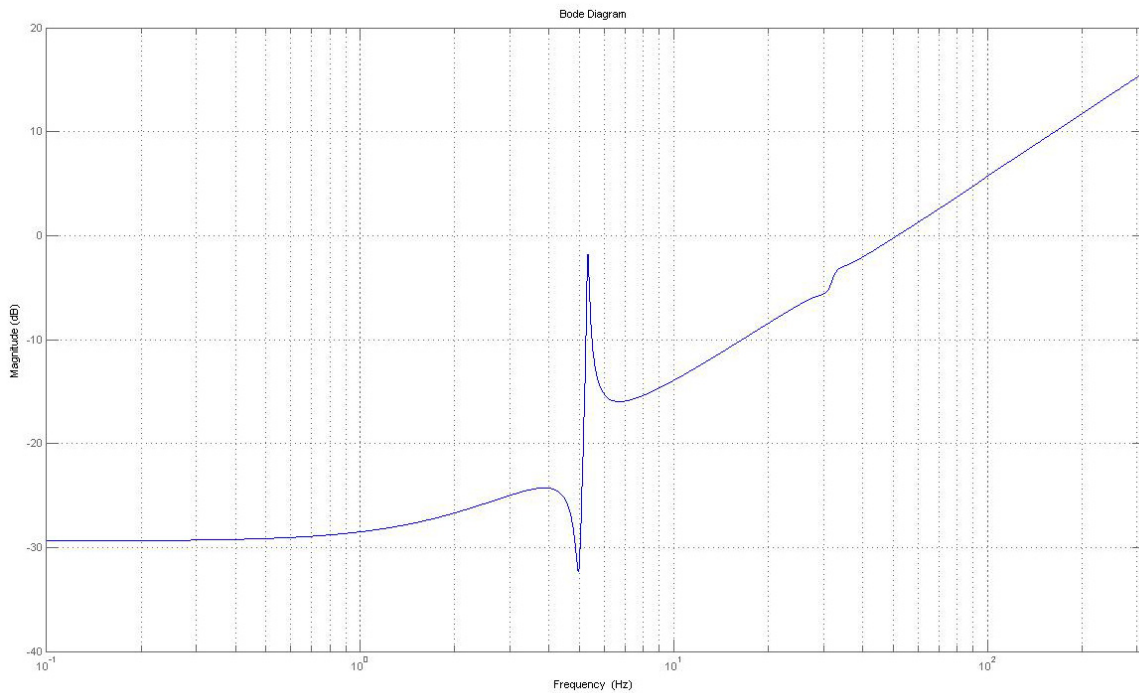


Figure 5.7 Bode Plot of Improper Gff

The ideal feedforward controller is an improper transfer function since the order of the numerator is greater than the denominator. The differentiator effect must be removed at high frequencies and the transfer function must be made proper. This can be achieved by implementing a low pass filter. A single order low pass filter with a cut-off frequency of 15 Hz has been used. It has been assumed that the angular rate of the hull is measured by a rate gyro with the same dynamic characteristics as the one for the inner-loop rate control [3].

Entering following Matlab® commands;

```
LP = tf([2*pi*15] , [1 2*pi*15]);
Gff2 = Gff * LP
bodemag(Gff2,w);
grid;
```

Matlab® commands outputs a proper feedforward controller Gff2 as follows;

```
-459.6 s^30 - 1.11e006 s^29 - 3.203e009 s^28 - 4.681e012 s^27 - 7.205e015 s^26 - 7.156e018 s^25 - 7.317e021 s^24
- 5.159e024 s^23 - 3.773e027 s^22 - 1.913e030 s^21 - 1.029e033 s^20 - 3.71e035 s^19 - 1.475e038 s^18
- 3.69e040 s^17 - 1.077e043 s^16 - 1.898e045 s^15 - 3.99e047 s^14 - 4.93e049 s^13 - 7.014e051 s^12
- 5.844e053 s^11 - 4.838e055 s^10 - 2.54e057 s^9 - 1.261e059 s^8 - 4.095e060 s^7 - 1.22e062 s^6
- 2.566e063 s^5 - 4.179e064 s^4 - 4.776e065 s^3 - 3.624e066 s^2 - 1.665e067 s - 1.649e056

-----
1597 s^30 + 3.99e006 s^29 + 1.145e010 s^28 + 1.721e013 s^27 + 2.641e016 s^26 + 2.699e019 s^25 + 2.754e022 s^24
+ 2.008e025 s^23 + 1.464e028 s^22 + 7.76e030 s^21 + 4.141e033 s^20 + 1.592e036 s^19 + 6.215e038 s^18
+ 1.714e041 s^17 + 4.821e043 s^16 + 9.732e045 s^15 + 1.934e048 s^14 + 2.864e050 s^13 + 3.829e052 s^12
+ 4.019e054 s^11 + 3.267e056 s^10 + 2.205e058 s^9 + 1.091e060 s^8 + 4.71e061 s^7 + 1.388e063 s^6
+ 3.837e064 s^5 + 6.522e065 s^4 + 9.53e066 s^3 + 7.474e067 s^2 + 4.903e068 s + 6.579e055
```

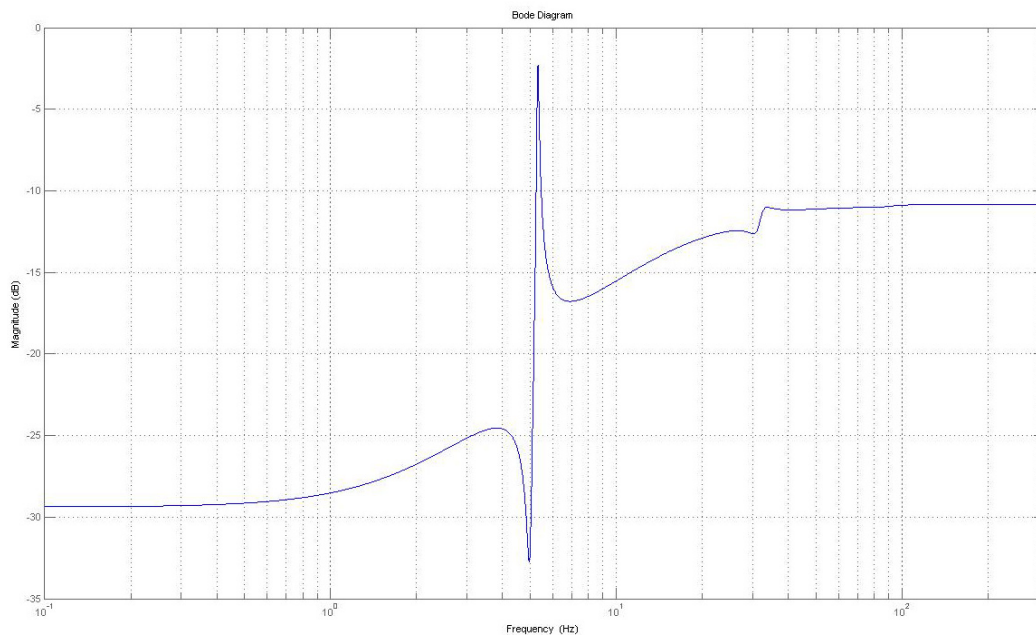


Figure 5.8 Bode Plot of Gff2, LP Filter is Added to Gff

The modified feedforward transfer function Gff2 needs to be further analyzed in terms of stability. Besides, since the order is quite high, some effort is necessary to reduce the order. For this purpose, “Hankel Singular Value Decomposition Method” is used. Matlab® contains a function set for hankel singular value decomposition analysis; “hsvd”.

This function computes the Hankel singular values hsv of the LTI models. In state coordinates that equalize the input-to-state and state-to-output energy transfers, the Hankel singular values measure the contribution of each state to the input/output behavior. Hankel singular values are to model order what singular values are to matrix rank. In particular, small Hankel singular values signal states that can be discarded to simplify the model (balred function is used). For models with unstable poles, hsvd only computes the Hankel singular values of the stable part and entries of hsv corresponding to unstable modes are set to Inf [9].

Entering following Matlab® command, the hankel singular value decomposition figure is obtained (Figure 5.9);

```
hsvd(Gff2);
```

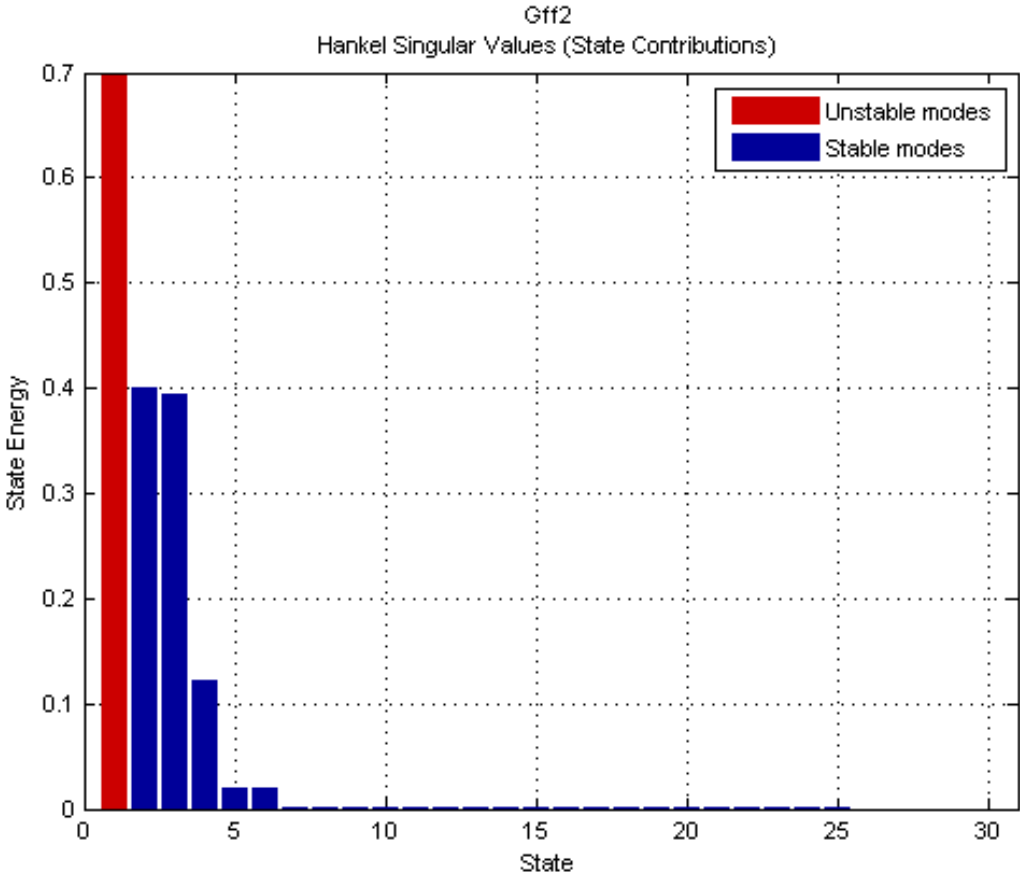


Figure 5.9 HSVD Plot for Gff2

From Figure 5.9, it is observed that feedforward transfer function Gff2 has one unstable mode out of its 30 modes. This unstable mode needs to be extracted. For this purpose, “stabsep” function of Matlab® is used.

`[GS,GNS]=stabsep` decomposes the LTI model into its stable and unstable parts

$$G = GS + GNS \quad (5.2)$$

Where GS contains all stable modes that can be separated from the unstable modes in a numerically stable way, and GNS contains the remaining modes. GNS is always strictly proper.

`[G1,GNS] = stabsep(G, 'abstol',ATOL,'reltol',RTOL)`

Specifies absolute and relative error tolerances for the stable/unstable decomposition. The frequency responses of G and GS + GNS should differ by no more than ATOL+RTOL*abs(G). Increasing these tolerances helps separate nearby stable and unstable modes at the expense of accuracy. The default values are ATOL=0 and RTOL=1e-8.

`[G1,G2]=stabsep(G, ..., 'Mode', MODE, 'Offset', ALPHA)`

Above command produces a more general stable/unstable decomposition where G1 includes all separable poles lying in the regions defined using offset ALPHA. This can be useful when there are numerical accuracy issues. For example, if you have a pair of poles close to, but slightly to the left of, the jw-axis, you can decide not to include them in the stable part of the decomposition if numerical considerations lead you to believe that the poles may be in fact unstable [9].

Entering following Matlab® commands, the unstable mode of Gff2 is extracted and the modified hankel singular value decomposition figure is obtained (Figure 5.10);

```
[Gff2s,Gff2ns]=stabsep(Gff2, 'AbsTol', 1e-5, 'Offset', 0.001);
hsvd(Gff2s);
Gff2s
```

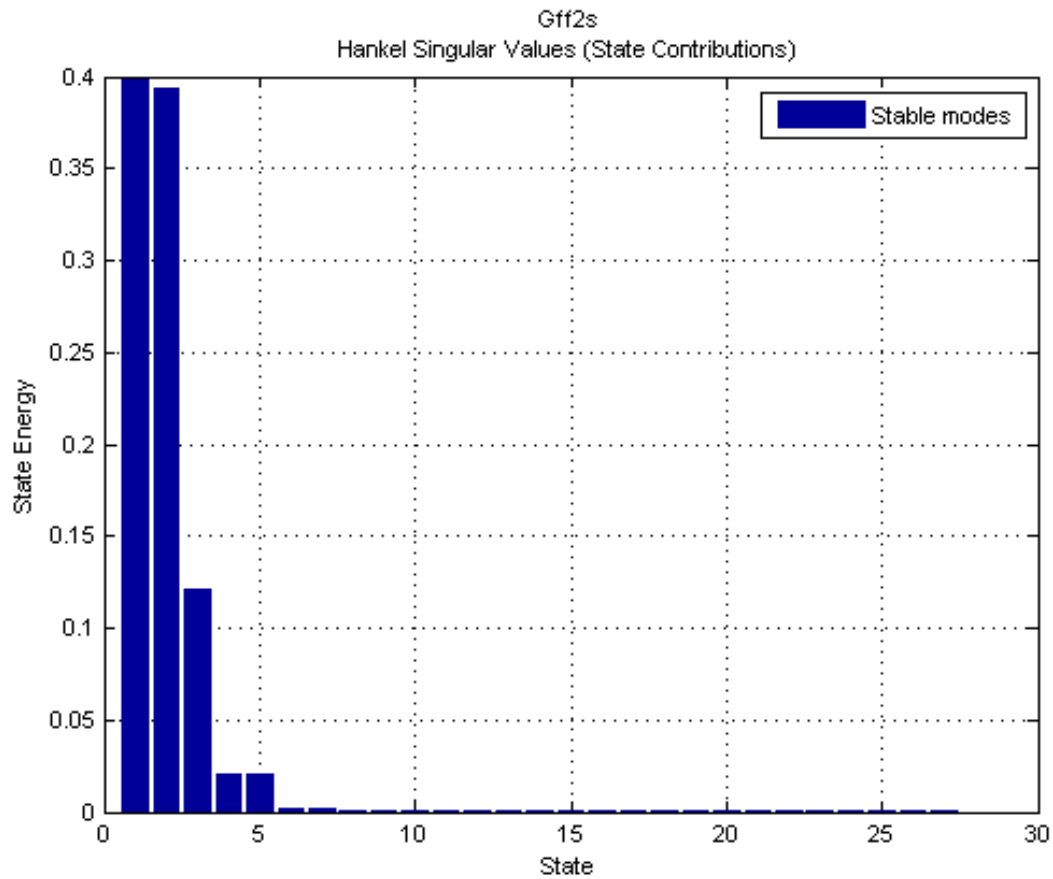


Figure 5.10 HSVD Plot for Gff2s (Stable Part of Gff2)

$$\begin{aligned}
 & -0.2879 s^{29} - 695.1 s^{28} - 2.006e006 s^{27} - 2.932e009 s^{26} - 4.512e012 s^{25} - 4.482e015 s^{24} - 4.583e018 s^{23} \\
 & - 3.231e021 s^{22} - 2.363e024 s^{21} - 1.198e027 s^{20} - 6.447e029 s^{19} - 2.324e032 s^{18} - 9.236e034 s^{17} - 2.311e037 s^{16} \\
 & - 6.746e039 s^{15} - 1.189e042 s^{14} - 2.499e044 s^{13} - 3.088e046 s^{12} - 4.393e048 s^{11} - 3.66e050 s^{10} - 3.03e052 s^9 \\
 & - 1.591e054 s^8 - 7.897e055 s^7 - 2.564e057 s^6 - 7.644e058 s^5 - 1.607e060 s^4 - 2.618e061 s^3 - 2.991e062 s^2 - 2.269e063 s \\
 & - 1.043e064 \\
 & \text{-----} \\
 & s^{29} + 2499 s^{28} + 7.174e006 s^{27} + 1.078e010 s^{26} + 1.654e013 s^{25} + 1.69e016 s^{24} + 1.725e019 s^{23} + 1.258e022 s^{22} \\
 & + 9.167e024 s^{21} + 4.86e027 s^{20} + 2.594e030 s^{19} + 9.97e032 s^{18} + 3.893e035 s^{17} + 1.074e038 s^{16} + 3.019e040 s^{15} \\
 & + 6.095e042 s^{14} + 1.211e045 s^{13} + 1.794e047 s^{12} + 2.398e049 s^{11} + 2.517e051 s^{10} + 2.046e053 s^9 + 1.381e055 s^8 \\
 & + 6.833e056 s^7 + 2.95e058 s^6 + 8.692e059 s^5 + 2.403e061 s^4 + 4.085e062 s^3 + 5.969e063 s^2 + 4.681e064 s + 3.07e065
 \end{aligned}$$

Feedforward controller Gff2s is implemented to the Simulink model as a LTI system block and the simulation is run as follows(Figure 5.11).

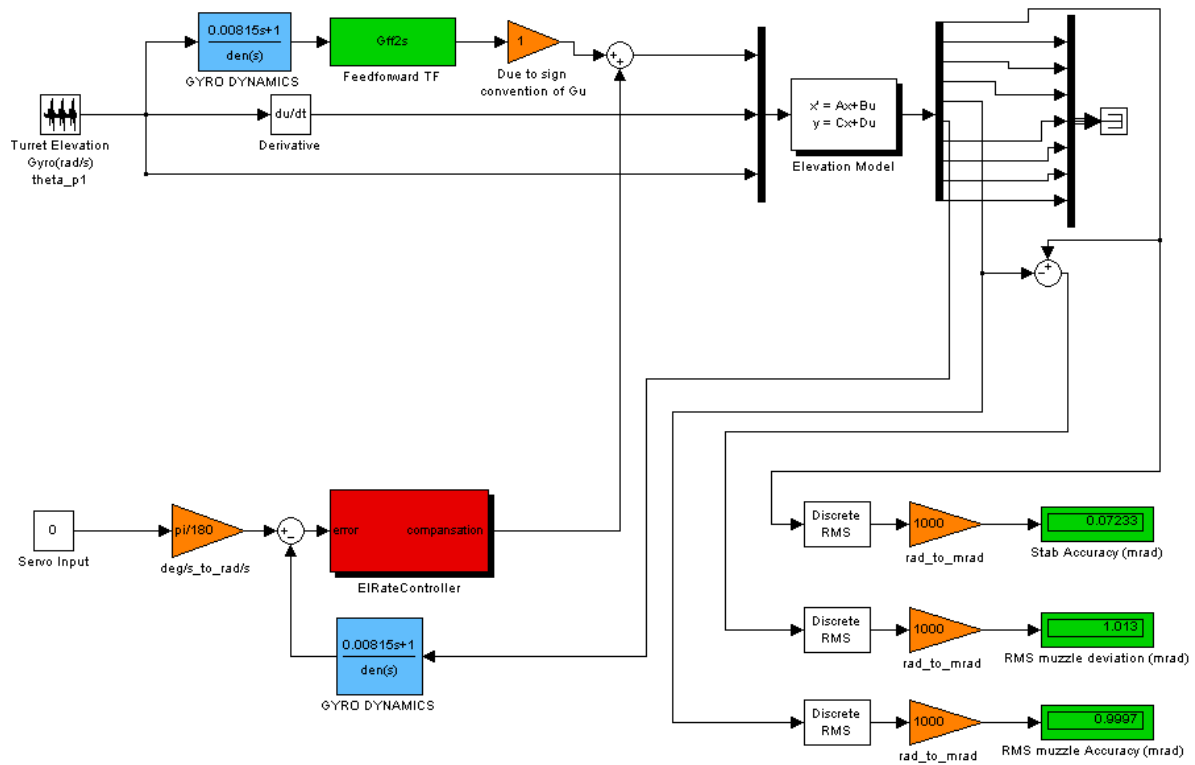


Figure 5.11 Feedforward Controller Simulation

Result is a significant improvement in the stabilization accuracy. Without feedforward controller, the stabilization accuracy was $860\mu\text{rad}$. When implemented, feedforward compensation reduced this value down to $72\mu\text{rad}$. This value is quite a super stabilization accuracy when compared to the general practical $500\mu\text{rad}$ requirement.

But it must be emphasized that no matter how good is the stabilization accuracy, muzzle deviation and muzzle stabilization accuracy values are at a level of $1000\mu\text{rad}$.

5.2 Azimuth Controller Design

In this section, azimuth controller schematics will be defined and a relevant controller will be developed using the 7-DOF state-space elevation model. The feedback controller will be designed by servo step response. The feedforward controller will be designed afterwards analyzing the disturbance rejectance characteristics. Aim and scope of this controller design effort will be kept at the level of a pre-determined stabilization performance and step response

criteria satisfaction. The controller satisfying those criteria will be accepted and no further optimization will be studied. Aim of this thesis is to study mainly the effects of the flexibilities between the muzzle and the trunnion. At every step, the muzzle deviation will be monitored with respect to the trunnion where the feedback gyro is positioned.

5.2.1 Azimuth Feedback Controller Design

7-DOF state-space azimuth model is driven by a step input having 10 deg/s amplitude and the disturbance inputs are set to zero (Figure 5.12). Trunnion angular velocity output of the model is monitored as the response. This output is then filtered with the gyro transfer function and fed back into a dual PI controller (Figure 5.13). The gyro transfer function is obtained from the vendor of a dynamically tuned rate gyro, being used in similar fire control systems.

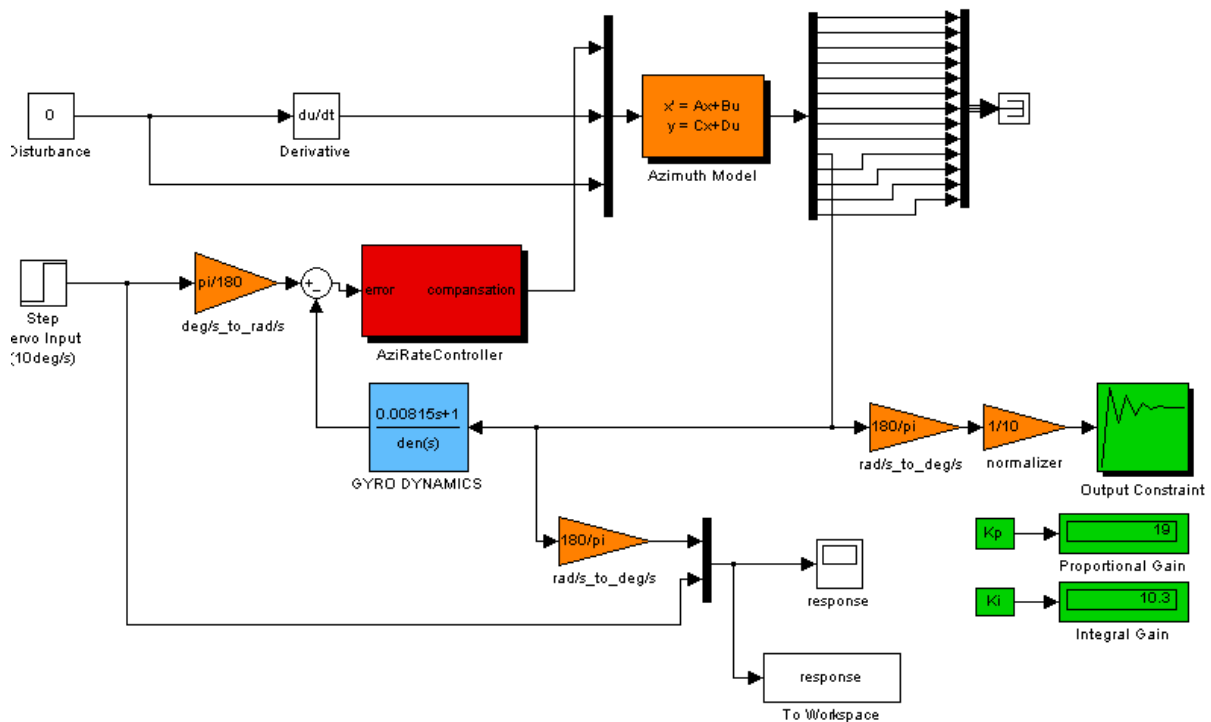


Figure 5.12 Simulink Model for Elevation Feedback Controller Design

Using a dual PI control scheme provides better disturbance characteristics especially in the low frequency region. PID scheme is not used since the derivative term has significant noise amplifying effects.

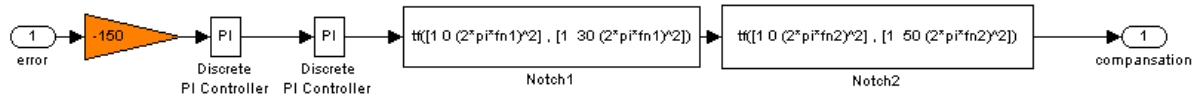


Figure 5.13 Dual PI Controller Block (Azimuth)

In association with the dual PI filter, two adjacent notch filters corresponding to the first and the third natural frequencies (6.62Hz, 42.63Hz) are used to obtain a feasible controller.

PI controller gains (K_p , K_i) are entered as parametric variables into the controller model, and the “Simulink Response Optimization Toolbox” is used to obtain the values satisfying the desired response of the system to the step input. An “Output Constraint” block is used to limit the response in time domain (Figure 5.14).

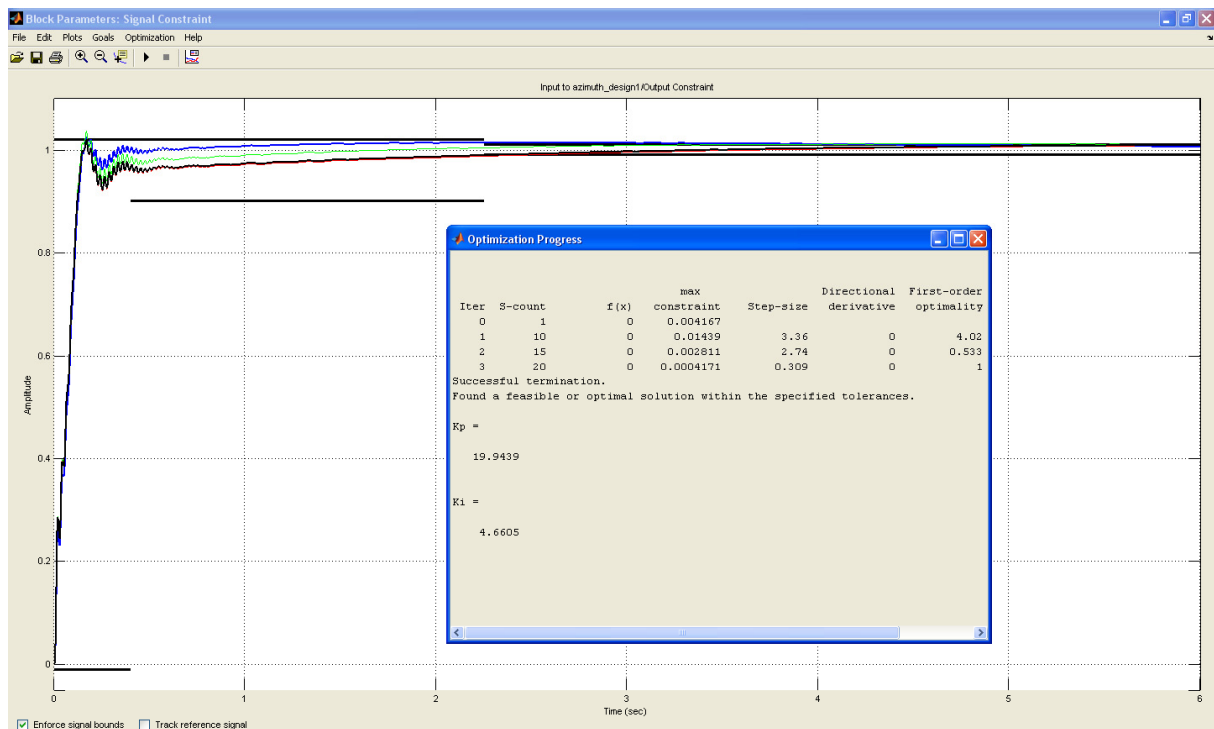


Figure 5.14 Output Constraints and Response Optimization (Azimuth)

In tank control systems, servo response is required to have a very low level of overshoot to the step input. Therefore the overshoot constraint is set to 2%. Settling time is set

to 2 seconds. When the optimization procedure is run, the proportional and the integral gains satisfying the response constraints are obtained as; $K_p = 19.9439$ and $K_i = 4.6605$. Rounding off to single significant digit after zero, the gains are used having values of “ $K_p = 19.9$ ” and “ $K_i = 4.7$ ”.

Before designing the feedforward controller, the disturbance data will be entered into the model and the stabilization performance will be measured. Normally, the way of measuring the stabilization performance is done by integrating the gyro output once to have the inertial position and measure the RMS value in a time period. But the position output is already in hand from the state-space model. Therefore, the trunnion position is entered into a discrete RMS model and the simulation is run (Figure 5.15).

At the same time, the muzzle deviation from the trunnion is monitored by taking the RMS value of the inertial position difference between the muzzle and the trunnion, and also the RMS value of muzzle inertial position (muzzle stabilization accuracy) is monitored.

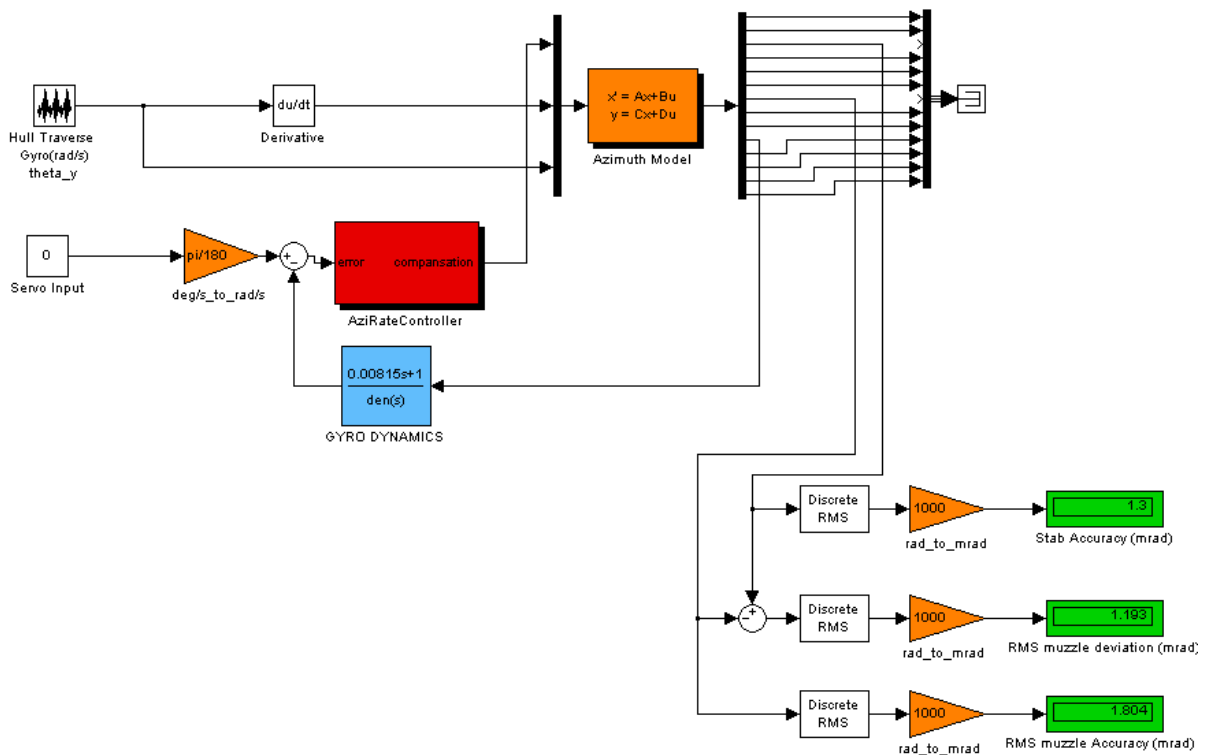


Figure 5.15 Azimuth Feedback Controller Stabilization Performance and Muzzle Deviation

Simulation has given the stabilization accuracy as 1.300 mrad, RMS muzzle deviation as 1.193 mrad and RMS muzzle stabilization accuracy of 1.804 mrad. This means that, if the fire control system would measure the stabilization error signal (from the trunnion gyro like in every existing fire control systems) and allow firing at a certain coincidence window by comparing the absolute value of the error signal with the limits of the window (typically 0.5 mrad, meaning the absolute value of the error signal is less than 0.5 mrad) the real line of fire would not be within the coincidence window because of the muzzle deviation.

It is not practical to install any feedback device to the gun muzzle because of the extreme shocks during gun fire. But the muzzle deviation can be calculated using the state-space model and this signal can be used for the coincidence during fire.

It is also impractical to try to stabilize the muzzle itself by using the model, since this time the trunnion would be in the wrong inertial position. When the gunner's sight is slave to the gun either (fixed if) mechanically or electronically, the extra error in the trunnion would be added to the sight inertial angular position and line of sight stabilization accuracy would get worse.

5.2.2 Azimuth Feedforward Controller Design

In this part, a feedforward controller is to be developed and the stabilization accuracies will be compared to the feedback controller only case. First, the feedforward controller is to be reviewed in general.

Effect of the disturbance on the output of the controller system can be reduced by measuring this disturbance and using a feedforward controller. The feed forward transfer function, G_{ff} , should be the inversion of the ratio of the disturbance transfer function and the nominal plant transfer function. It should be remembered that the G_{ff} must be stable since it acts in open loop (Figure5.6) [5].

To form G_{ff} , first G_d and G_u are to be obtained from the relevant input/output channels of the state-space elevation model. G_u is the transfer function of the model between the first input and the sixth output. G_d is the sum of the transfer functions of the model between the second and third input and the tenth output. The tenth output is the trunnion azimuth angular

velocity, where the feedback gyro is mounted. First input is the servo reference signal input, and the second and third inputs are the disturbances in azimuth.

Following Matlab[®] commands are entered to obtain G_{ff} ;

```
[NUM1, DEN]=ss2tf(Aaz, Baz, Caz, Daz, 1);
Gu=tf(NUM1(10, :), DEN);
[NUM2, DEN]=ss2tf(Aaz, Baz, Caz, Daz, 2);
[NUM3, DEN]=ss2tf(Aaz, Baz, Caz, Daz, 3);
DER = tf([1 0], 1);
Gd1= DER * tf(NUM2(10, :), DEN);

f=logspace(-1, 2.5, 5000);
w=2*pi*f;

Gd2= tf(NUM3(10, :), DEN);
Gd = Gd1 + Gd2;
Gff = -Gd/Gu;
bodemag(Gff, w);
grid;
```

Matlab[®] output for Gff;

```
1.277 s^42 + 4128 s^41 + 1.456e007 s^40 + 2.743e010 s^39 + 5.278e013 s^38 + 6.797e016 s^37 + 9.046e019 s^36
+ 8.613e022 s^35 + 8.757e025 s^34 + 6.455e028 s^33 + 5.287e031 s^32 + 3.096e034 s^31 + 2.109e037 s^30
+ 9.934e039 s^29 + 5.747e042 s^28 + 2.184e045 s^27 + 1.089e048 s^26 + 3.323e050 s^25 + 1.444e053 s^24
+ 3.503e055 s^23 + 1.336e058 s^22 + 2.536e060 s^21 + 8.532e062 s^20 + 1.237e065 s^19 + 3.673e067 s^18
+ 3.917e069 s^17 + 1.024e072 s^16 + 7.527e073 s^15 + 1.718e076 s^14 + 7.718e077 s^13 + 1.504e080 s^12
+ 3.28e081 s^11 + 5.064e083 s^10 + 6.317e084 s^9 + 7.154e086 s^8 + 5.416e087 s^7 + 3.632e089 s^6
+ 1.599e090 s^5 + 2.337e090 s^4 + 1.121e090 s^3 - 7.034e079 s^2 + 1.471e069 s - 1.025e058
-----
1.819e-012 s^41 + 1.183e-008 s^40 - 15.2 s^39 - 4.9e004 s^38 - 1.75e008 s^37 - 3.315e011 s^36
- 6.476e014 s^35 - 8.443e017 s^34 - 1.144e021 s^33 - 1.106e024 s^32 - 1.145e027 s^31 - 8.561e029 s^30
- 7.109e032 s^29 - 4.199e035 s^28 - 2.879e038 s^27 - 1.352e041 s^26 - 7.791e043 s^25 - 2.895e046 s^24
- 1.42e049 s^23 - 4.117e051 s^22 - 1.733e054 s^21 - 3.839e056 s^20 - 1.399e059 s^19 - 2.302e061 s^18
- 7.296e063 s^17 - 8.577e065 s^16 - 2.368e068 s^15 - 1.861e070 s^14 - 4.466e072 s^13 - 2.059e074 s^12
- 4.249e076 s^11 - 8.672e077 s^10 - 1.479e080 s^9 - 1.585e081 s^8 - 2.127e083 s^7 - 1.215e084 s^6
- 1.09e086 s^5 - 2.717e086 s^4 - 1.713e086 s^3 + 1.507e079 s^2 - 6.202e068 s + 6.384e057
```

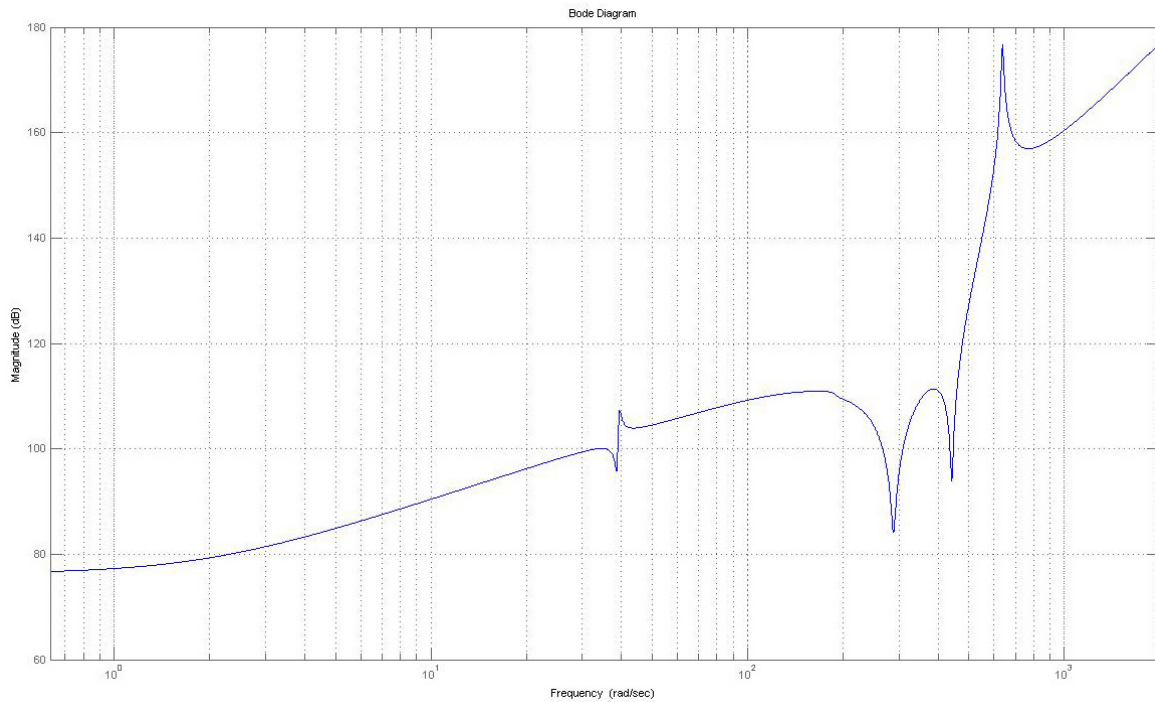


Figure 5.16 Bode Plot of Improper Gff (Azimuth)

The ideal feedforward controller is an improper transfer function since the order of the numerator is greater than the denominator (Figure 5.16). The differentiator effect must be removed at high frequencies and the transfer function must be made proper. This can be achieved by implementing a low pass filter. After some commissioning, four single order low pass filters with cut-off frequencies of 11.5 Hz has been used. It has been assumed that the angular rate of the hull is measured by a rate gyro with the same dynamic characteristics as the one for the inner-loop rate control [3].

Entering following Matlab[®] commands;

```
LP = tf([2*pi*11.5] , [1 2*pi*11.5]);
Gff2 = Gff * LP * LP * LP * LP ;
bodemag(Gff2,w);
grid;
```

Matlab[®] commands outputs a proper feedforward controller Gff2 as follows;

$$\begin{aligned}
& 3.481e007 s^{42} + 1.125e011 s^{41} + 3.97e014 s^{40} + 7.476e017 s^{39} + 1.439e021 s^{38} + 1.853e024 s^{37} \\
& + 2.466e027 s^{36} + 2.348e030 s^{35} + 2.387e033 s^{34} + 1.76e036 s^{33} + 1.441e039 s^{32} + 8.439e041 s^{31} \\
& + 5.749e044 s^{30} + 2.708e047 s^{29} + 1.567e050 s^{28} + 5.953e052 s^{27} + 2.969e055 s^{26} + 9.059e057 s^{25} \\
& + 3.936e060 s^{24} + 9.549e062 s^{23} + 3.643e065 s^{22} + 6.914e067 s^{21} + 2.326e070 s^{20} + 3.372e072 s^{19} \\
& + 1.001e075 s^{18} + 1.068e077 s^{17} + 2.791e079 s^{16} + 2.052e081 s^{15} + 4.682e083 s^{14} + 2.104e085 s^{13} \\
& + 4.1e087 s^{12} + 8.94e088 s^{11} + 1.381e091 s^{10} + 1.722e092 s^9 + 1.95e094 s^8 + 1.476e095 s^7 \\
& + 9.902e096 s^6 + 4.359e097 s^5 + 6.37e097 s^4 + 3.056e097 s^3 - 1.917e087 s^2 + 4.009e076 s - 2.794e065
\end{aligned}$$

$$\begin{aligned}
& 1.819e-012 s^{45} + 1.236e-008 s^{44} - 15.2 s^{43} - 5.34e004 s^{42} - 1.896e008 s^{41} - 3.836e011 s^{40} \\
& - 7.489e014 s^{39} - 1.042e018 s^{38} - 1.409e021 s^{37} - 1.464e024 s^{36} - 1.501e027 s^{35} - 1.223e030 s^{34} \\
& - 9.958e032 s^{33} - 6.539e035 s^{32} - 4.328e038 s^{31} - 2.326e041 s^{30} - 1.267e044 s^{29} - 5.615e046 s^{28} \\
& - 2.522e049 s^{27} - 9.248e051 s^{26} - 3.414e054 s^{25} - 1.036e057 s^{24} - 3.117e059 s^{23} - 7.82e061 s^{22} \\
& - 1.896e064 s^{21} - 3.909e066 s^{20} - 7.518e068 s^{19} - 1.256e071 s^{18} - 1.876e073 s^{17} - 2.46e075 s^{16} \\
& - 2.764e077 s^{15} - 2.684e079 s^{14} - 2.162e081 s^{13} - 1.412e083 s^{12} - 7.77e084 s^{11} - 3.591e086 s^{10} \\
& - 1.354e088 s^9 - 4.339e089 s^8 - 1.112e091 s^7 - 2.061e092 s^6 - 3.385e093 s^5 - 7.665e093 s^4 \\
& - 4.669e093 s^3 + 4.107e086 s^2 - 1.691e076 s + 1.74e065
\end{aligned}$$

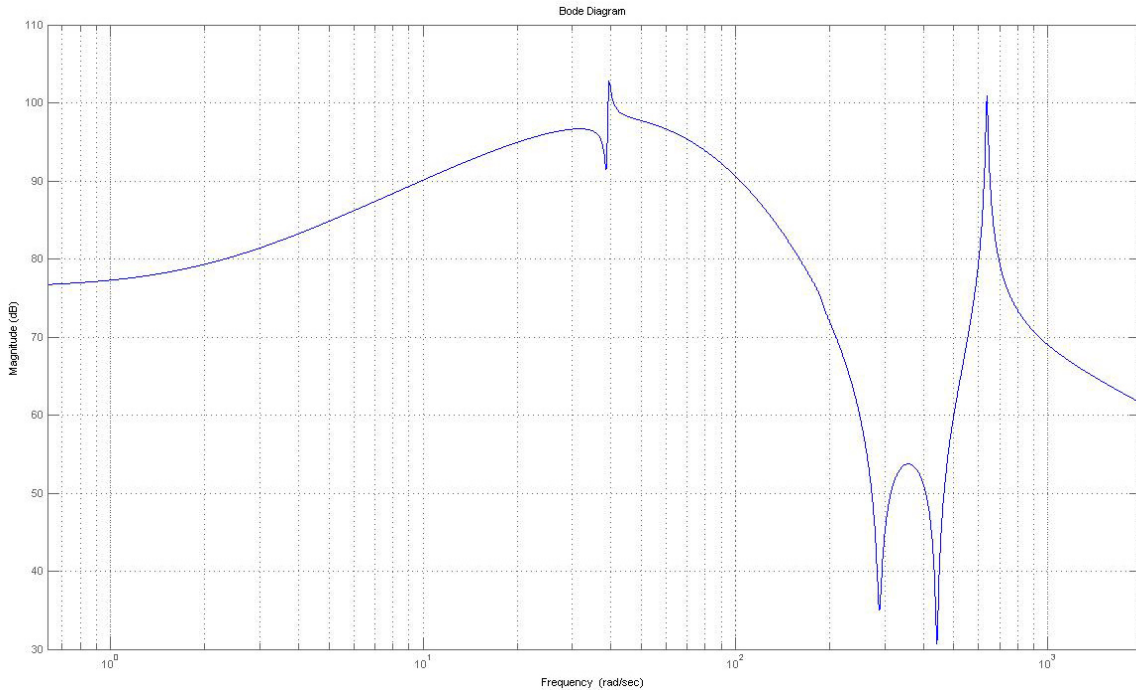


Figure 5.17 Bode Plot of Gff2, LP Filter is Added to Gff

The modified feedforward transfer function Gff2 needs to be further analyzed in terms of stability (Figure 5.17). Besides, since the order is quite high, some effort is necessary to reduce the order. For this purpose, “Hankel Singular Value Decomposition Method” is used.

Entering following Matlab® command, the hankel singular value decomposition figure is obtained (Figure 5.18);

```
hsvd(Gff2);
```

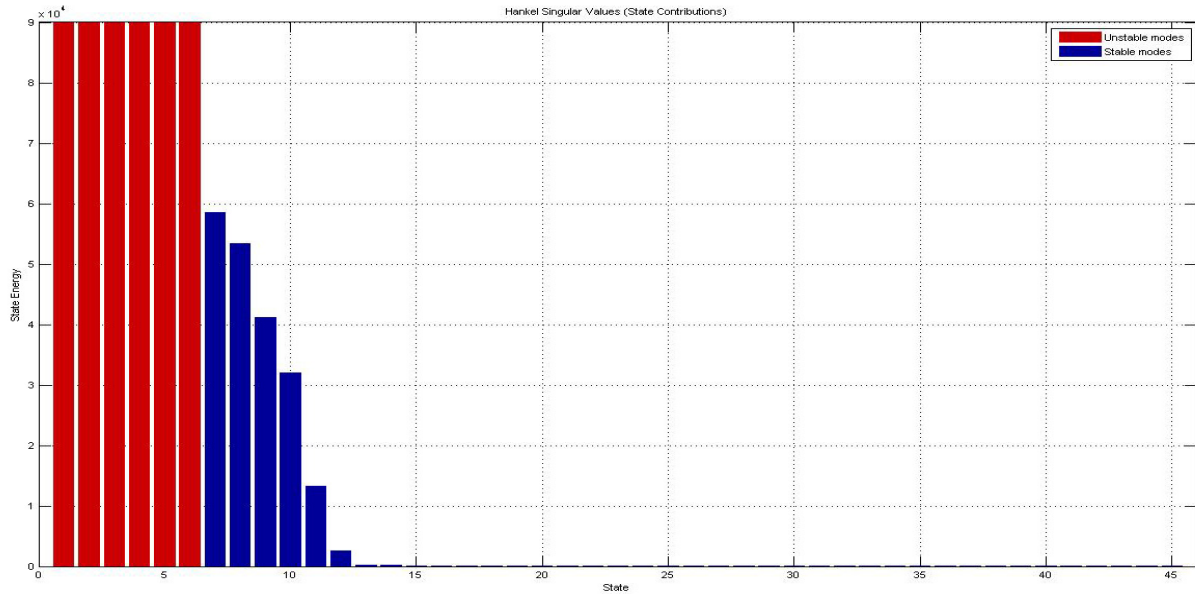


Figure 5.18 HSVD Plot for Gff2

From Figure 5.18, it is observed that feedforward transfer function Gff2 has six unstable modes out of its 45 modes. This unstable modes need to be extracted. For this purpose, “stabsep” function of Matlab® is used. Furthermore, like in feedback controller, two notch filters corresponding to the first and the third natural frequencies of the open loop system has been added to the feedforward transfer function.

Entering following Matlab® commands, the unstable modes of Gff2 is extracted and the modified hankel singular value decomposition figure is obtained (Figure 5.19);

```
fn1=6.62; %First natural frequency

NF1=tf([1 0 (2*pi*fn1)^2] , [1 30 (2*pi*fn1)^2]); %Notch against
first natural frequency

fn2=42.63; %Third natural frequency

NF2=tf([1 0 (2*pi*fn2)^2] , [1 50 (2*pi*fn2)^2]); %Notch
against third natural frequency

[Gff2s,Gff2ns]=stabsep(Gff2,'AbsTol',1e-5,'Offset',3);
Gff2s=Gff2s*NF1*NF2
```


hsvd(Gff2s);

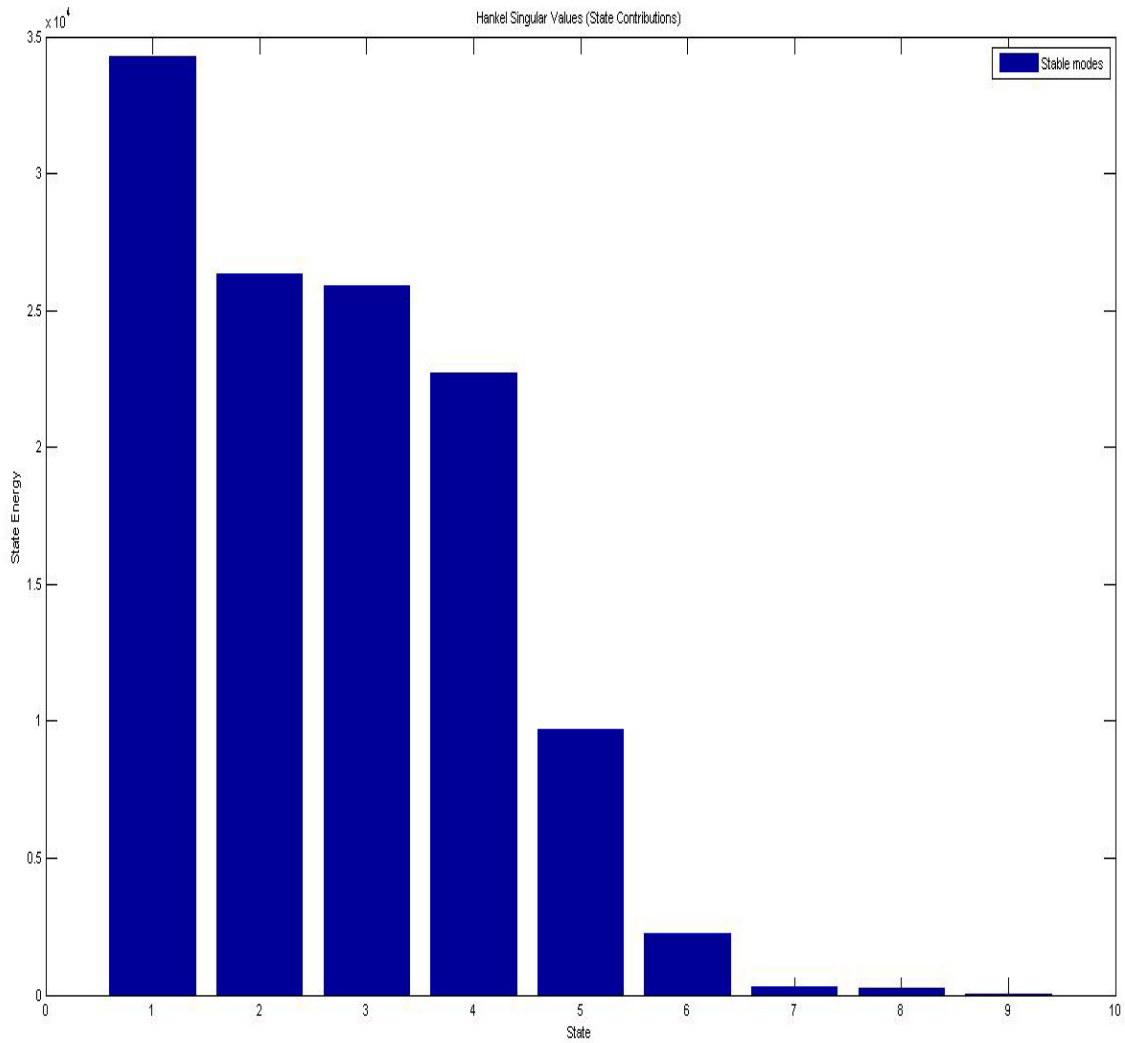


Figure 5.19 HSVD Plot for Gff2s (Stable Part of Gff2)

Gff2s;

$$\begin{aligned}
 & -2.709e005 s^8 - 4.094e012 s^7 - 6.038e013 s^6 - 5.67e017 s^5 - 5.15e018 s^4 \\
 & - 2.007e022 s^3 - 6.005e022 s^2 - 3.305e025 s - 8.879e025 \\
 & \text{-----} \\
 & s^9 + 2.892e006 s^8 + 1.067e009 s^7 + 3.743e011 s^6 + 8.076e013 s^5 + 9.451e015 s^4 \\
 & + 6.401e017 s^3 + 2.693e019 s^2 + 7.182e020 s + 9.786e021
 \end{aligned}$$

It can be seen that the order of the initial feedforward transfer function has been reduced from 45 to 8.

Feedforward controller Gff2s is implemented to the Simulink model as a LTI system block and the simulation is run as follows (Figure 5.20).

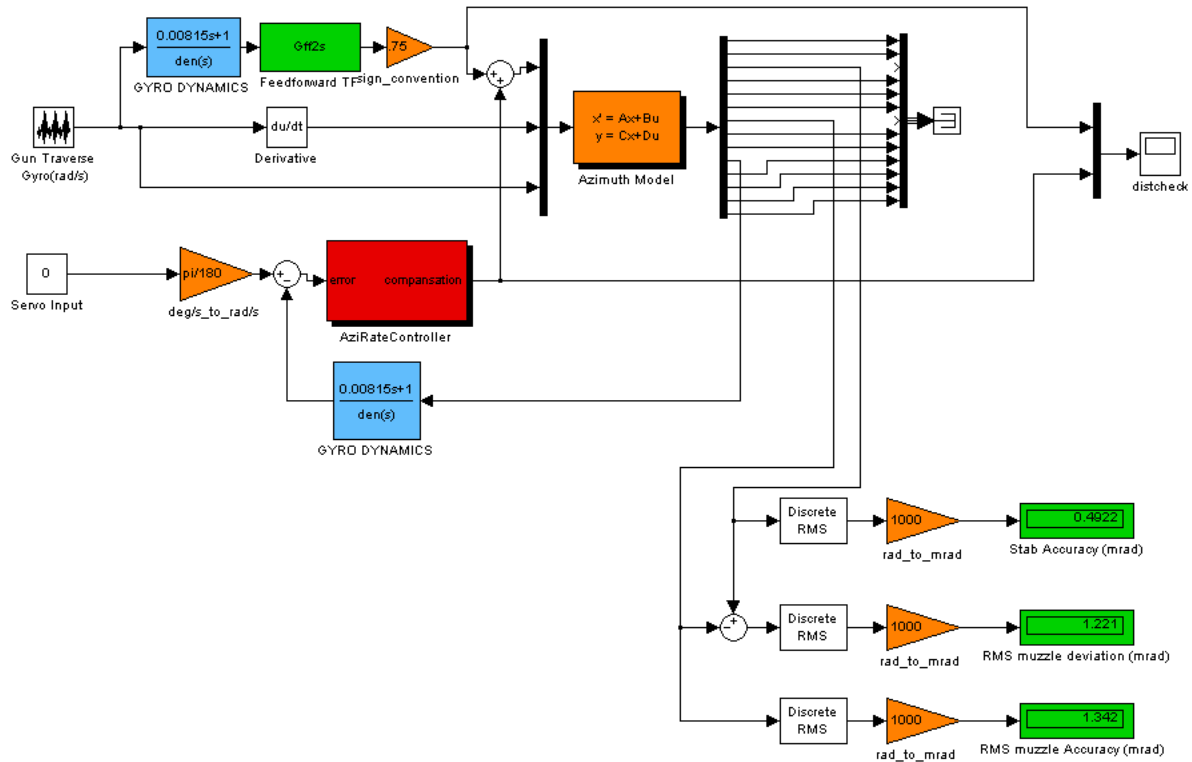


Figure 5.20. Feedforward Controller Simulation

Result is a significant improvement in the stabilization accuracy. Without feedforward controller, the stabilization accuracy was 1300 μ rad. When implemented, feedforward compensation reduced this value down to 492 μ rad. This value is fair as a stabilization accuracy when compared to the general practical 500 μ rad requirement.

But it must be emphasized again that no matter how good is the stabilization accuracy, muzzle deviation and muzzle stabilization accuracy values are at a level of 1000 μ rad.

CHAPTER 6

COINCIDENCE FIRING DESIGN

In this section, a coincidence algorithm will be developed for the stabilization controller. First the physical factors and requirements will be identified, and then a solution will be proposed. Simulations will be run with the developed coincidence algorithm and the effectiveness will be monitored.

6.1 Coincidence Algorithm Necessity

In previous chapters, simulations showed that no matter how successful a stabilization controller is designed, gun flexibility always exists (Figure 6.1). And the muzzle deflections are at the order of a few mrad's, meaning a few meters at 1km. It is apparent that the typical hit probabilities of a main battle tank cannot be achieved if there is no control over the fire permit and inhibit as the gunner pulls the trigger.

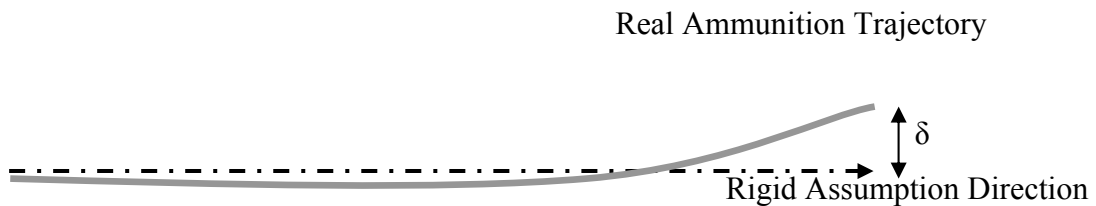


Figure 6.1. Effect of Flexibility of the Barrel

Classical coincidence checks, existing in many tanks, only monitors the current stabilization error signal (signal entering into the controller) and permits fire only if the current error signal value is within a certain margin (e.g. $\pm 0.5\text{mrad}$), as the gunner pulls the trigger. But, this method is insufficient since the muzzle is still not monitored i.e. gun flexibility is not taken into account.

6.2 Coincidence Algorithm Design

Since a detailed model has been formed in this thesis, it is possible to take the deflection of the muzzle with respect to the trunnion, where the feedback gyro is located, and develop an enhanced coincidence check. The algorithm to be proposed will use the fixed time delay between the trigger is pulled and the ammunition exit from the muzzle of the barrel. It is inevitable to take this effect into account since the muzzle will move into another inertial angular orientation during this delay period and the precise inertial position of the muzzle has to be predicted.

Definition of this time delay is from the gunner's fire command, T_0 , (by pulling the trigger) up to the ammunition leaves the barrel muzzle, T_1 , (Figure 6.2). Therefore several factors contribute; time for the firing electronics activating the chemical reaction in the primer capsule at the back of the cartridge, time for the chemical to burn and time for the projectile to accelerate and reach the end of the barrel (muzzle). For different ammunition types, this delay differs, so it is a variable having ammunition dependency and the fire control computer should use the selected ammunition's value for this variable while checking the coincidence.

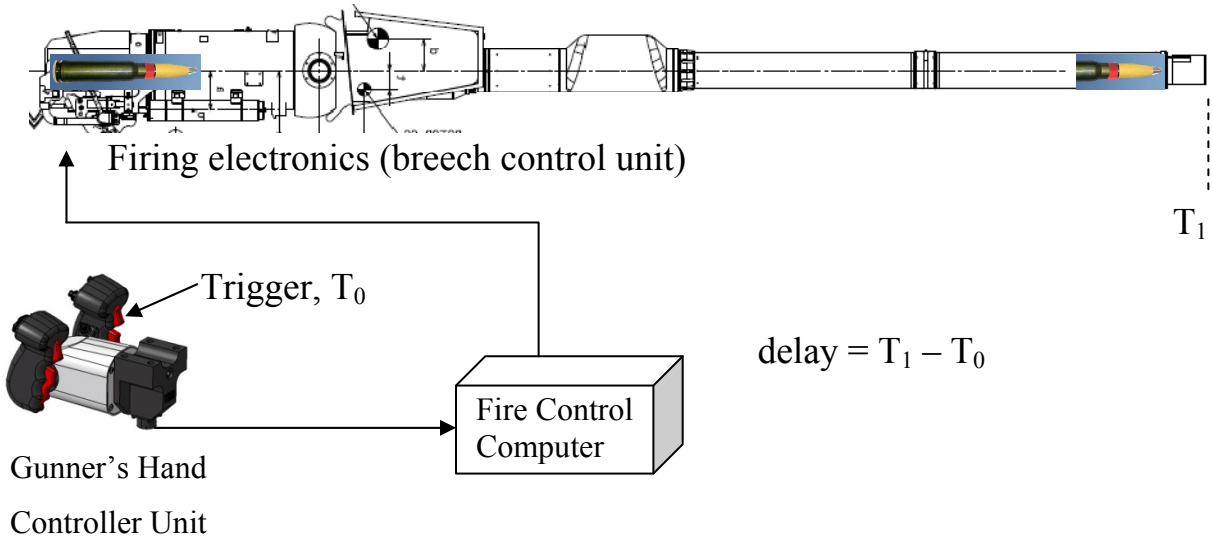


Figure 6.2. Fixed Firing Delay Between the Trigger and the Muzzle

Angular orientation of the muzzle will be predicted for a prediction horizon of exactly the fixed time delay ahead. For this reason, plant and controller models will be run parallel to the real model which we will assume the physical system. Measured disturbance signals will be used to predict the future disturbance values and the predicted disturbance signal will be entered into the model running in parallel to the real model (Figure 6.3).

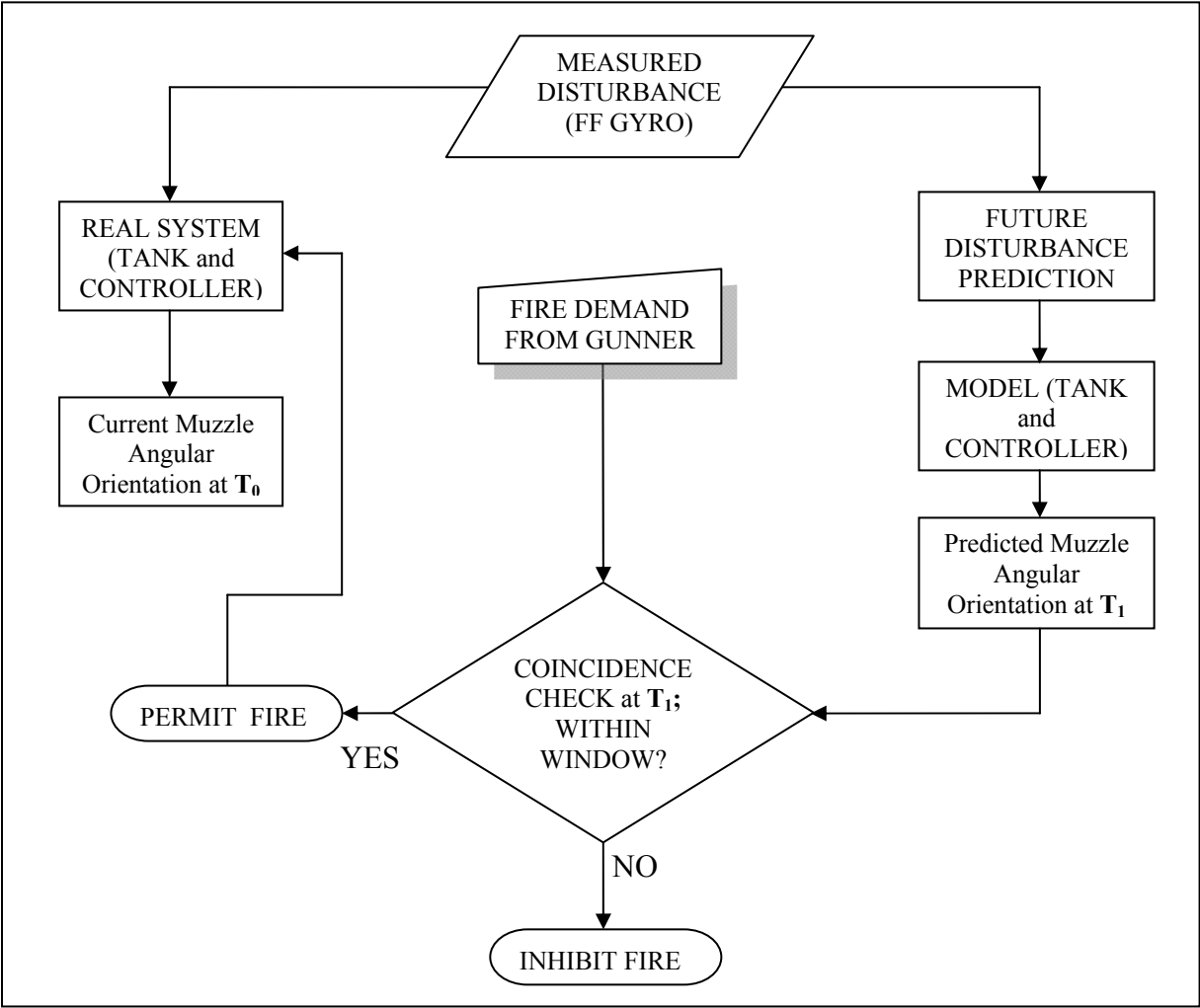


Figure 6.3. Coincidence Algorithm

Then the muzzle angular velocity output of the plant and controller (this is the predicted muzzle angular orientation at the delay time later prediction horizon) with respect to the predicted disturbance will be monitored to permit/inhibit fire signal if this value is within a coincidence window (Figure 6.4).

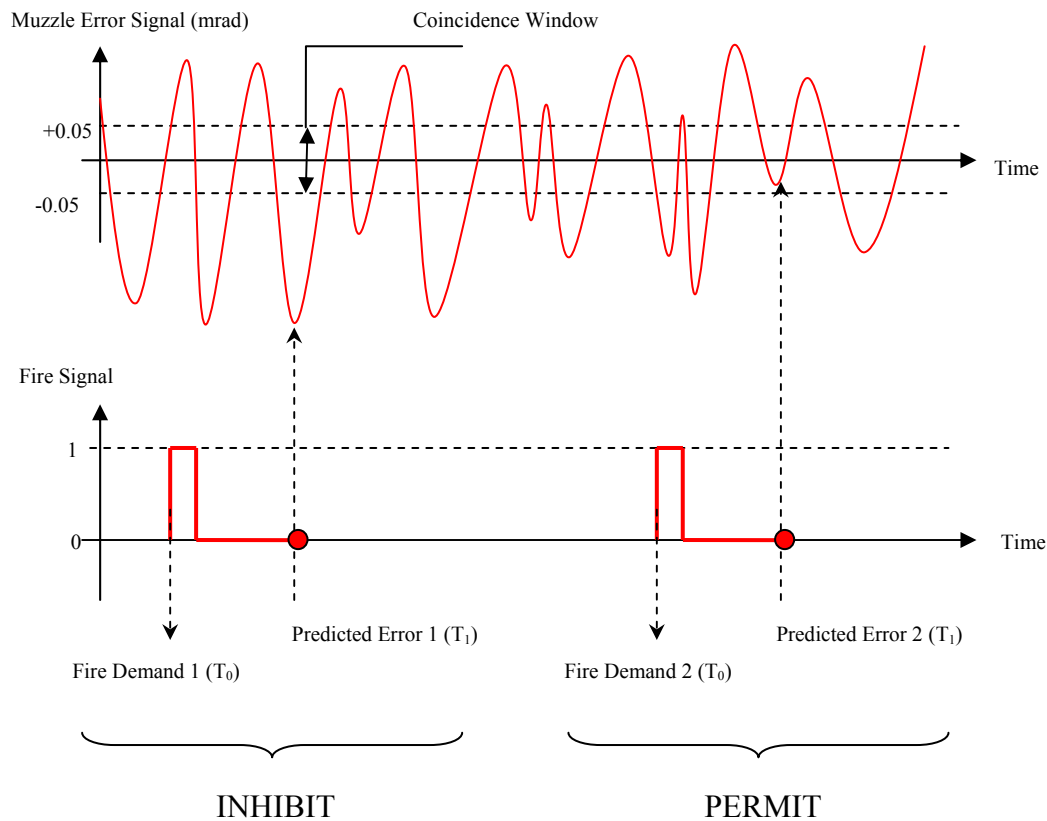


Figure 6.4. Graphical Representation of Coincidence Algorithm

In the first attempt to fire (Fire Demand 1), predicted muzzle stabilization error signal at T_1 (angular orientation) is out of the coincidence and the fire is inhibited. But in the second attempt to fire (Fire Demand 2), predicted muzzle stabilization error signal at T_1 is within the coincidence and the fire is permitted.

In order to predict the future disturbance, measured disturbance signal with the feedforward gyro signal will be used. This signal has already been used for the feedforward controller design in Chapter 5. Autoregressive (AR) modeling method will be used to predict the future prediction of the disturbance time-series. A brief explanation about the AR time series analysis background is as follows [10];

A time series is defined as a sequence of vectors (or scalars) which depend on time t ; $\{x(t_0), x(t_1), \dots, x(t_{i-1}), x(t_i), x(t_{i+1}), \dots\}$ and it is the output of some process P that creates the disturbance to the stabilization loop for our case (Figure 6.5).

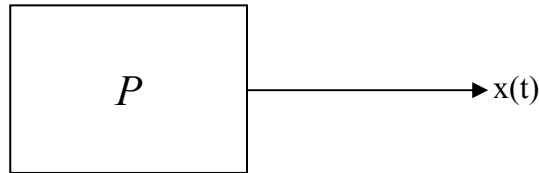


Figure 6.5. Stochastic Process Time Series Representation

Extending backward from time t , we have time series $\{x[t], x[t-1], \dots\}$ which is the measured disturbance data sampled at 500Hz. With the measured disturbance data in hand, next step is to estimate x at some future time; $\hat{x}[t + s] = f(x[t], x[t-1], \dots)$, where s is called the horizon of prediction. For our case, s is the total number of sample time steps between times T_0 and T_1 . This problem will be solved by using the autoregressive modeling. An AR[p] assumes that at its heart is an Infinite Impulse Filter (IIR) applied to some (unknown) internal signal, $\varepsilon[t]$, and p is the order of that filter;

$$x[t] = \sum_{i=1}^p \alpha_i x[t - i] + \varepsilon[t] \tag{6.1}$$

If on average $\varepsilon[t]$ is small relative to $x[t]$, then we can estimate $x[t]$ using;

$$\hat{x}[t] \equiv x[t] - \varepsilon[t] = \sum_{i=1}^p w_i x[t - i] \tag{6.2}$$

This is an FIR filter. The w_i 's are estimates of the α_i 's. To estimate AR[p] parameters, there are several methods [9];

a) Burg's lattice-based method: Solves the lattice filter equations using the harmonic mean of forward and backward squared prediction errors.

b) Forward-backward approach: Minimizes the sum of a least- squares criterion for a forward model, and the analogous criterion for a time-reversed model.

c) Geometric lattice approach: Similar to Burg’s method, but uses the geometric mean instead of the harmonic mean during minimization.

d) Least-squares approach: Minimizes the standard sum of squared forward-prediction errors.

e) Yule-Walker approach: Solves the Yule-Walker equations, formed from sample covariances.

$$x[t] \approx \hat{x}[t] = \sum_{i=1}^p w_i x[t - i]$$

$$\begin{bmatrix} x[p + 1] \\ x[p + 2] \\ \vdots \end{bmatrix} = \begin{bmatrix} x[1] & x[2] & \dots & x[p] \\ x[2] & x[3] & \dots & x[p + 1] \\ \vdots & \vdots & \ddots & \vdots \end{bmatrix} \cdot \underbrace{\begin{bmatrix} w_1 \\ w_2 \\ \vdots \\ w_p \end{bmatrix}}_{\mathbf{w}}$$

(6.3)

Time series disturbance modeling / time series modeling method is being used in various applications; Active noise cancellation, speech recognition, active structural vibration control and residual optical jitter suppression [11].

Time-series autoregressive modeling and prediction implementation will be done using “*System Identification Toolbox*” commands of the Matlab® software. “*ar*” command in Matlab® estimate parameters of autoregressive model for scalar time series[9]. Command syntax is as follows; $m = ar(y,n,approach>window)$. y is the data to be used to create the model and n is the order of the model.

Portion of the past measured disturbance data will be used to create the model and the k -step ahead prediction will be done by using this model, rest of the measured data (current measurement) with the “*predict*” command. Command syntax is: $yp = predict(m,data)$.

To run the commands within the Simulink environment, a Matlab® function has been written as;

```
function denemem= deneme(u)
myvect = [u(1);u(2);u(3);u(4);u(5);u(6);u(7);u(8);u(9);u(10)];
mdl=ar(myvect,3,0.002);
yhat_cell=predict(mdl,myvect,5);
yhat=yhat_cell{1,1};
denemem=yhat(length(yhat));
%TIME SERIES PREDICTION USING SYSTEM IDENTIFICATION TOOLBOX
%5-step ahead prediction for disturbance signal using Auto-
Regression,
%Order of the model is 3,
%Model is updated at every solver step
%Sample time is 0.002s
```

The disturbance signal is connected to the following Simulink sub-system as (Figure6.6);

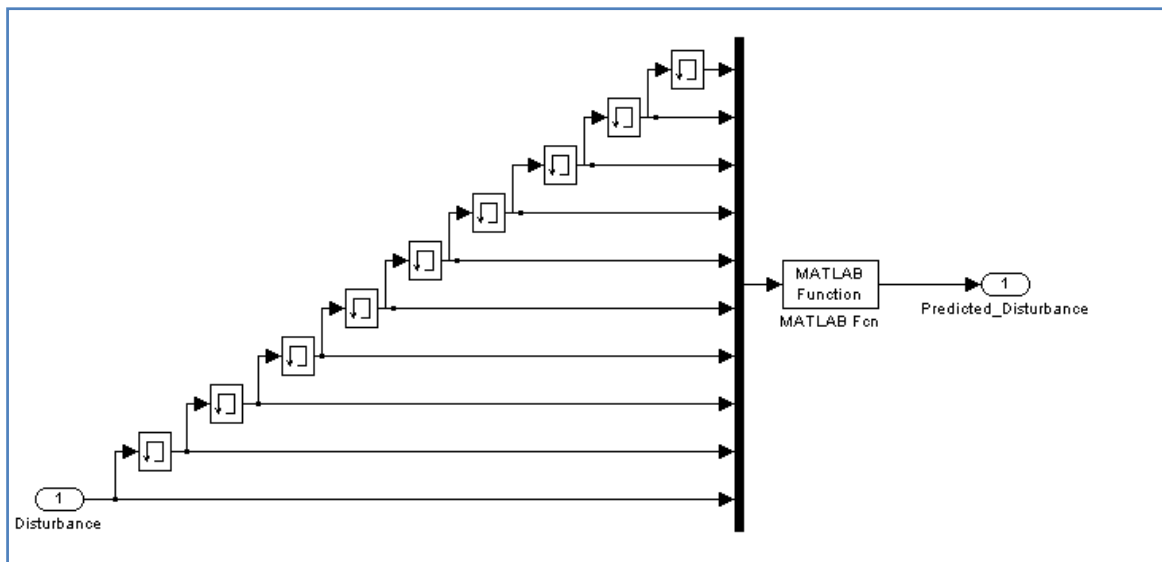


Figure 6.6. AR-Prediction Sub-system

Then the following Simulink model has been prepared to implement the coincidence algorithm (Figure6.7). This model uses the elevation 5-dof model and the stabilization controller developed in Chapter 5. The model is doubled and the first one is assumed as the real tank, the second one as the observer model. The real system is fed by the disturbance itself and the observer model is fed by the 5 step predicted disturbance signal. It is assumed that the delay time between gunner triggering and the ammunition exit from the muzzle is 5 solver steps (10msec). Total simulation time is 80.8 sec and a periodic fire trigger signal having a time period of 0.8 sec and 12.5% (0.1sec) pulse width has been modeled as the gunner fire demand. By this way 100 periodic fire signals has been created and the output of the coincidence algorithm is stored. A very tight coincidence window (0.05mrad) has been selected. If the muzzle angular orientation of the observer model using the 5-step ahead predicted disturbance signal is within the 0.05mrad coincidence and if the trigger is pulled, the system permits fire. Otherwise inhibits.

If the external ballistics ammunition dispersion effects are not taken into account, keeping the coincidence window as narrow as ± 0.05 mrad provides a ± 5 cm window at a target standing at 1 km. For a target distance of 5km, this value becomes ± 25 cm. A standard NATO tank target is a target board having 2500mm by 2500mm dimensions.

Normally, the first round hit probability value for a tank is calculated from the hit point coordinates at the 2500mm by 2500mm target board. Since the coincidence allows fire practically only if the target will be hit without any deviation from the center of the target board (aiming point), one can claim that by using this coincidence algorithm a 100% first round hit probability is achieved. The permitted fire signal results has been counted and the percentage of the permit signals within the total fire attempts has been calculated as 80% since the total number of inhibit signals is 20 out of 100 (Figure6.8).

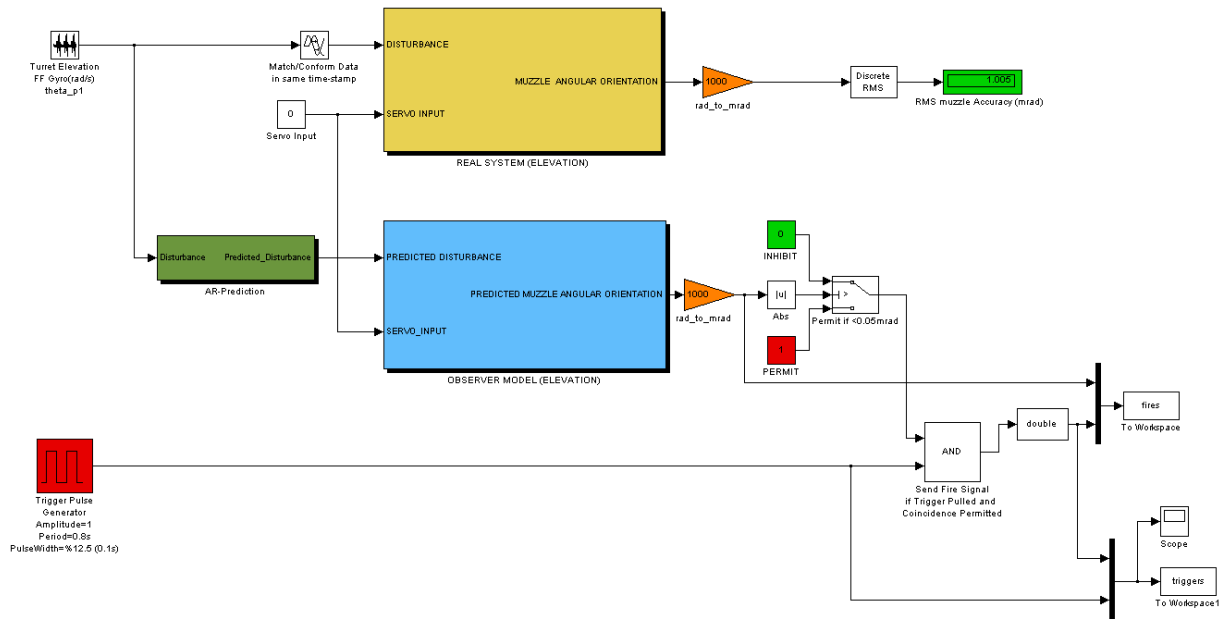


Figure 6.7. Coincidence Simulation Model

Sustaining fire signal for 0.1sec by adjusting the trigger signal pulse-width increase the percentage of the permit signals while the coincidence algorithm adjusts the correct timing to send the signal within this 0.1sec period. After simulation is complete, following Matlab® commands have been written to create the plot (Figure6.8) for the trigger and coincidence results together with the predicted muzzle angular orientation;

```
plot(fires.time(1:40428,1),fires.signals.values(1:40428,1),'b');
grid; hold on; grid;
```

```
plot(triggers.time(1:40428,1),triggers.signals.values(1:40428,1),'g'
);
grid; hold on;
```

```
plot(triggers.time(1:40428,1),triggers.signals.values(1:40428,2),'r'
);
```

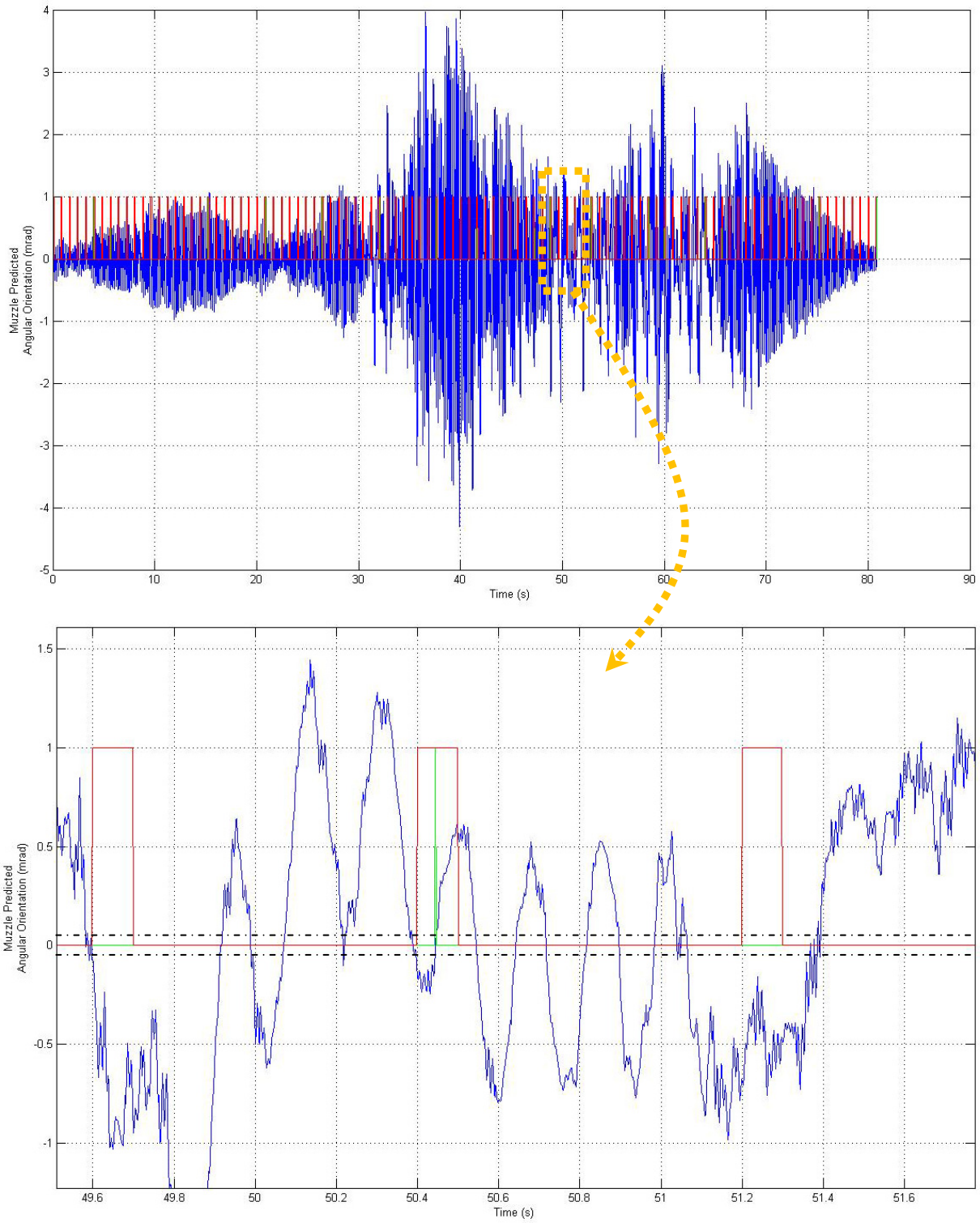


Figure 6.8. Fire Demand (red), Coincidence Check Result (green), Muzzle Orientation (blue) ,
Coincidence Window (black-dashed)

Applying the coincidence in just elevation axis has given very good results. Eighty out of a hundred fire demands have satisfied the 0.05mrad coincidence criteria. Now, the same coincidence criteria will be applied for both elevation and traverse axes. Hundred firing attempts will be made again, and the output will be plot in time domain. For this reason, a new Simulink model has been prepared by combining the models for elevation and traverse (Figure6.9).

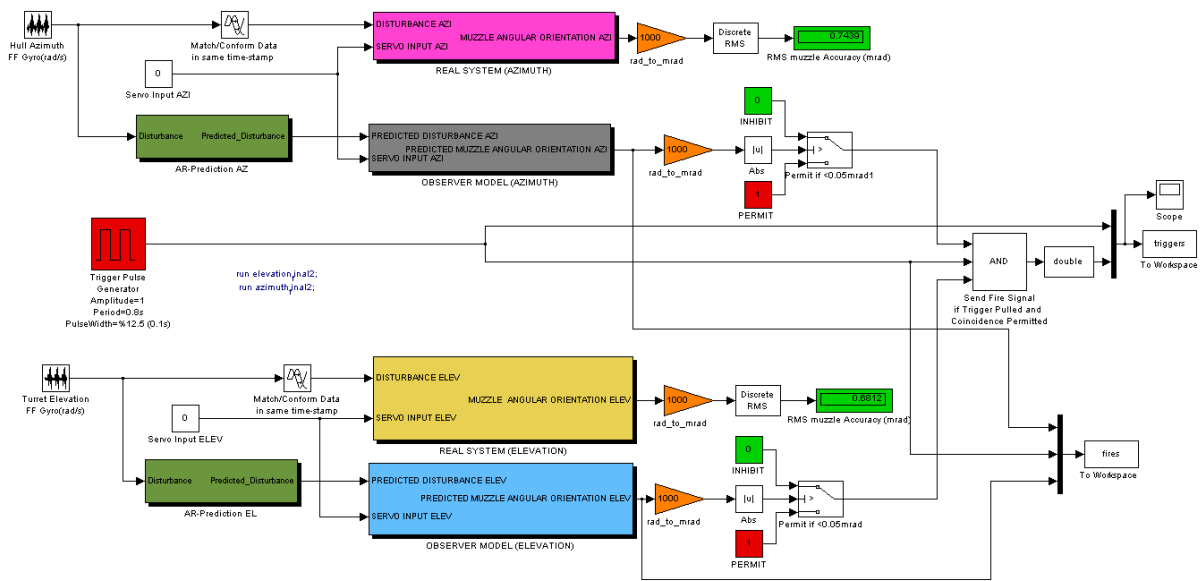


Figure 6.9. Two Axes Coincidence Simulation Model

After simulation is complete, following Matlab® commands have been written to create the plot (Figure6.10) for the trigger and coincidence results together with the predicted muzzle angular orientation;

```
plot(fires.time(1:40428,1),fires.signals.values(1:40428,1),'b');
grid; hold on;
plot(fires.time(1:40428,1), fires.signals.values(1:40428,3),'m');
grid; hold on;
plot(triggers.time(1:40428,1),triggers.signals.values(1:40428,1),'r'
); grid; hold on;
plot(triggers.time(1:40428,1),triggers.signals.values(1:40428,2),'g'
);
```

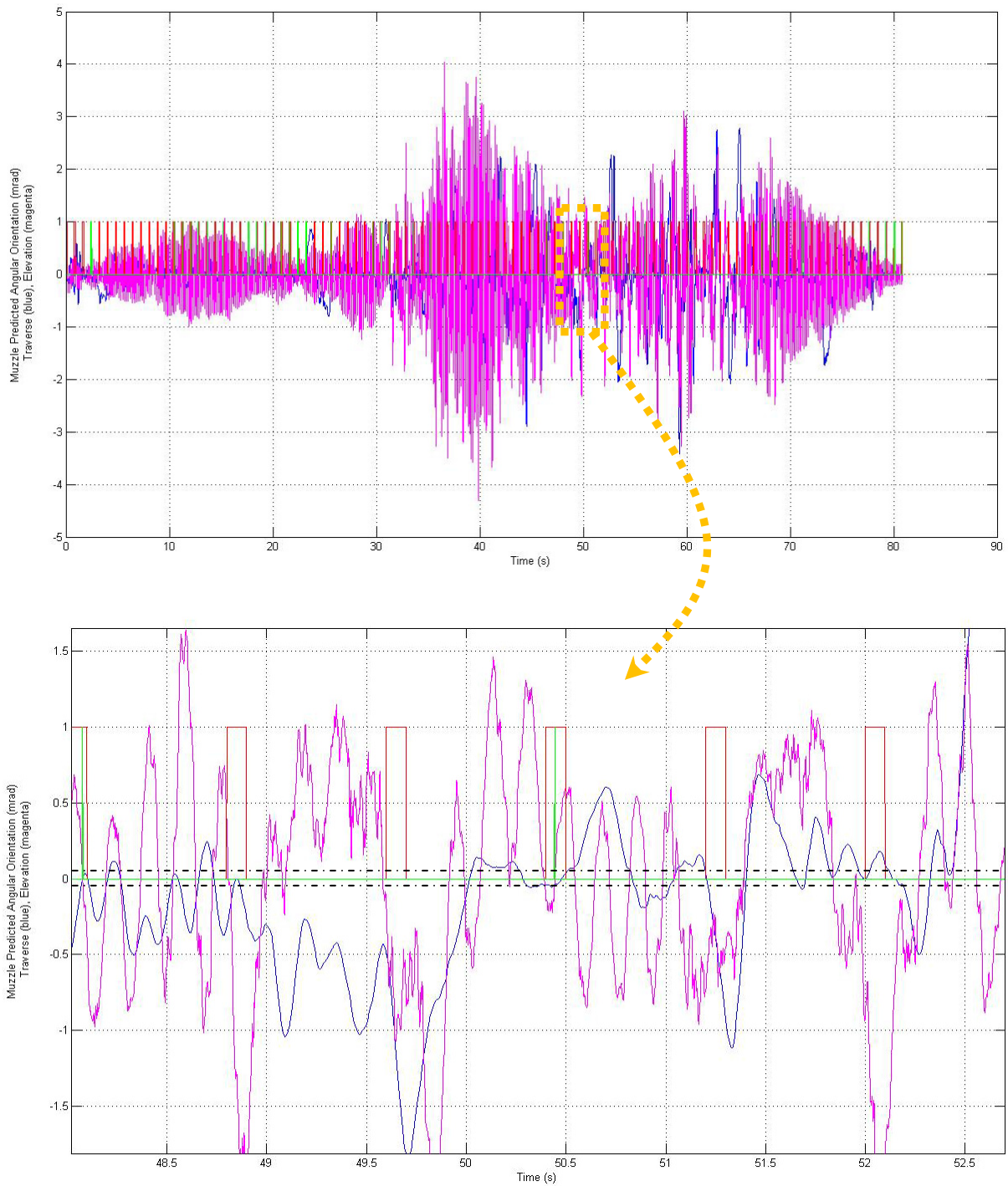


Figure 6.10. Fire Demand (red), Coincidence Check Result (green), Muzzle Orientation (Traverse: blue, Elevation: red), Coincidence Window (black-dashed)

Reviewing the simulation outputs, it can still be said that the first round hit probability is still 100% in theory, this time for both axes. But, applying the coincidence in traverse, it is observed that the permit signals ratio over a hundred fire demand is reduced to 31%. This is due to the low stabilization accuracy of the traverse axis (0.49mrad-RMS) compared to the elevation axis (0.07mrad-RMS), and it is not because of the gun flexibility. Gun flexibility muzzle deviation order is very close for both axes.

6.3 Three Dimensional Visual Simulation Design

For better visualization of the study of this thesis, an animation environment which is using the Matlab® and Simulink simulation outputs as inputs has been designed. This environment has been formed by using Microsoft Visual C++ and associated OpenGL (Open Graphics Library) library commands. Simulink “3D Animation Toolbox” has not been selected since the graphical ability of this toolbox is very limited compared to OpenGL capabilities.

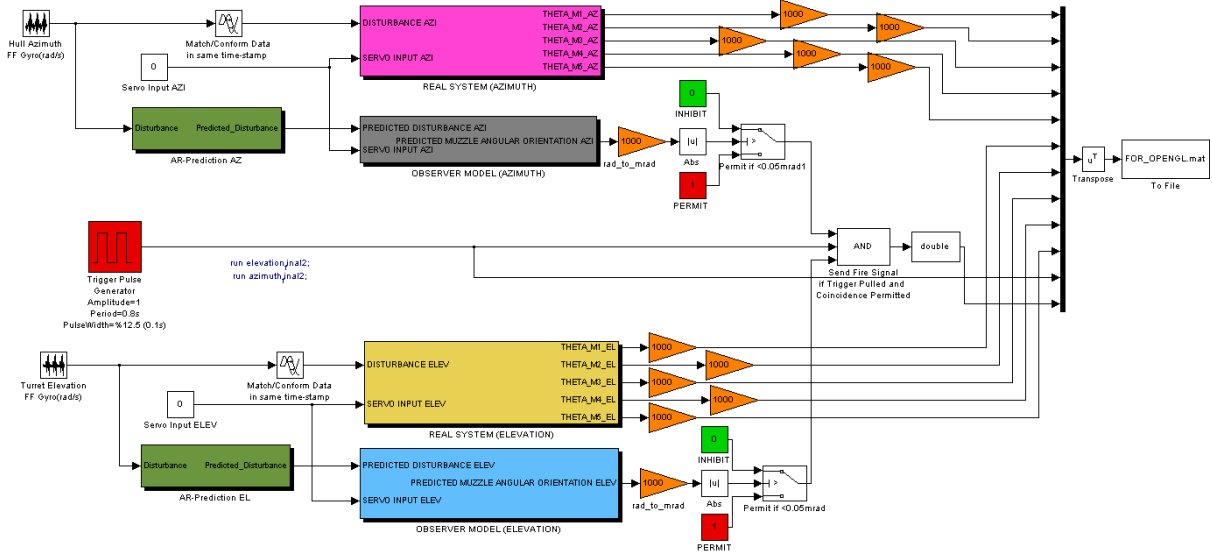


Figure 6.11. Simulink Model for Creating OpenGL Animation Data

In order to give simulation outputs to animation environment, disturbances in azimuth and elevation axes, angular orientation states of the discrete parts in both axes and the fire demands with the coincidence result has been stored in a “.mat” file (Figure6.11). This file has been read by the animation code (Figure6.12) to animate the multi-body simulation.

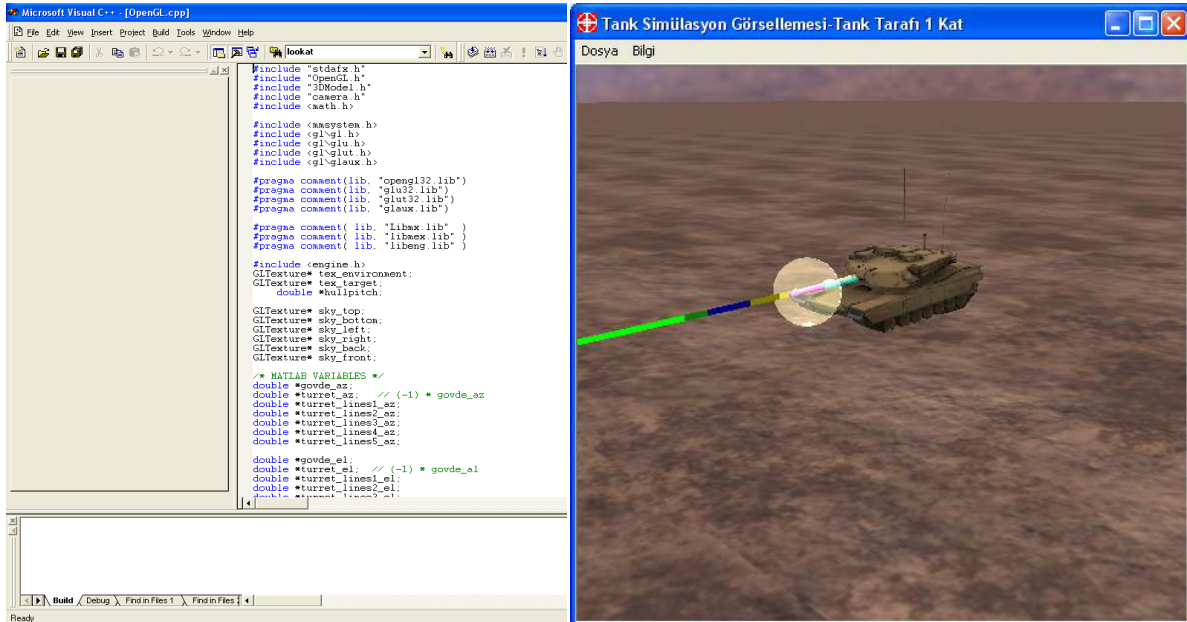


Figure 6.12. A View From Animation Code and The Compiled Application Window

CHAPTER 7

MUZZLE RATE OBSERVABILITY AND MUZZLE RATE STABILIZATION

In this section, gun muzzle will be stabilized instead of closing the stabilization loop by feedback and feedforward gyros and running a coincidence algorithm as in previous chapters. An observer for muzzle rates will be studied and the results will be analyzed

7.1 Observability

Implementing a state feedback controller $u(k) = Kx(k)$ requires the entire state vector $x(k)$, but sensors often provide only the measurements of output[12] (Figure7.1).

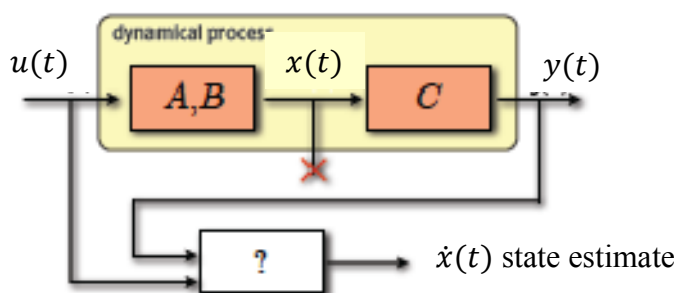


Figure 7.1. General State Estimation

Consider an input free continuous system;

$$\begin{aligned} \dot{x}(t) &= A x(t), x(t_0) = x_0 \\ y(t) &= C x(t) \end{aligned} \tag{7.1}$$

with $x \in \mathbb{R}^n, y \in \mathbb{R}^p, A \in \mathbb{R}^{n \times n}, C \in \mathbb{R}^{p \times n}$ knowledge of x_0 is sufficient to determine $x(t)$ at any time instant since;

$$x(t) = e^{A(t-t_0)} x(t_0) \tag{7.2}$$

The problem is to find $x(t_0)$ from the available measurements in equation (7.1).

$$\begin{aligned}
y(t_0) &= Cx(t_0) \\
\dot{y}(t_0) &= C\dot{x}(t_0) = CAx(t_0) \\
\ddot{y}(t_0) &= C\ddot{x}(t_0) = CA^2x(t_0) \\
&\vdots \\
y^{(n-1)}(t_0) &= Cx^{(n-1)}(t_0) = CA^{(n-1)}x(t_0)
\end{aligned} \tag{7.3}$$

Aim is to generate n linearly independent algebraic equations in n unknowns of the state vector $x(t_0)$. Equations (7.3) are a system of np linear algebraic equations and can be put in matrix form as;

$$\begin{bmatrix} y(t_0) \\ \dot{y}(t_0) \\ \ddot{y}(t_0) \\ \vdots \\ y^{(n-1)}(t_0) \end{bmatrix}^{(np) \times 1} = \begin{bmatrix} C \\ CA \\ CA^2 \\ \vdots \\ CA^{n-1} \end{bmatrix}^{(np) \times n} * x(t_0) = \theta x(t_0) = Y(t_0) \tag{7.4}$$

where θ is the observability matrix. The initial condition $x(t_0)$ can be determined uniquely from equation (7.4) if and only if the observability matrix has the full rank, i.e. $rank(\theta) = n$. Therefore observability can be stated as; the linear system with equation (7.1) with measurements with equation (7.2) is observable if and only if the observability matrix θ has full rank.

7.2 Muzzle Rate Observability

In our 7-dof azimuth and 5-dof elevation state space model case, C matrices takes the following forms since the feedback signals are only from the feedback gyro, $\dot{\theta}_{m1}$ for both;

$$C_{az}^{14 \times 14} = \begin{bmatrix} 0 & 0 & 0 & 0 & 0 & 0 & 0 & 0 & 0 & 0 & 0 & 0 & 0 & 0 \\ 0 & 0 & 0 & 0 & 0 & 0 & 0 & 0 & 0 & 0 & 0 & 0 & 0 & 0 \\ 0 & 0 & 0 & 0 & 0 & 0 & 0 & 0 & 0 & 0 & 0 & 0 & 0 & 0 \\ 0 & 0 & 0 & 0 & 0 & 0 & 0 & 0 & 0 & 0 & 0 & 0 & 0 & 0 \\ 0 & 0 & 0 & 0 & 0 & 0 & 0 & 0 & 0 & 0 & 0 & 0 & 0 & 0 \\ 0 & 0 & 0 & 0 & 0 & 0 & 0 & 0 & 0 & 0 & 0 & 0 & 0 & 0 \\ 0 & 0 & 0 & 0 & 0 & 0 & 0 & 0 & 0 & 0 & 0 & 0 & 0 & 0 \\ 0 & 0 & 0 & 0 & 0 & 0 & 0 & 0 & 0 & 0 & 0 & 0 & 0 & 0 \\ 0 & 0 & 0 & 0 & 0 & 0 & 0 & 0 & 0 & 0 & 0 & 0 & 0 & 0 \\ 0 & 0 & 0 & 0 & 0 & 0 & 0 & 0 & 0 & 1 & 0 & 0 & 0 & 0 \\ 0 & 0 & 0 & 0 & 0 & 0 & 0 & 0 & 0 & 0 & 0 & 0 & 0 & 0 \\ 0 & 0 & 0 & 0 & 0 & 0 & 0 & 0 & 0 & 0 & 0 & 0 & 0 & 0 \\ 0 & 0 & 0 & 0 & 0 & 0 & 0 & 0 & 0 & 0 & 0 & 0 & 0 & 0 \\ 0 & 0 & 0 & 0 & 0 & 0 & 0 & 0 & 0 & 0 & 0 & 0 & 0 & 0 \end{bmatrix}$$

$$C_{el}^{10 \times 10} = \begin{bmatrix} 0 & 0 & 0 & 0 & 0 & 0 & 0 & 0 & 0 & 0 \\ 0 & 0 & 0 & 0 & 0 & 0 & 0 & 0 & 0 & 0 \\ 0 & 0 & 0 & 0 & 0 & 0 & 0 & 0 & 0 & 0 \\ 0 & 0 & 0 & 0 & 0 & 0 & 0 & 0 & 0 & 0 \\ 0 & 0 & 0 & 0 & 0 & 1 & 0 & 0 & 0 & 0 \\ 0 & 0 & 0 & 0 & 0 & 0 & 0 & 0 & 0 & 0 \\ 0 & 0 & 0 & 0 & 0 & 0 & 0 & 0 & 0 & 0 \\ 0 & 0 & 0 & 0 & 0 & 0 & 0 & 0 & 0 & 0 \\ 0 & 0 & 0 & 0 & 0 & 0 & 0 & 0 & 0 & 0 \\ 0 & 0 & 0 & 0 & 0 & 0 & 0 & 0 & 0 & 0 \end{bmatrix}$$

By running the following code in MATLAB, observability analysis has been done as;

```

%*****
%*****MUZZLE STABILIZATION CHAPTER7*****
%****BY: TURKER KARAYUMAK, METU MECHANICAL ENGINEERING*****
%*****

%*****RUN MODEL PARAMETERS*****
elevation_final3;
azimuth_final3;

%*****FORM NEW C MATRICES*****

Caz=zeros(14);
Caz(10,10)=1;           %Gyro feedback signal in az
Cel=zeros(10);
Cel(6,6)=1;           %Gyro feedback signal in el
THETA_az=obsv(Aaz,Caz); %Azimuth observability matrix
rank(THETA_az)
THETA_el=obsv(Ael,Cel); %Azimuth observability matrix
rank(THETA_el)

```

The output is 4 for both axes. Therefore since ranks of observability matrix of both systems seem less than their orders, both can be thought as unobservable. To determine which

states are observable, a canonical observable transformation (observable stair case formation) will be made such that;

$$\begin{aligned} \begin{bmatrix} \dot{x}_{uo} \\ \dot{x}_o \end{bmatrix} &= \begin{bmatrix} A_{uo} & A_{12} \\ 0 & A_o \end{bmatrix} \begin{bmatrix} x_{uo} \\ x_o \end{bmatrix} + \begin{bmatrix} B_{uo} \\ B_o \end{bmatrix} u \\ y &= [0 \quad C_o] \begin{bmatrix} x_{uo} \\ x_o \end{bmatrix} \\ \bar{A} &= TAT^T, \bar{B} = TB, \bar{C} = CT^T \end{aligned} \quad (7.5)$$

Where T is the similarity transformation matrix and transformed system has a staircase form with the unobservable modes in A_{uo} . Transformed matrix portions (C_o, A_o) is observable and the eigenvalues of A_{uo} are the unobservable modes. Following commands have been added to the previous m file;

```
[Abar_az, Bbar_az, Cbar_az, T_az, k_az] = obsvf(Aaz, Baz, Caz)
sum(k_az)
[Abar_el, Bbar_el, Cbar_el, T_el, k_el] = obsvf(Ael, Bel, Cel)
sum(k_el)
Abar_az, Bbar_az, Cbar_az, T_az, k_az] = ctrbf(Aaz, Baz, Caz)
sum(k_az)
[Abar_el, Bbar_el, Cbar_el, T_el, k_el] = ctrbf(Ael, Bel, Cel)
sum(k_el)
```

The outputs for observable state numbers are 14 for azimuth and 10 for elevation. From this result, both axes models seem fully observable. The problem with the observability analysis could be the numerical rank of the observability matrices [34]. With the last two command sets, controllability has also been checked and the controllable state numbers are 14 for azimuth and 10 for elevation. Our 7-dof azimuth and 5-dof elevation state space models are full state controllable and observable. When the default tolerance “ $tol = \max(\text{size}(A)) * \text{eps}(\text{norm}(A))$ ” is changed for the Matlab function “ $\text{rank}(A, tol)$ ” as;

```
rank(THETA_az, 1)
rank(THETA_el, 1)
```

The results are 14 for the azimuth and 10 for the elevation. Therefore, Matlab function “rank” should be used carefully not to cause any mislead [34].

7.3 Luenberger Observer and Muzzle Rate Stabilization

An observer is a mathematical structure that combines sensor output and plant excitation signals with models of the plant and sensor [13]. An observer provides feedback signals that are superior to the sensor output alone. The Luenberger observer combines five elements (Figure 7.2):

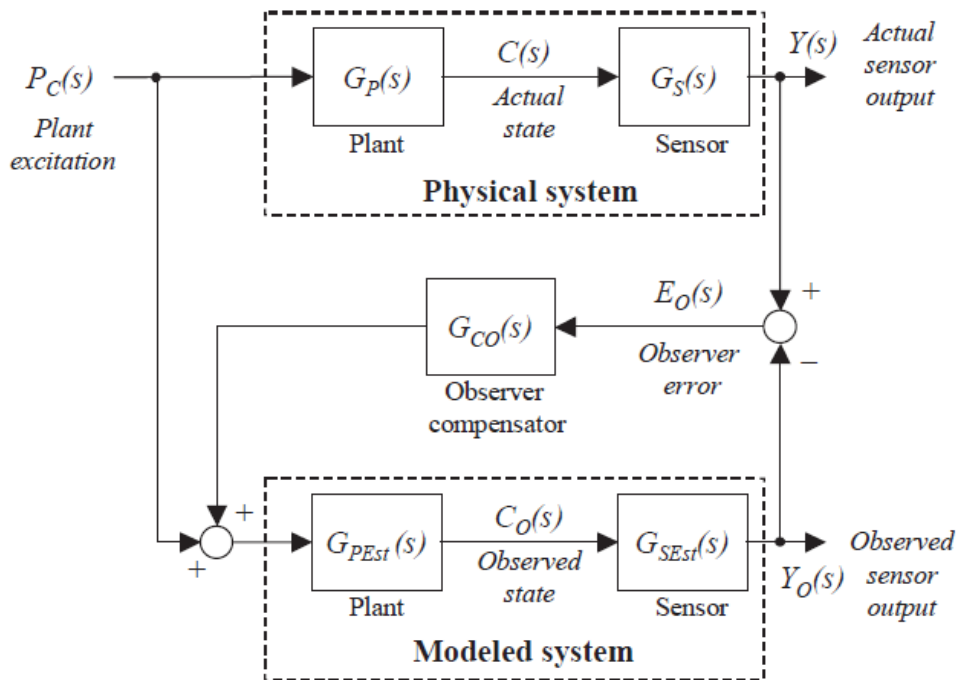


Figure 7.2. General Form of the Luenberger Observer

- a sensor output, $Y(s)$,
- a power converter output (plant excitation), $PC(s)$,
- a model (estimation) of the plant, $GPEst(s)$,
- a model of the sensor, $GSEst(s)$, and
- a PI or PID observer compensator, $GCO(s)$.

In our physical case, there is a single sensor for each axis, a dual axes feedback gyro, integrated onto and measuring the angular rates of the trunnion (part θ_{m1}) in azimuth and elevation, $\dot{\theta}_{m1AZ}$ & $\dot{\theta}_{m1EL}$, and a feedforward gyro for each axis, measuring the disturbance in appropriate direction. The study will be extended for the case that a linear accelerometer is

utilized physically at the muzzle, measuring \dot{z}_5 (Figure3.1) and \dot{y}_5 (Figure3.2). This data will be used to generate the muzzle rates and stabilization of the muzzle directly unlike the method used in the previous chapters (Figure7.3).

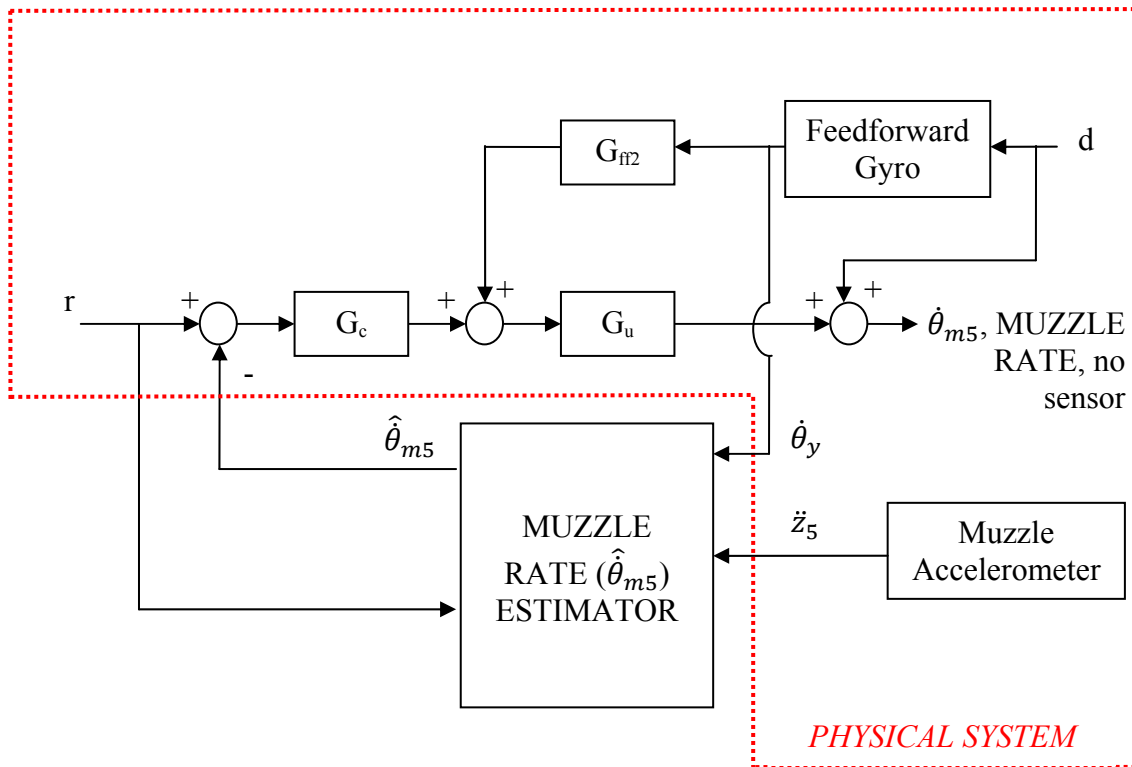


Figure 7.3. Muzzle Rate Stabilization Scheme

Elevation and azimuth models developed in Chapter 3 will be assumed as the physical system. By modifying the model parameters slightly, an estimator model will be formed and a Luenberger Observer will be constructed to correct the accelerometer output signals (Figure7.4). For the new control schematics, feedback (G_c) and feedforward (G_{ff2}) controllers will be re-tuned. It should be remembered that z is the linear degree of freedom in azimuth and θ_y is the yaw disturbance again for azimuth. Their respective nomenclatures in elevation are y and θ_p .

With the development of micro fabrication technology, Micro-Electro-Mechanical System (MEMS) which integrated mechanical sensors and actuators with electrical circuits has been broadly applied to various fields such as airbags in automotives, bio-medical area, and military system.

MEMS technology gives possibility to integrate complex systems into a small single chip with low cost and multiple functions. However, the miniaturized devices also reduce the signal to noise ratio (SNR) and the dynamic range (DR), and also increase the system uncertainties during the manufacturing process [14].

Inertial MEMS sensors including MEMS accelerometers and gyroscopes occupy more than 20% of MEMS markets. MEMS accelerometers alone have the second largest sales volume after pressure sensors. As an acceleration and deceleration sensor, MEMS accelerometers have been extensively applied to airbag deployment systems in automobiles [15].

Figure 7.5 shows the performance and cost of different MEMS fabrication technologies which can be used to manufacture MEMS accelerometers. Capacitive sensing mechanism structure is the most popular in MEMS accelerometer.

As shown in Figure 7.5, bulk and surface micromachining technologies are two particular methods used in fabricating capacitive sensing accelerometers. Compared to surface micro-machined accelerometers, the bulk micromachined devices have high sensitivity and low noise floor since they have large mass and more sensing capacitors. However, the surface micromachined devices are low cost and easy to be integrated with signal processing circuits [16] while low cost and easy implementation are always two desirable features in MEMS.

Moreover, capacitive sensing mechanism is currently the most popular sensing technology in MEMS accelerometer. Compared to other two sensing mechanisms which are piezoresistive sensing and tunnel current sensing, capacitive sensing has the advantages of low power dissipation, low cost, and low temperature coefficients [15]. Therefore, in this thesis, we will utilize a muzzle accelerometer, based on surface micro-machined capacitive technology.

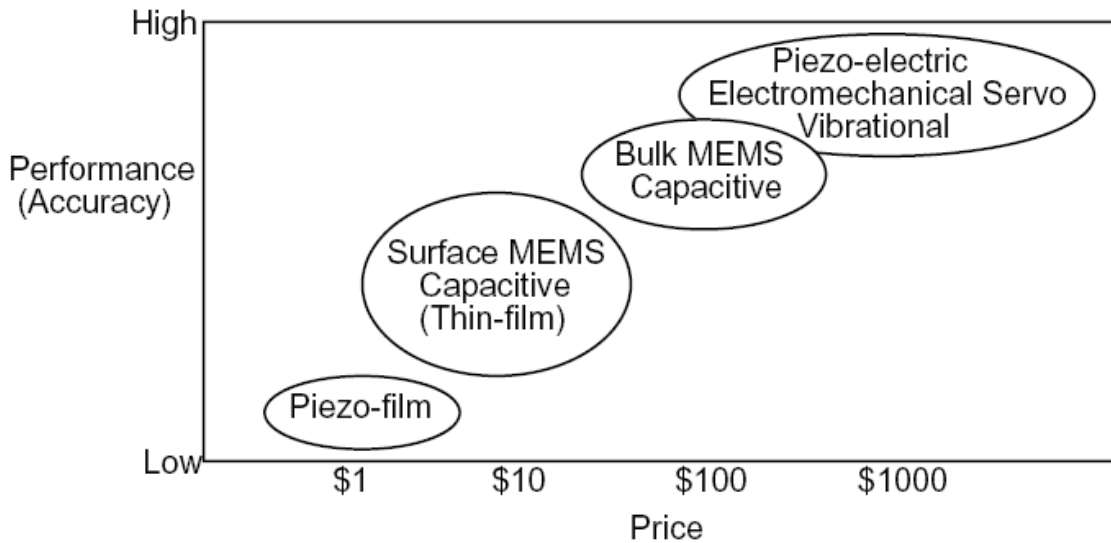


Figure 7.5. Performance and Cost of Different MEMS accelerometer [15]

Moreover, capacitive sensing mechanism is currently the most popular sensing technology in MEMS accelerometer. Compared to other two sensing mechanisms which are piezoresistive sensing and tunnel current sensing, capacitive sensing has the advantages of low power dissipation, low cost, and low temperature coefficients [15]. Therefore, in this thesis, we will utilize a muzzle accelerometer, based on surface micro-machined capacitive technology.

Brownian noise caused by damping effect and electronic noise from CMOS readout circuit are two major noise sources in both bulk and surface micromachined capacitive accelerometers. Brownian noise is higher in surface micromachined accelerometers than in bulk micromachined ones because of the small mass of a surface micro-machined accelerometer. Noise floor is the measurement of the signal created by noise sources and unwanted signals. We cannot detect a signal if its value is under noise floor. The value of noise floor normally changes with different frequency and has a unit relates to frequency. The Brownian noise in surfaced micro-machined accelerometers has the noise floor between $10\sim 100\mu g/\sqrt{Hz}$. The noise floor of electronic noise in the surface micromachined accelerometer is above $20\mu g/\sqrt{Hz}$ and is much more critical than the one in the bulk micromachined accelerometers because of the lower capacitance in surface micro-machined accelerometers[14].

Besides noise, the sensing accuracy of low-cost surface micro-machined accelerometer is also limited by the nonlinearities and system uncertainties due to fabrication imperfections. Therefore, a feedback controller is essential for surface micro-machined accelerometers to compensate for the fabrication imperfections and improve its performance. It can reduce the offsets caused by mechanical imperfections and increase the bandwidth, sensitivity and dynamic range of accelerometers. Nevertheless, noise is still a challenging problem to the surface micro-machined accelerometers even with a feedback controller. This leads the use Kalman filter to reduce the noise. The Kalman filter functions as an observer in feedback control [14].

Three major capacitive sensing accelerometer circuit designs for accelerometers are reported in current literature. They are modulation/demodulation voltage sensing [16, 17, 18], current sensing [19] and switch capacitor charge sensing [20]. The most popular method is switch capacitor read-out circuit sensing, which is also the sensing method for the accelerometer used in this thesis. The modulation/demodulation voltage sensing is more accurate than the switch capacitor charge sensing, but it requires more electronic components such as buffer, amplifier, and high speed sampling switch. The modulation/demodulation voltage sensing is expensive and makes the fabrication process complicated. The current sensing is noisy as mentioned in [19].

In addition, two major control methods are applied in capacitive accelerometers. They are force-to-rebalance closed-loop control [18, 21] and a compensator in $\Delta\Sigma$ loop control [22, 23, 24, 25]. Currently, most MEMS products use open-loop control method instead of closed-loop control due to their space limit and their low requirements for dynamic range. The complication and high cost of closed-loop operation also limit its use. However, compared to open-loop control method, closed-loop control is more robust against noise and external disturbances. Force-to-rebalance closed-loop control has been applied in Analog Devices' recent ADXL series MEMS accelerometers. A readout circuit and a $\Delta\Sigma$ loop with feed-back compensator have been introduced in [22], [23], [24] and [25]. The $\Delta\Sigma$ modulators are also called over-sampling Analog to Digital (AD) converters. A digital signal has higher noise immunity than that of analog signal. In addition, the digital signal can be easily implemented using powerful digital signal process (DSP) algorithm [14].

The bulk micro-machined accelerometer in [22] gives a lower noise floor at $3.7 \mu g / \sqrt{Hz}$, because it has a big mass of 10^{-6} kg and and large capacitance at μF level and also uses

$\Delta\Sigma$ compensator control. In [26], bulk micro-machining technology shows a more significant noise floor at $2,200 \mu g/\sqrt{Hz}$ due to nonlinearities and uncertain parameter effects through open-loop control method. The capacitive accelerometer in [23] shows more noise at $1,600 \mu g/\sqrt{Hz}$ since it uses surface micro-machined process with smaller mass at 10^{-9} kg and capacitance at pF . All of the accelerometers in [17], [18], [24] and [25] are surface micro-machined accelerometers with modulation voltage sensing. But they use different control methods including open-loop control [17], force-to-rebalance control [18] and $\Delta\Sigma$ compensator [24] [25]. In [24], an advanced sensing method named chopper stabilized voltage modulation is used and makes the noise floor at $4.6 \mu g/\sqrt{Hz}$. Force-to-rebalance control method in [18] gives a $500 \mu g/\sqrt{Hz}$ noise floor which is larger than open-loop control in [17] at $200 \mu g/\sqrt{Hz}$ because of controller post-set [14]. From above the literature review, we can see the more complicated and advanced sensing and control methods we use, the smaller noise floor we will obtain.

Although different fabrication methods (such as surface and bulk micro-machining fabrications) could affect the performances of MEMS accelerometers in noise rejection and sensitivity, appropriate sensing and control strategy could compensate for the mechanical imperfections and improve the performance of accelerometers. The growing applications of control designs have been investigated and used to overcome the noise problems caused by low cost surface micromachined fabrication[14]. In this thesis, we will implement a readily available surface micro-machined MEMS capacitive accelerometer with switch capacitive sensing and force-to-rebalance control strategy.

For the muzzle accelerometer, a modified version of Analog Devices ADXL203 MEMS accelerometer model will be implemented in the thesis. Sensor model created in Simulink[®] readily available will be taken from the manufacturer's development tools and will be modified to conform the maximum range. ADXL203 MEMS accelerometer has a maximum range of $\pm 1.7g$. But in our case, simulation results show that muzzle has $\pm 6.5g$ linear acceleration level transverse to azimuth axis and $\pm 3.8g$ linear acceleration level transverse to elevation axis. Therefore, maximum scale will be extended to $\pm 8g$ by modifying the original sensor model. To accomplish this, sensitivity line in the constants of the original .m file has been changed from $1V/g$ to $1*(1.7/8) V/g$.

Figure7.6 shows the simulink blocks for the modified ADXL203 model. The .m file used to load the axes models and the accelerometer constants file has been written as follows;

```

%*****MUZZLE STABILIZATION CHAPTER7*****
%BY: TURKER KARAYUMAK, METU MECHANICAL ENGINEERING*****
%*****

%*****RUN MODEL PARAMETERS*****
elevation_final3;
azimuth_final3;

%*****READ ACCELEROMETER CONSTANTS*****

%   ADXL203_constants.m from AnalogDevices, Inc.
%   Coefficients for 5V operation only
%   Model coefficients

stg   = .75           % g   - Self test magnitude
a     = 8.374e-10    %     - X,Y axis beam coefficient
b     = 5.788e-6     %     - X,Y axis beam coefficient
sens  = 1.0          % V/g  - Sensitivity (original)
sens  = 1.0*(1.7/8) % V/g  - Sensitivity (modified)
bf    = 50           % Hz   - 3db frequency set by ext. cap.
K     = 12.54*sens   %     - Amplifier gain
e     = 2.27e-5      %     - Demod filter effects
h     = 1/(6.28*bf)  %     - Output filter coefficient
w     = 8.250e-10    %     - Z axis beam coefficient
g     = 2.872e-5     %     - Z axis beam coefficient
zx    = 0            %     - Z response factor, Xchannel
zy    = 0            %     - Z response factor, Ychannel
yx    = 0            %     - Y response factor, Xchannel
xy    = 0            %     - X response factor, Ychannel

%*****OBSERVER COMPENSATORS*****
Kp_co_az=1; %Azimuth observer compensator proportional gain
Ki_co_az=15; %Azimuth observer compensator integrator gain
Kd_co_az=0; %Azimuth observer compensator derivative gain

Kp_co_el=1; %Elevation observer compensator proportional gain
Ki_co_el=15; %Elevation observer compensator integrator gain
Kd_co_el=0; %Elevation observer compensator derivative gain

```

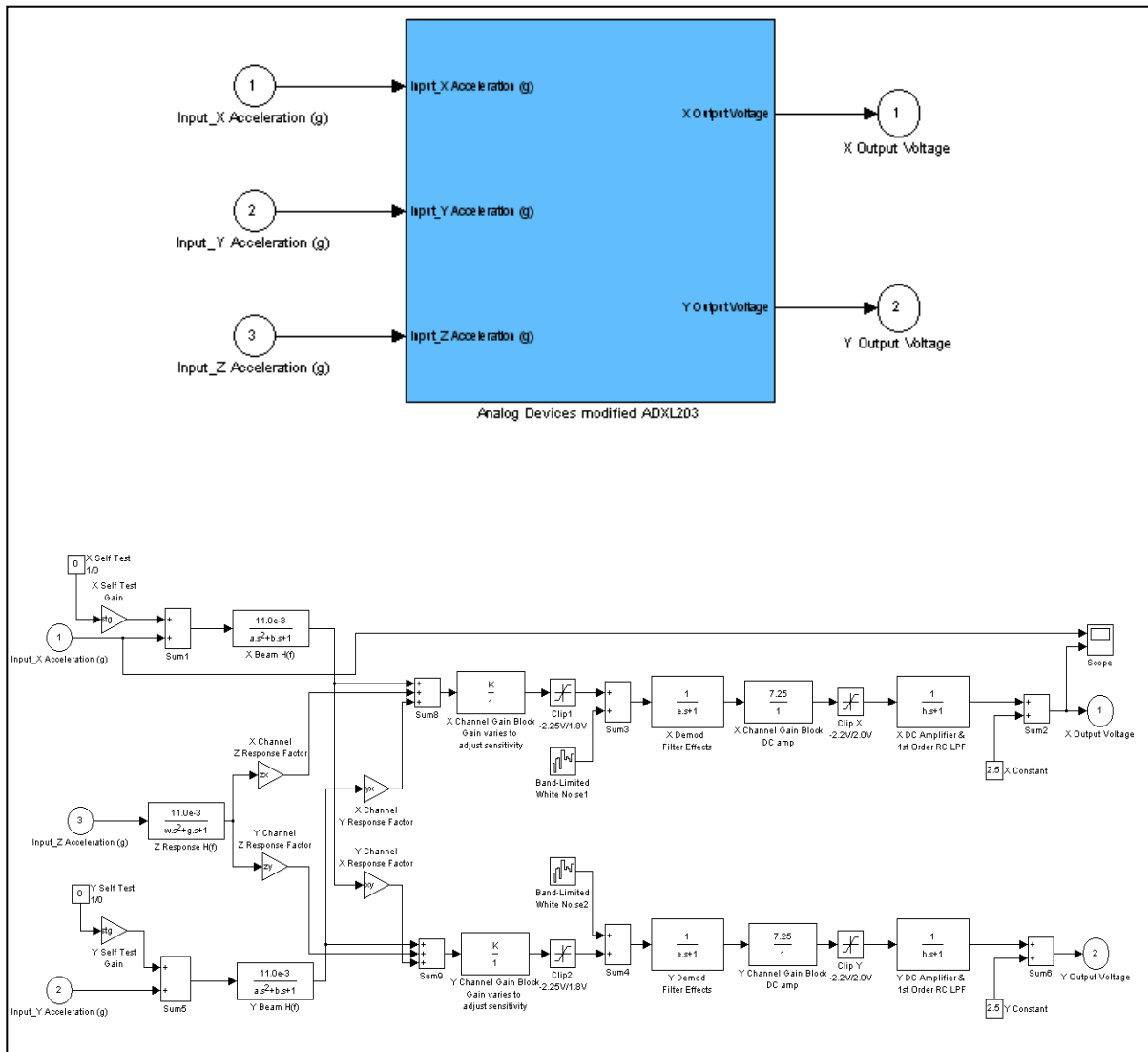


Figure 7.6. Modified Analog Devices ADXL203 MEMS Accelerometer Behavioral Model

Input acceleration in the 3rd axis stands for the cross coupling of the acceleration in this axis to other two axes, being measured. But it can be seen in the .m code that *zx*, *zy*, *yx* and *xy* all set to zero, meaning no axis cross couples to any of the other. This is the manufacturer’s specification.

7.3.2 Muzzle Rate Stabilization

After creating the muzzle accelerometer behavioral model, muzzle rate stabilization scheme (Figure 7.3) has been formed and run in Simulink® (Figure 7.7).

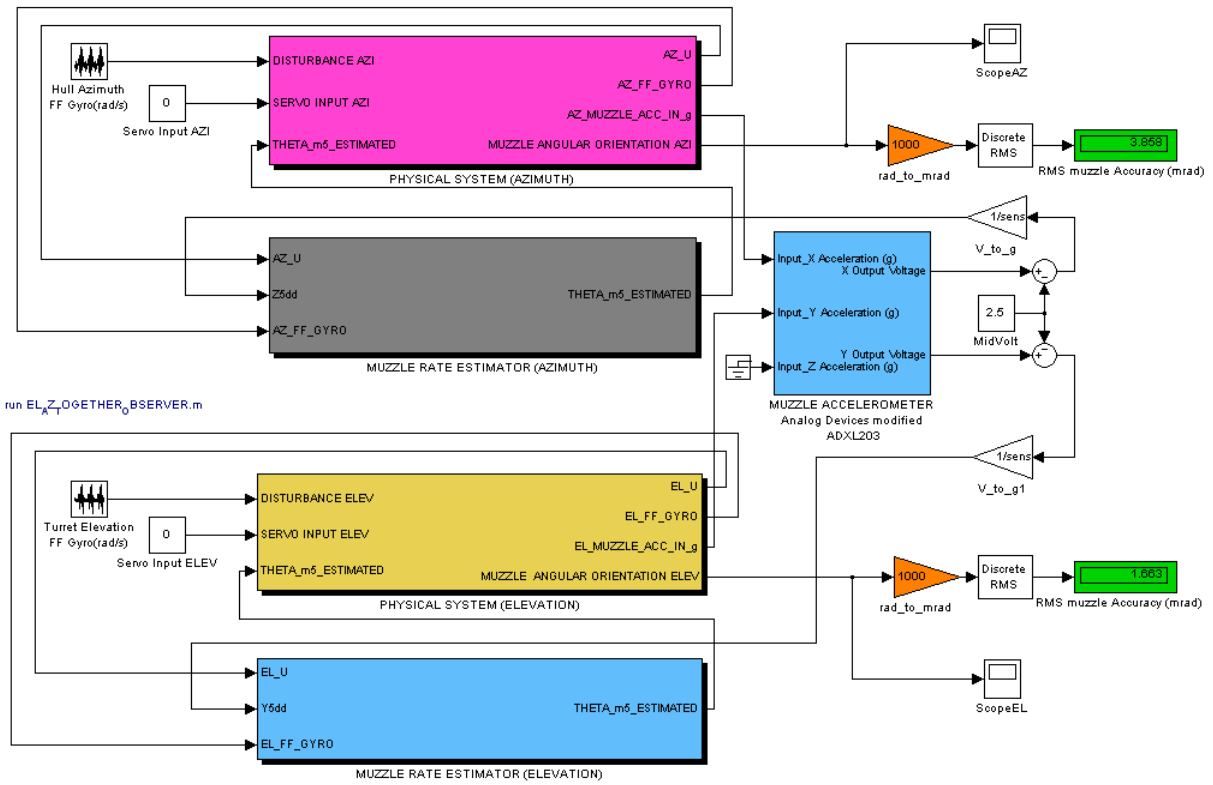


Figure 7.7. Muzzle Rate Stabilization Scheme

Physical system block (Figure 7.8) represent the real system, in which the loop has been closed by the estimated muzzle rate, $\hat{\theta}_{m5}$.

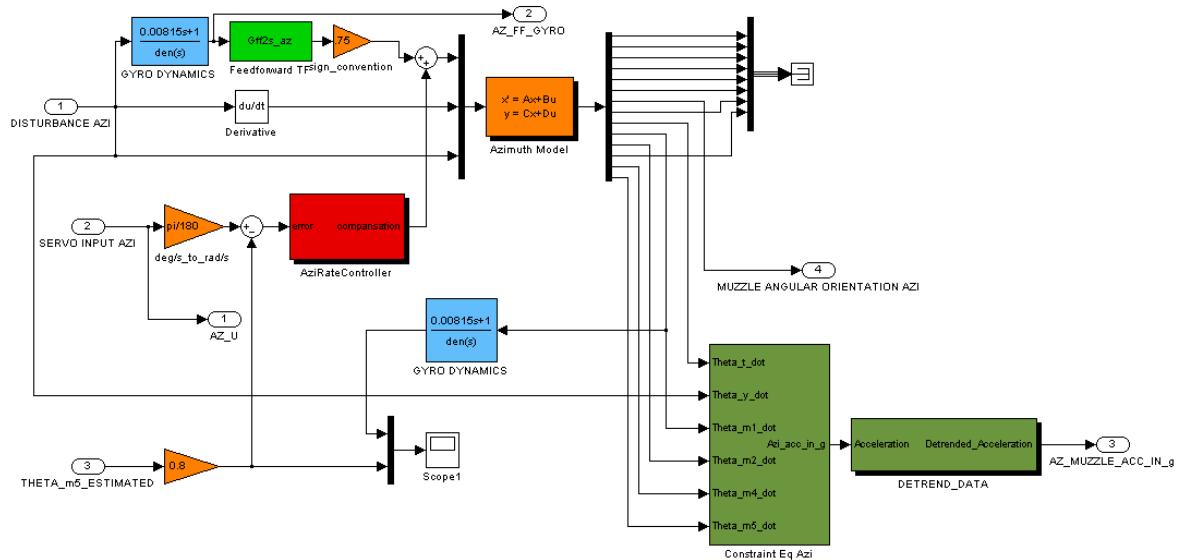


Figure 7.8. Physical System Block (Azimuth)

Linear acceleration output (\ddot{z}_5, \dot{y}_5) of the constraint equations block (Figure 7.9) has been de-trended with a detrend block (Figure 7.10), in which a Matlab function is fed with the 10 sample data buffer.

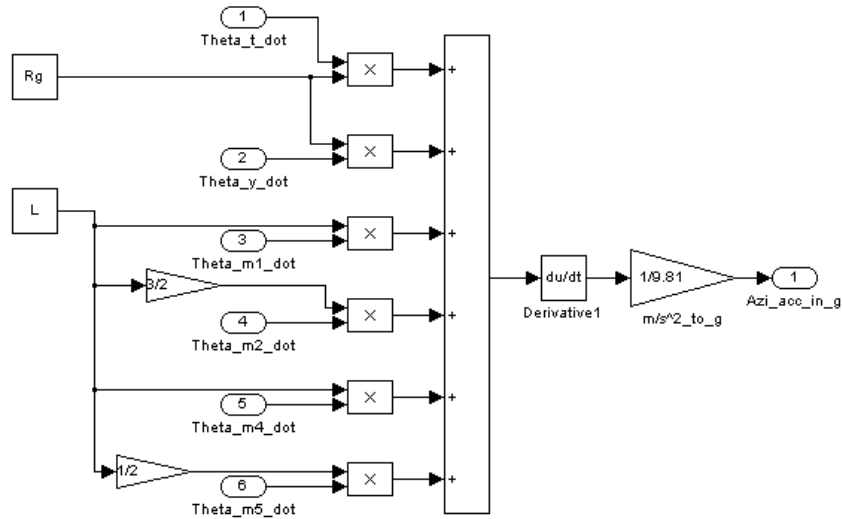


Figure 7.9. Constraint Equations Block

Simple Matlab function “my_detrend” uses the function ”detrend” over a buffered data being stored as a 1x10 vector.

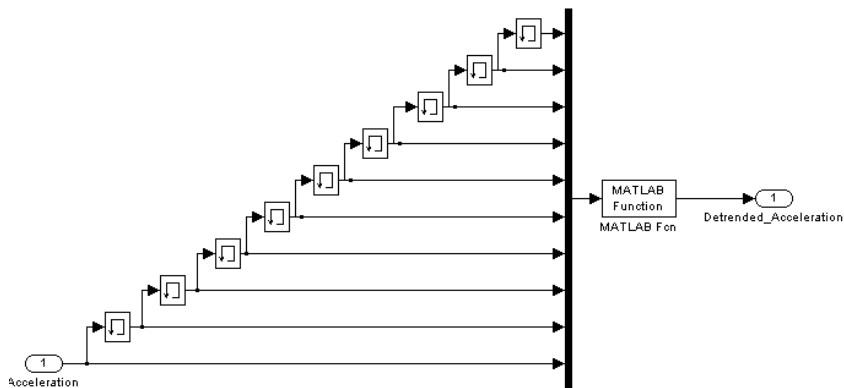


Figure 7.10. Detrend Block

```
function denemem= my_detrend(u)
myvect = [u(1);u(2);u(3);u(4);u(5);u(6);u(7);u(8);u(9);u(10)];
y=detrend(myvect,'linear',10);
denemem=y(1);
%Sample time is 0.002s
```

Muzzle rate estimator block includes the modeled system and the estimator compensator (Figure 7.11).

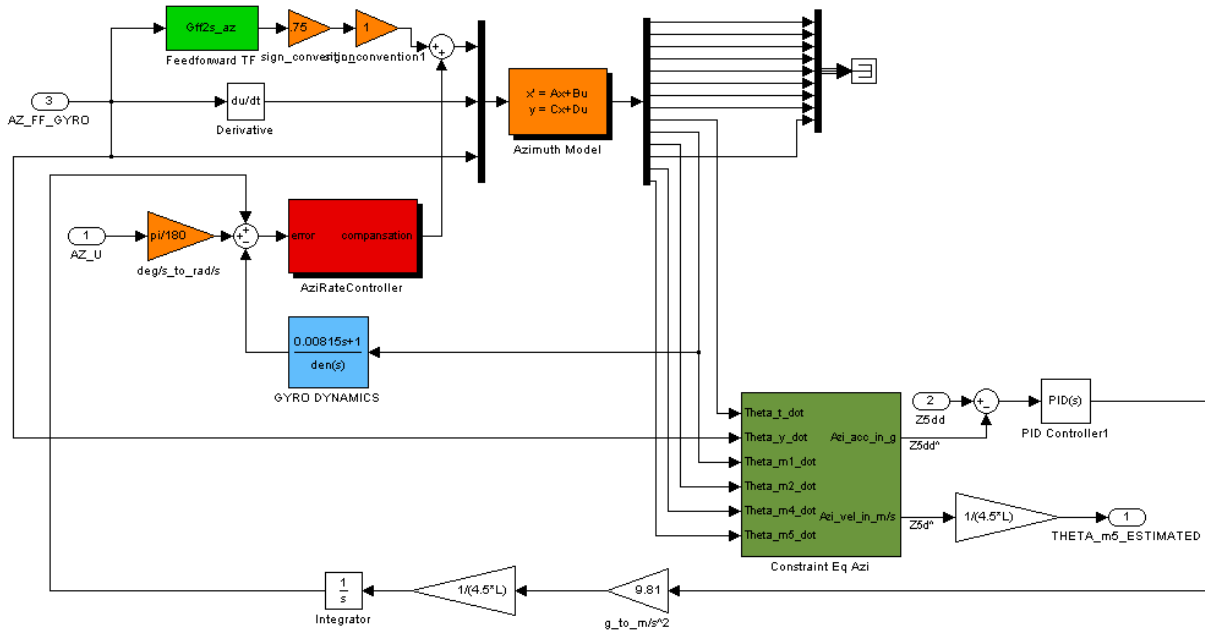


Figure 7.11. Muzzle Rate Estimator Block

Similarly, the same detrend block has been implemented to the constraint equations block of the muzzle rate estimator (Figure 7.12), this time for \hat{z}_5 and \hat{y}_5 .

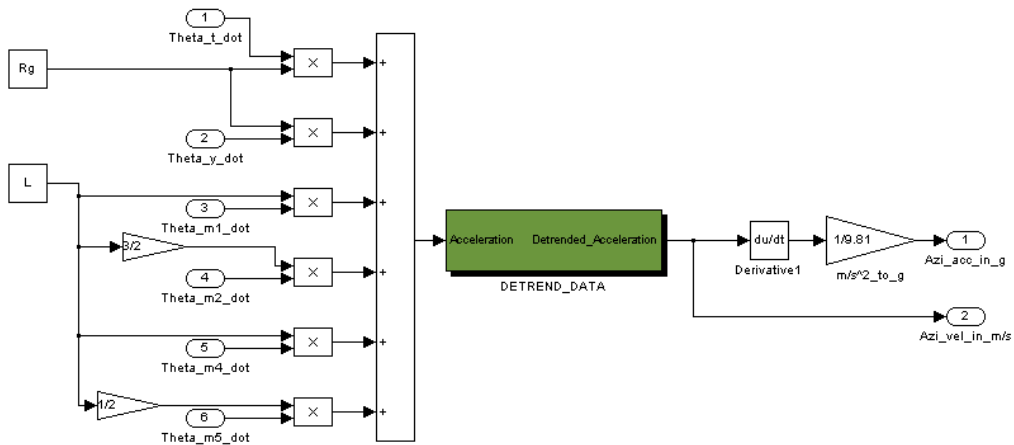


Figure 7.12. Muzzle Rate Estimator Constraint Equations Block

As the estimator compensator, a PID scheme was tried (Figure 7.11). But after several trials, derivative term was observed to cause excessive oscillations in the predicted muzzle rate outputs because of the noise in the MEMS accelerometer output. Therefore derivative gains are entered as zeros to yield in a PI scheme for both axes.

When the simulation is run, the muzzle stabilization accuracy is calculated as 3.858mrad in azimuth and 1.663mrad in elevation. These accuracies do not meet the 0.5mrad requirement for both elevation and azimuth despite a huge amount of commissioning effort has been made to reach these levels. This result is not surprise since in the last simulation model, the feedback gyro has not been used and the loop has been closed by a simple MEMS accelerometer.

Then what could be the benefit of using a muzzle accelerometer? The right idea would be to use the muzzle accelerometer, which is output refined by an estimator, together with the feedback gyro, although this gyro measures the angular rates of the trunnion ($\dot{\theta}_{m1}$), where it can practically be located at. Stabilize the gun using the rate gyro as conventionally done in Chapter 5 and use the refined accelerometer output to monitor the muzzle deflection just like a dynamic muzzle reference system is utilized. Then either give the necessary corrections to the drives as servo inputs or use the information to predict the future deflection values in the coincidence algorithm as have been done in Chapter 6.

CHAPTER 8

CONCLUSION AND FUTURE WORK

Ultimate performance criteria for a main battle tank is the “First Round Hit Probability (FRHP)” figure, no matter how good is the gun and turret stabilization performance is. The final decision maker to enable or inhibit a fire trigger request made by a tank gunner is the coincidence algorithm. The performance of the coincidence algorithm directly influences the FRHP figure. Major contribution of this thesis to the literature is the complex coincidence algorithm design, which is absent in most of the fire control systems in use and in literature as well. Existing coincidence algorithms only monitor the stabilization error signal measured with the feedback gyro mounted on the trunnion and permits fire if this error signal is within a pre-defined range. These conventional coincidence algorithms do not consider the muzzle deflection due to barrel flexure and the time elapsed by the ammunition from being fired in the breech until exit from the muzzle. Proposed complex coincidence algorithm by this study takes the barrel flexure and the time delay into account and predicts the future orientation of the muzzle to permit or inhibit the fire trigger request by the gunner. By the use of this proposed technique, a 100% FRHP level can be achieved in theory.

In this study, a parametric model for a main battle tank electric gun turret drive system stabilization controller has been developed. Main scope was the study of the muzzle deviation due to barrel flexibility. Traverse and elevation dynamics has been modeled to include the drive-line and barrel flexibilities. Order of the models has been kept large enough to cover the frequencies dominant in the interest scope but at the same time low enough to create a parametric model which can be used in real-time fire control computers.

Therefore a 5-dof elevation and a 7-dof traverse models have been implemented. These models have been used to design a classical feedback and feedforward controllers

which performed good enough to meet 0.5mrad stabilization accuracies. Meanwhile, the theory of the feedforward control has been presented and the effect on enhancing the stabilization accuracy has been monitored. Instability of the feedforward controller and methods to remove the instabilities by reducing the order of the controller transfer function by “*Hankel Singular Value Decomposition*” has been implemented.

After satisfactory results have been obtained from the stabilization controller, a special coincidence algorithm has been implemented by time-series analysis of the disturbance signal which is constantly being measured by the feedforward gyro. Necessity of predicting the future muzzle angular orientation due to the latency in fire is discussed and by using autoregressive modeling of the disturbance signal, future values of the disturbance signal has been entered into the observer model. The prediction horizon has been set to the time delay value between the trigger is pulled by the gunner and the ammunition exit from the muzzle. By checking the future coincidence within a very narrow window (0.05mrad) a 100% first round hit probability in theory has been achieved. This is assured since the coincidence inhibited the fire signals which were to miss the aiming point with a large error.

Finally a different control strategy has been tried. Instead of a conventional feedback and feedforward stabilization controller which use an enhanced coincidence algorithm, effort has been given to stabilize the muzzle itself. Since a fiber optic rate gyro cannot be mounted on the gun muzzle due to excessive shocks induced during tank fire and other practical design concerns, a MEMS accelerometer has been used as a muzzle rate predictor. Raw signal output of the MEMS accelerometer has been refined by using a Luenberger observer. Although a plenty of commissioning effort has been given to have satisfactory stabilization accuracies, the muzzle stabilization accuracy has been obtained as 3.858mrad in azimuth and 1.663mrad in elevation, which are more than 0.5mrad satisfaction criteria. Although the stabilization accuracy satisfaction criteria couldn't be achieved, the result was very good at the order of magnitude, especially in the vicinity of a fiber optic feedback gyro which has a commercial value around 10,000\$ and instead using a 10\$ MEMS accelerometer. With the fiber optic feedback gyro and feedforward gyro implemented in Chapter5, stabilization accuracy values for elevation was 0.492mrad in azimuth and 0.072mrad in elevation which met the 0.5mrad requirement

As a future work, elevation and traverse models can be made more complex by adding enhanced friction models including the static and dynamic behavior [29]. Imbalance can be added as well and the effect of cant angles both on imbalance moment and static deflection on barrel can be studied. Electric gun turret drive system modeling can be enhanced by implementing the drive servomotor and gearbox characteristics. A servo-amplifier model can also be added to see the effects of amplifier efficiencies. System identification methods can be used to try different control schemes like “*General Predictive Control*”. Time-series analysis and future prediction can be studied by implementing neural network architecture. Also a MEMS type rate gyro can be tried for muzzle stabilization instead of the MEMS accelerometer study.

Despite the inexistence of the studies listed as the future work, the methodology and level of complexity kept for this thesis is quite appropriate and effective for real-time hardware implementation of a fire control computer.

REFERENCES

- [1] **Ogorkiewicz, R.M. (1991)**, *"Technology of Tanks Vol.1, Vol.2"*, Jane's Information Group Limited.

- [2] **Regelin, K.(1980)**, *"Armoured Vehicles"*, International Defense Review.

- [3] **Purdy, J.D. (2005)**, *"Introduction to Weapon and Gun Control Systems for Main Battle Tanks"*, Class Presentations, Cranfield University - Royal Military College of Science.

- [4] **Şahin, S. (2001)**, *"Stabilization and Orientation of a Tank Gun"*, M.S. Thesis, METU Mechanical Engineering Department, Ankara.

- [5] **Afacan, K. (2004)**, *"Modeling and Control of a Stabilization System"*, M.S. Thesis, METU Mechanical Engineering Department, Ankara.

- [6] **Karayumak, T. (2003)**, *"Design and Manufacturing of a Two Degrees of Freedom Gyro Stabilized Opto-Mechanical Platform"*, M.S. Thesis, METU Mechanical Engineering Department, Ankara.

- [7] **Sandu, C., Freeman, J.S. (2003)**, *"Three-Dimensional Multibody Tracked Vehicle Modeling and Simulation"*, A Technical Paper, Michigan Technological University.

- [8] **Hameed, A. (2005)**, *"Gun Dynamics"*, Class Presentations, Cranfield University - Royal Military College of Science.

- [9] **MathWorks (2010)**, “*MATLAB® 7.11*”, Product Help Documentations.
- [10] **Touretzky, D., Laskowski, K. (2006)**, “*Neural Networks for Time Series Prediction*”, Artificial Neural Networks Lecture Class Presentations, Carnegie Mellon University.
- [11] **Moon, S., Cole, D., Clark, R. (2005)**, “*Real-time Implementation of Adaptive Feedback and Feedforward Generalized Predictive Control Algorithm*”, A Technical Paper, Duke University.
- [12] **Bemporad, A. (2010)**, “*Observability Analysis*”, Automatic Control Lecture Class Presentations, University of Trento.
- [13] **Ellis, G. (2002)**, “*Observers in Control Systems*”, Academic Press.
- [14] **Zhang, K. (2010)**, “*Sensing and Control of MEMS Accelerometers Using Kalman Filter*”, M.S. Thesis, Cleveland State University Electrical Engineering Department.
- [15] **Thai-Ran, H. (2008)**, “*MEMS & Microsystems: Design, Manufacture, and Nanoscale Engineering*”, Wiley Interscience.
- [16] **Bernstein, J. (1999)**, “*Low-Noise MEMS Vibration Sensor for Geophysical Application*”, Journal of Microelectromechanical System, vol.8, no. 4, pp. 433-438.

- [17] **Zhang, G. (1998)**, “*Design and Simulation of a COMS-MEMS Accelerometer*”, M. S. Thesis, Carnegie Mellon University Department of Electrical and Computer Engineering.
- [18] **Doscher, J.** “*Using iMEMS Accelerometers in Instrument Applications*”, Analog Devices Technical Note, available at <http://www.analog.com/industry/iMEMS/Library/>.
- [19] **Fedder, G.K. (1997)**, “*Simulation of Microelectromechanical System*”, Doctoral Dissertation, University of California at Berkeley Department of Electrical Engineering and Computer Sciences.
- [20] **Smith, T. (1994)**, “*A 15b Electromechanical Sigma-Delta Converter for Acceleration Measurements*”, in *Proc. of IEEE Int. Solid-State Circuits Conf. Digest of Technical Papers*, pp. 160-161, San Francisco, CA.
- [21] **Chau, K. H., Lewis, S., Zhao, Y. (1995)**, “*An Integrated Force-Balanced Capacitive Accelerometer for Low-G Applications*”, in *Proc. 8th Int. Conf. Solid-State Sensors and Actuators, and Eurosensors IX*, pp. 593-596, Stockholm, Sweden.
- [22] **Yazdi, N., Najafi, K. (1999)**, “*An Interface IC for A Capacitive μ Accelerometer*”, in *Proc. of IEEE Int. Solid-State Circuit Conf. Digest of Technical Papers*, pp. 274-275, San Francisco, CA.
- [23] **Lu, C., Lemkin, M., Boser, B. (1995)**, “*A Monolithic Surface Micromachined Accelerometer with Digital Output*”, in *Proc. of IEEE Solid-state Circuit Conf. Digest of Technical Papers*, pp.160-161, San Francisco, CA.

- [24] Kraft, M. (1997), "*Closed-loop Digital Accelerometer employing oversampling conversion*", Ph.D. Dissertation, Coventry University, School of Engineering, UK.
- [25] Zhang, G. (2002), "*Sensing and Control Electronics for Low-Mass Low-Capacitance MEMS Accelerometer*", Ph.D. Dissertation, Carnegie Mellon University.
- [26] Motorola, "*XMMAS40G10D micromachined accelerometer*", Datasheet, Phoenix AZ, available at www.datasheetarchive.com/XMMAS40G10D-datasheet.html.
- [27] Scholar, C., Ma, Z.D., Perkins, N.C., "*Modeling Tracked Vehicles Using Vibration Modes: Development and Implementation*", A Technical Paper, University of Michigan.
- [28] Wong, J. Y. (1993), "*Theory of Ground Vehicles*", John Wiley, New York.
- [29] Pongpunwattana, A. (1999), "*Modelling and Control of a Single-link Flexible Robotic Arm Under the Influence of Mechanical Friction*", M.S. Thesis, University of Washington Mechanical Engineering Department.
- [30] Purdy, D. J., (1998), "*Main Battle Tank Stabilisation Ratio Enhancement Using Hull Rate Feedforward*", J. Battlefield Tech. Vol. 1, No. 2, July 1998.
- [31] Purdy, D. J., (2006), "*Gun Barrel Models for Use in Weapon Control System Investigations*", J. Battlefield Tech. Vol. 9, No. 1, March 2006.

[32] Purdy, D. J., (1996), *“Modelling and Simulation of a Weapon Control System for a Main Battle Tank”*, The 8th US Army Symposium on Gun Dynamics, Newport, Rhode Island, May 1996.

[33] Purdy, D. J., (1994), *“High Precision Tip Angle Control of a Flexible Beam with Drive Line Dynamics”*, Institution of Electrical Engineers international conference “Control '94”, Warwick University 1994.

[34] Paige, C. C., (1981), *“Properties of Numerical Algorithms Related to Computing Controllability”*, IEEE Transactions on Automatic Control Vol. AC-26, No. 1, February 1981.

Appendix A1 – Derivation of M, C and K Matrices for Traverse Axis

FBD of Pinion

$$kd(\theta_d - \theta_p) - fdR_p = 0$$

$$\implies f_d = \frac{kd}{R_p}(\theta_d - \theta_p)$$

FBD of Turret

$$I_t \theta_{tdd} = I_a \theta_{ydd} + \frac{kd}{R_p}(\theta_d - \theta_p)R_t - f_m I R_g - k(g(\theta_t - \theta_m)) - ct(\theta_{td} - \theta_{yd})$$

$$\implies I_t \theta_{tdd} = I_a \theta_{ydd} + \frac{kd}{R_p}(\theta_d - \theta_p)R_t - \left[m_1 \left(R_g \theta_{tdd} + R_g \theta_{ydd} - \frac{1}{2} \theta_{m1dd} \right) + \left[m_2 \left(R_g \theta_{tdd} + R_g \theta_{ydd} + L \cdot \theta_{m1dd} + \frac{1}{2} L \cdot \theta_{m2dd} \right) + m_3 \left(R_g \theta_{tdd} + R_g \theta_{ydd} + L \cdot \theta_{m1dd} + \frac{3}{2} L \cdot \theta_{m2dd} - \frac{1}{2} L \cdot \theta_{m3dd} \right) + m_4 \left(R_g \theta_{tdd} + R_g \theta_{ydd} + L \cdot \theta_{m1dd} + \frac{3}{2} L \cdot \theta_{m2dd} + \frac{1}{2} L \cdot \theta_{m4dd} \right) + m_5 \left(R_g \theta_{tdd} + R_g \theta_{ydd} + L \cdot \theta_{m1dd} + \frac{3}{2} L \cdot \theta_{m2dd} + L \cdot \theta_{m4dd} + \frac{1}{2} L \cdot \theta_{m5dd} \right) \right] R_g - k(g(\theta_t - \theta_m)) - ct(\theta_{td} - \theta_{yd})$$

FBD of Drive

$$I_d \theta_{ddd} = T_d - cd \cdot \theta_{dd} - kd(\theta_d - \theta_p)$$

RESULTANT SET OF EQNS .

$$15 \cdot \theta_{m5dd} = kb(\theta_{m4} - \theta_{m5}) + cb(\theta_{m4d} - \theta_{m5d}) - \frac{1}{2} L \cdot m_5 \left(R_g \theta_{tdd} + R_g \theta_{ydd} + L \cdot \theta_{m1dd} + \frac{3}{2} L \cdot \theta_{m2dd} + L \cdot \theta_{m4dd} + \frac{1}{2} L \cdot \theta_{m5dd} \right)$$

$$14 \cdot \theta_{m4dd} = kb(\theta_{m3} - \theta_{m4}) + cb(\theta_{m3d} - \theta_{m4d}) - kb(\theta_{m4} - \theta_{m5}) - cb(\theta_{m4d} - \theta_{m5d}) - \frac{1}{2} L \cdot \left[m_4 \left(R_g \theta_{tdd} + R_g \theta_{ydd} + L \cdot \theta_{m1dd} + \frac{3}{2} L \cdot \theta_{m2dd} + \frac{1}{2} L \cdot \theta_{m4dd} \right) + 2m_5 \left(R_g \theta_{tdd} + R_g \theta_{ydd} + L \cdot \theta_{m1dd} + \frac{3}{2} L \cdot \theta_{m2dd} + L \cdot \theta_{m4dd} + \frac{1}{2} L \cdot \theta_{m5dd} \right) \right]$$

$$13 \cdot \theta_{m3dd} = kb(\theta_{m2} - \theta_{m3}) + cb(\theta_{m2d} - \theta_{m3d}) - kb(\theta_{m3} - \theta_{m4}) - cb(\theta_{m3d} - \theta_{m4d}) - \frac{1}{2} L \cdot \left[m_3 \left(R_g \theta_{tdd} + R_g \theta_{ydd} + L \cdot \theta_{m1dd} + \frac{3}{2} L \cdot \theta_{m2dd} - \frac{1}{2} L \cdot \theta_{m3dd} \right) + 2m_4 \left(R_g \theta_{tdd} + R_g \theta_{ydd} + L \cdot \theta_{m1dd} + \frac{3}{2} L \cdot \theta_{m2dd} + \frac{1}{2} L \cdot \theta_{m4dd} \right) + 2m_5 \left(R_g \theta_{tdd} + R_g \theta_{ydd} + L \cdot \theta_{m1dd} + \frac{3}{2} L \cdot \theta_{m2dd} + L \cdot \theta_{m4dd} + \frac{1}{2} L \cdot \theta_{m5dd} \right) \right]$$

$$12 \cdot \theta_{m2dd} = kb(\theta_{m1} - \theta_{m2}) + cb(\theta_{m1d} - \theta_{m2d}) - kb(\theta_{m2} - \theta_{m3}) - cb(\theta_{m2d} - \theta_{m3d}) - \frac{1}{2} L \cdot \left[m_2 \left(R_g \theta_{tdd} + R_g \theta_{ydd} + L \cdot \theta_{m1dd} + \frac{1}{2} L \cdot \theta_{m2dd} \right) + 2m_3 \left(R_g \theta_{tdd} + R_g \theta_{ydd} + L \cdot \theta_{m1dd} + \frac{3}{2} L \cdot \theta_{m2dd} - \frac{1}{2} L \cdot \theta_{m3dd} \right) + 2m_4 \left(R_g \theta_{tdd} + R_g \theta_{ydd} + L \cdot \theta_{m1dd} + \frac{3}{2} L \cdot \theta_{m2dd} + \frac{1}{2} L \cdot \theta_{m4dd} \right) + 2m_5 \left(R_g \theta_{tdd} + R_g \theta_{ydd} + L \cdot \theta_{m1dd} + \frac{3}{2} L \cdot \theta_{m2dd} + L \cdot \theta_{m4dd} + \frac{1}{2} L \cdot \theta_{m5dd} \right) \right]$$

$$11 \cdot \theta_{m1dd} = k(g(\theta_t - \theta_m)) + m_1 \left(R_g \theta_{tdd} + R_g \theta_{ydd} - \frac{1}{2} \theta_{m1dd} \right) \eta_1 - kb(\theta_{m1} - \theta_{m2}) - cb(\theta_{m1d} - \theta_{m2d}) - \left[m_2 \left(R_g \theta_{tdd} + R_g \theta_{ydd} + L \cdot \theta_{m1dd} + \frac{1}{2} L \cdot \theta_{m2dd} \right) + m_3 \left(R_g \theta_{tdd} + R_g \theta_{ydd} + L \cdot \theta_{m1dd} + \frac{3}{2} L \cdot \theta_{m2dd} - \frac{1}{2} L \cdot \theta_{m3dd} \right) + m_4 \left(R_g \theta_{tdd} + R_g \theta_{ydd} + L \cdot \theta_{m1dd} + \frac{3}{2} L \cdot \theta_{m2dd} + \frac{1}{2} L \cdot \theta_{m4dd} \right) + m_5 \left(R_g \theta_{tdd} + R_g \theta_{ydd} + L \cdot \theta_{m1dd} + \frac{3}{2} L \cdot \theta_{m2dd} + L \cdot \theta_{m4dd} + \frac{1}{2} L \cdot \theta_{m5dd} \right) \right] L$$

$$I_t \theta_{tdd} = I_a \theta_{ydd} + \frac{kd}{R_p}(\theta_d - \theta_p)R_t - \left[m_1 \left(R_g \theta_{tdd} + R_g \theta_{ydd} - \frac{1}{2} \theta_{m1dd} \right) + \left[m_2 \left(R_g \theta_{tdd} + R_g \theta_{ydd} + L \cdot \theta_{m1dd} + \frac{1}{2} L \cdot \theta_{m2dd} \right) + m_3 \left(R_g \theta_{tdd} + R_g \theta_{ydd} + L \cdot \theta_{m1dd} + \frac{3}{2} L \cdot \theta_{m2dd} - \frac{1}{2} L \cdot \theta_{m3dd} \right) + m_4 \left(R_g \theta_{tdd} + R_g \theta_{ydd} + L \cdot \theta_{m1dd} + \frac{3}{2} L \cdot \theta_{m2dd} + \frac{1}{2} L \cdot \theta_{m4dd} \right) + m_5 \left(R_g \theta_{tdd} + R_g \theta_{ydd} + L \cdot \theta_{m1dd} + \frac{3}{2} L \cdot \theta_{m2dd} + L \cdot \theta_{m4dd} + \frac{1}{2} L \cdot \theta_{m5dd} \right) \right] R_g - k(g(\theta_t - \theta_m)) - ct(\theta_{td} - \theta_{yd})$$

$$I_d \theta_{ddd} = T_d - cd \cdot \theta_{dd} - kd \left(\theta_d - \frac{R_t}{R_p} \theta_t \right)$$

Re-arranging the equations so as to cast into the following form;

$$M \theta_{dd} + C \dot{\theta}_d + K \theta = I u$$

$$\theta = \begin{bmatrix} \theta_d \\ \dot{\theta}_d \end{bmatrix} \quad \theta = \begin{bmatrix} \theta_d \\ \dot{\theta}_d \end{bmatrix} \quad \theta = \begin{bmatrix} \theta_d \\ \dot{\theta}_d \end{bmatrix}$$

$$u = \begin{bmatrix} T_d \\ \theta_{ydd} \\ \theta_{yd} \end{bmatrix}$$

Solving first 6 eqns for θ and the last for T_d ;

$$-4kb\theta_m + 4kb\theta_n - 4cb\theta_m + 4cb\theta_n + 2LmSRg\theta_{ydd} + 2L^2mSRg\theta_{ydd} + 3L^2mSRg\theta_{ydd} + 2L^2mSRg\theta_{ydd} + (415 + L^2mSRg\theta_{ydd}) = -2LmSRg\theta_{ydd}$$

$$4kb\theta_m - 8kb\theta_n + 4kb\theta_m - 4cb\theta_m + 4cb\theta_n - 8cb\theta_m + 4cb\theta_n - (2LmSRg + 4LmSRg)\theta_{ydd} - (2m_4L^2 + 4m_5L^2)\theta_{m1dd} - (3m_4L^2 + 6m_5L^2)\theta_{m2dd} - (m_4L^2 + 414 + 4m_5L^2)\theta_{m4dd} - 2m_5L^2\theta_{m5dd} = 2LmSRg(m_4 + 2m_5)\theta_{ydd}$$

$$4kb\theta_m - 8kb\theta_n + 4kb\theta_m + 4cb\theta_m - 8cb\theta_m + 4cb\theta_n - (2LmSRg + 4LmSRg + 4LmSRg)\theta_{ydd} - (2m_3L^2 + 4m_4L^2 + 4m_5L^2)\theta_{m1dd} - (3m_3L^2 + 6m_4L^2 + 6m_5L^2)\theta_{m2dd} + (m_3L^2 - 413)\theta_{m3dd} - (2m_4L^2 + 4m_5L^2)\theta_{m4dd} - 2m_5L^2\theta_{m5dd} = 2LmSRg(m_3 + 2m_4 + 2m_5)\theta_{ydd}$$

$$4kb\theta_m - 8kb\theta_n + 4kb\theta_m + 4cb\theta_m - 8cb\theta_m + 4cb\theta_n - (4LmSRg + 2LmSRg + 4LmSRg + 4LmSRg)\theta_{ydd} - (4m_4L^2 + 2m_5L^2 + 4m_5L^2)\theta_{m1dd} - (6m_4L^2 + 6m_5L^2 + 412 + m_5L^2 + 6m_4L^2)\theta_{m2dd} + 2m_5L^2\theta_{m3dd} - (4m_4L^2 + 2m_5L^2)\theta_{m4dd} - 2m_5L^2\theta_{m5dd} = 2LmSRg(m_2 + 2m_3 + 2m_4 + 2m_5)\theta_{ydd}$$

$$2ktg\theta - (2ktg + 2ktg\theta_m + 2kb\theta_n - 2cb\theta_m + 2cb\theta_n - (2LmSRg + 2LmSRg + 2LmSRg + 2LmSRg - 2m\eta_1 R_g)\theta_{ydd} - (211 + 2m_2L^2 + 2m_4L^2 + 2m_5L^2 + 2m\eta_1)\theta_{m1dd} - (3m_2L^2 + 3m_4L^2 + 3m_5L^2 + m_2L^2)\theta_{m2dd} + m_2L^2\theta_{m3dd} - (2m_4L^2 + m_4L^2)\theta_{m4dd} - m_5L^2\theta_{m5dd} = 2Rg(-m\eta_1 + m_2L + m_3L + m_4L + m_5L)\theta_{ydd}$$

$$2kdR\theta - \left(2ktgR_p + 2kdR\left(\frac{R_t}{R_p}\right)\theta + 2ktgR_p\theta_m - 2ctR_p\theta_d - (2R_g^2R_{pm3} + 2R_g^2R_{pm2} + 2R_g^2R_{pm1} + 2R_g^2R_{pm4} + 2R_g^2R_{pm5} + 21R_p)\theta_{dd} - (2R_gR_{pm4} + 2R_gR_{pm5} - R_gR_{pm1} + 2R_gR_{pm2} + 2R_gR_{pm3})\theta_{m1dd} - (3R_gR_{pm4} + 3R_gR_{pm5} + 3R_gR_{pm3} + R_gR_{pm2})\theta_{m2dd} + R_gR_{pm3}\theta_{m3dd} - (2R_gR_{pm5} + R_gR_{pm4})\theta_{m4dd} - R_gR_{pm5}\theta_{m5dd} = 2R_p(m_1R_g^2 + m_2R_g^2 + m_3R_g^2 + m_4R_g^2 + m_5R_g^2 - I_d)\theta_{ydd} - 2ctR_p\theta_{yd} \right)$$

$$kdR_p\theta - kdR\theta + cdR_p\theta_{dd} + IdR_p\theta_{ddd} = R_pT_d$$

$$M_1 = \begin{bmatrix} 0 & 2 \cdot L \cdot m5 \cdot Rg & 2 \cdot L^2 \cdot m5 & 3 \cdot L^2 \cdot m5 & 0 & 2 \cdot L^2 \cdot m5 & (4 \cdot I5 + L^2 \cdot m5) \\ 0 & -(2 \cdot L \cdot m4 \cdot Rg + 4 \cdot L \cdot m5 \cdot Rg) & -(2 \cdot m4 \cdot L^2 + 4 \cdot m5 \cdot L^2) & -(3 \cdot m4 \cdot L^2 + 6 \cdot m5 \cdot L^2) & 0 & -(m4 \cdot L^2 + 4 \cdot I4 + 4 \cdot m5 \cdot L^2) & -(2 \cdot m5 \cdot L^2) \\ 0 & -(2 \cdot L \cdot m3 \cdot Rg + 4 \cdot L \cdot m4 \cdot Rg + 4 \cdot L \cdot m5 \cdot Rg) & -(2 \cdot m3 \cdot L^2 + 4 \cdot m4 \cdot L^2 + 4 \cdot m5 \cdot L^2) & -(3 \cdot m3 \cdot L^2 + 6 \cdot m4 \cdot L^2 + 6 \cdot m5 \cdot L^2) & (m3 \cdot L^2 - 4 \cdot I3) & -(2 \cdot m4 \cdot L^2 + 4 \cdot m5 \cdot L^2) & -(2 \cdot m5 \cdot L^2) \\ 0 & -(4 \cdot L \cdot m3 \cdot Rg + 2 \cdot L \cdot m2 \cdot Rg + 4 \cdot L \cdot m5 \cdot Rg + 4 \cdot L \cdot m4 \cdot Rg) & -(4 \cdot m4 \cdot L^2 + 2 \cdot m2 \cdot L^2 + 4 \cdot m5 \cdot L^2 + 4 \cdot m3 \cdot L^2) & -(6 \cdot m3 \cdot L^2 + 6 \cdot m5 \cdot L^2 + 4 \cdot I2 + m2 \cdot L^2 + 6 \cdot m4 \cdot L^2) & 2 \cdot m3 \cdot L^2 & -(4 \cdot m5 \cdot L^2 + 2 \cdot m4 \cdot L^2) & -(2 \cdot m5 \cdot L^2) \\ 0 & -(2 \cdot L \cdot m3 \cdot Rg + 2 \cdot L \cdot m2 \cdot Rg + 2 \cdot L \cdot m5 \cdot Rg + 2 \cdot L \cdot m4 \cdot Rg - 2 \cdot m1 \cdot \eta1 \cdot Rg) & -(2 \cdot I1 + 2 \cdot m2 \cdot L^2 + 2 \cdot m4 \cdot L^2 + 2 \cdot m5 \cdot L^2 + 2 \cdot m3 \cdot L^2 + m1 \cdot \eta1) & -(3 \cdot m3 \cdot L^2 + 3 \cdot m5 \cdot L^2 + 3 \cdot m4 \cdot L^2 + m2 \cdot L^2) & m3 \cdot L^2 \cdot \theta m3_{dd} & -(2 \cdot m5 \cdot L^2 + m4 \cdot L^2) & -(m5 \cdot L^2) \\ 0 & -(2 \cdot Rg^2 \cdot Rp \cdot m3 + 2 \cdot Rg^2 \cdot Rp \cdot m2 + 2 \cdot Rg^2 \cdot Rp \cdot m1 + 2 \cdot Rg^2 \cdot Rp \cdot m4 + 2 \cdot Rg^2 \cdot Rp \cdot m5 + 2 \cdot I1 \cdot Rp) & -(2 \cdot Rg \cdot Rp \cdot m4 \cdot L + 2 \cdot Rg \cdot Rp \cdot m3 \cdot L - Rg \cdot Rp \cdot m1 + 2 \cdot Rg \cdot Rp \cdot m2 \cdot L + 2 \cdot Rg \cdot Rp \cdot m5 \cdot L) & -(3 \cdot Rg \cdot Rp \cdot m4 \cdot L + 3 \cdot Rg \cdot Rp \cdot m5 \cdot L + 3 \cdot Rg \cdot Rp \cdot m3 \cdot L + Rg \cdot Rp \cdot m2 \cdot L) & Rg \cdot Rp \cdot m3 \cdot L & -(2 \cdot Rg \cdot Rp \cdot m5 \cdot L + Rg \cdot Rp \cdot m4 \cdot L) & -(Rg \cdot Rp \cdot m5 \cdot L) \\ Id \cdot Rp & 0 & 0 & 0 & 0 & 0 & 0 \end{bmatrix}$$

$$C_1 = \begin{pmatrix} 0 & 0 & 0 & 0 & 0 & -4 \cdot cb & 4 \cdot cb \\ 0 & 0 & 0 & 0 & 4 \cdot cb & -8 \cdot cb & 4 \cdot cb \\ 0 & 0 & 0 & 4 \cdot cb & -8 \cdot cb & 4 \cdot cb & 0 \\ 0 & 0 & 4 \cdot cb & -8 \cdot cb & 4 \cdot cb & 0 & 0 \\ 0 & 0 & -2 \cdot cb & 2 \cdot cb & 0 & 0 & 0 \\ 0 & -2 \cdot ct \cdot Rp & 0 & 0 & 0 & 0 & 0 \\ cd \cdot Rp & 0 & 0 & 0 & 0 & 0 & 0 \end{pmatrix} \quad K_1 = \begin{bmatrix} 0 & 0 & 0 & 0 & 0 & -4 \cdot kb & 4 \cdot kb \\ 0 & 0 & 0 & 0 & 4 \cdot kb & -8 \cdot kb & 4 \cdot kb \\ 0 & 0 & 0 & 4 \cdot kb & -8 \cdot kb & 4 \cdot kb & 0 \\ 0 & 0 & 4 \cdot kb & -8 \cdot kb & 4 \cdot kb & 0 & 0 \\ 0 & 2 \cdot ktg & -2 \cdot (ktg + kb) & 2 \cdot kb & 0 & 0 & 0 \\ 2 \cdot kd \cdot Rt & -2 \cdot \left(ktg \cdot Rp + kd \cdot \frac{Rt^2}{Rp} \right) & 2 \cdot ktg \cdot Rp & 0 & 0 & 0 & 0 \\ kd \cdot Rp & -kd \cdot Rt & 0 & 0 & 0 & 0 & 0 \end{bmatrix} \quad I_1 = \begin{bmatrix} 0 & -2 \cdot L \cdot m5 \cdot Rg & 0 \\ 0 & 2 \cdot L \cdot Rg \cdot (m4 + 2 \cdot m5) & 0 \\ 0 & 2 \cdot L \cdot Rg \cdot (m3 + 2 \cdot m4 + 2 \cdot m5) & 0 \\ 0 & 2 \cdot L \cdot Rg \cdot (m2 + 2 \cdot m3 + 2 \cdot m4 + 2 \cdot m5) & 0 \\ 0 & 2 \cdot Rg \cdot (-m1 \cdot \eta1 + m2 \cdot L + m3 \cdot L + m4 \cdot L + m5 \cdot L) & 0 \\ 0 & 2 \cdot Rp \cdot (m1 \cdot Rg^2 + m2 \cdot Rg^2 + m3 \cdot Rg^2 + m4 \cdot Rg^2 + m5 \cdot Rg^2 - I_a) & -2 \cdot ct \cdot Rp \\ Rp & 0 & 0 \end{bmatrix}$$

Appendix A2 – MATLAB® m-file for Traverse Axis

```

%*****
%*****AZIMUTH AXIS 7-DOF MODELING*****
%***BY: TURKER KARAYUMAK, METU MECHANICAL ENGINEERING*****
%*****

```

```
clear all;
```

```
%*****MODEL PARAMETERS*****
```

```

Id=25;      %Azimuth Drive Inertia (kg.m^2)
It=45000;   %Turret Inertia (kg.m^2)
m1=2500;    %Mass of Gun Part 1 (kg) (Includes Gun Breech)
m2=125;     %Mass of Gun Part 2 (kg)
m3=150;     %Mass of Gun Part 3 (kg)
m4=125;     %Mass of Gun Part 4 (kg)
m5=100;     %Mass of Gun Part 5 (kg) (This is the Gun Muzzle)
L=1;        %Length of each gun part except Part 1 (m)
I1=1000;    %Inertia of Gun Part 1 (kg.m^2)
I2=9.5;     %Inertia of Gun Part 2 (kg.m^2)
I3=9.5;     %Inertia of Gun Part 3 (kg.m^2)
I4=9.5;     %Inertia of Gun Part 4 (kg.m^2)
I5=9.5;     %Inertia of Gun Part 5 (kg.m^2)
cd=150;     %Drive viscous friction (N*m*s/rad)
ct=9e4;     %Turret viscous friction (N*m*s/rad)
ctg=1e4;    %Turret to gun(m1) viscous friction (N*m*s/rad)
ktg=4.5e8;  %Turret to gun(m1) stiffness (N*m/rad)
kd=2e6;     %Drive stiffness (N*m/rad)
cb=2e3;     %Gun parts joint viscous friction (N*m*s/rad) (Between m1,m2,m3,m4,m5)

```

```

kb=4e6;      %Gun parts joint stiffnesses (N*m/rad) (Between m1,m2,m3,m4,m5)
Rp=0.08;    %Pinion Pitch Circle Radius (m)
Rg=0.9;     %Turret rotation center to Turret-Gun_m1 Joint Distance
Rt=1.1;     %Turret Ring Gear Pitch Circle Radius (m)
Ia=It+(m1+m2+m3+m4+m5)*Rg^2; %Total azimuth inertia (turret + gun) (kg.m^2)
eta=0.5;    %Trunnion to CG of breech (m1) part (m)

```

```

%*****SYSTEM MATRICES*****

```

```

%Mass Matrix

```

```

M1=[0,          2*L*Rg*m5,          ,          2*L^2*m5,          ,          3*L^2*m5,          ,          0,          ,          2*L^2*m5,          ,          4*I5+ L^2*m5 ;
    0,          -2*L*Rg*(m4+2*m5),          ,          -2*L^2*(m4+2*m5),          ,          -3*L^2*(m4+2*m5),          ,          0,          ,          -L^2*(m4+4*m5)-4*I4,          ,          -2*L^2*m5 ;
    0,          -2*L*Rg*(m3+2*m4+2*m5),          ,          -2*L^2*(m3+2*m4+2*m5),          ,          -3*L^2*(m3+2*m4+2*m5),          ,          -4*I3+m3*L^2,          ,          -2*L^2*(m4+2*m5),          ,          -2*L^2*m5 ;
    0,          -2*L*Rg*(2*m3+m2+2*m5+2*m4),          ,          -2*L^2*(m2+2*m3+2*m4+2*m5),          ,          -4*I2-L^2*(m2+6*m3+6*m4+6*m5),          ,          2*m3*L^2,          ,          -2*L^2*(m4+2*m5),          ,          -2*L^2*m5 ;
    0,          -2*Rg*(L*(m3+m2+m5+m4)-m1*eta),          ,          -2*(I1+L^2*(m2+m3+m4+m5))-eta*m1,          ,          -L^2*(m2+3*m3+3*m4+3*m5),          ,          m3*L^2,          ,          -L^2*(m4+2*m5),          ,          -L^2*m5 ;
    0,          -2*Rp*(Rg^2*(m3+m2+m1+m4+m5)+It),          ,          -2*Rg*Rp*L*(m2+m3+m4+m5)+Rg*Rp*m1,          ,          -Rg*Rp*L*(m2+3*m3+3*m4+3*m5),          ,          Rg*Rp*m3*L,          ,          -Rg*Rp*L*(m4+2*m5),          ,          -Rg*Rp*L*m5 ;
Id*Rp,          0,          ,          0,          ,          0,          ,          0,          ,          0,          ,          0 ];
```

```

%Damping Matrix

```

```

C1=[0,          ,0,          ,0,          ,0,          , -4*cb,          , 4*cb ;
    0,          ,0,          ,0,          ,0,          , 4*cb,          , -8*cb,          , 4*cb ;
    0,          ,0,          ,0,          , 4*cb,          , -8*cb,          , 4*cb,          , 0 ;
    0,          ,0,          , 4*cb,          , -8*cb,          , 4*cb,          , 0,          , 0 ;
    0,          ,0,          , -2*cb,          , 2*cb,          , 0,          , 0,          , 0 ;
    0,          , -2*ct*Rp,          , 0,          , 0,          , 0,          , 0,          , 0 ;
cd*Rp,          ,0,          ,0,          ,0,          ,0,          ,0,          ,0 ];
```

```

%Stiffness Matrix

```

```

K1=[0,          ,0,          ,0,          ,0,          , -4*kb,          , 4*kb;
    0,          ,0,          ,0,          ,0,          , 4*kb,          , -8*kb,          , 4*kb;
    0,          ,0,          ,0,          , 4*kb,          , -8*kb,          , 4*kb,          , 0;
    0,          ,0,          , 4*kb,          , -8*kb,          , 4*kb,          , 0,          , 0;
    0,          , 2*ktg,          , -2*(ktg+kb),          , 2*kb,          , 0,          , 0,          , 0;
    2*kd*Rt,          , -2*(ktg*Rp+kd*(Rt^2/Rp)),          , 2*ktg*Rp,          , 0,          , 0,          , 0,          , 0;
kd*Rp,          , kd*Rt,          , 0,          , 0,          , 0,          , 0,          , 0];
```



```

%Inertia Matrix
I1=[0 , -2*L*Rg*m5 , 0 ;
0 , 2*L*Rg*(m4+2*m5) , 0 ;
0 , 2*L*Rg*(m3+2*m4+2*m5) , 0 ;
0 , 2*L*Rg*(m2+2*m3+2*m4+2*m5) , 0 ;
0 , 2*Rg*(m2*L+m3*L+m4*L+m5*L-eta*m1) , 0 ;
0 , 2*Rp*(Rg^2*(m1+m2+m3+m4+m5)-Ia) , -2*ct*Rp ;
Rp , 0 , 0 ];
```

```

%*****UNDAMPED FREE-VIBRATIONS NATURAL FREQUENCIES OF THE SYSTEM*****
```

```

eigenvalues=eig(inv(M1)*K1);
naturalfrequencies=(1/(2*pi))*sqrt(eigenvalues);
naturalfrequencies_sorted=sort(naturalfrequencies)
```

114

```

%*****STATE SPACE REPRESENTATION*****
```

```

%State Variables;
%x=[angpos_drive;pos_turret;angpos_M1;angpos_M2;angpos_M3;angpos_M4;angpos_M5;
% angvel_drive;angvel_turret;angvel_M1;angvel_M2;angvel_M3;angvel_M4;angvel_M5]
%u=[Td ; angacc_hull ; angvel_hull]
```

```

A=[(eye(7)*0) , eye(7) ;
-inv(M1)*K1 , -inv(M1)*C1];
```

```

B=[0,0,0;0,0,0;0,0,0;0,0,0;0,0,0;0,0,0;0,0,0; -inv(M1)*I1];
```

```
C=eye(14);

D=[0,0,0;0,0,0;0,0,0;0,0,0;0,0,0;0,0,0;0,0,0;0,0,0;0,0,0;0,0,0;0,0,0;0,0,0;0,0,0;0,0,0;0,0,0];
```

```
%*****FREQUENCY RESPONSE AND *****
f=logspace(-1,2.5,5000);
w=2*pi*f;
t=0:0.001:10;339
```

```
[m,p]=bode(A,B,C,D,1,w);
md=20*log10(m);
```

```
%*****FEEDBACK CONTROLLER TUNE*****
[NUM1,DEN]=ss2tf(Aaz,Baz,Caz,Daz,1);
Gu=tf(NUM1(10,:),DEN);
% figure(1),bode(Gu,w);
fn1=6.62; %First natural frequency
NF1=tf([1 0 (2*pi*fn1)^2] , [1 30 (2*pi*fn1)^2]);%Notch against first natural frequency
fn2=42.63; %Third natural frequency
NF2=tf([1 0 (2*pi*fn2)^2] , [1 50 (2*pi*fn2)^2]);%Notch against third natural frequency
% figure(2),bode(NF1*NF2,w)
% figure(3),bode(Gu*NF1*NF2,w)
```

```

% Kp=19;
% Ki=10.3;
Kp=19.9;
Ki=4.7; %19.12.2009

```

```

%*****FEEDFORWARD TRANSFER FUNCTION*****
% [NUM1,DEN]=ss2tf(Aaz,Baz,Caz,Daz,1);
% Gu=tf(NUM1(10,:),DEN);
[NUM2,DEN]=ss2tf(Aaz,Baz,Caz,Daz,2);
[NUM3,DEN]=ss2tf(Aaz,Baz,Caz,Daz,3);
DER = tf([1 0],1);
Gd1= DER * tf(NUM2(10,:),DEN);
f=logspace(-1,2.5,5000);
w=2*pi*f;
Gd2= tf(NUM3(10,:),DEN);
Gd = Gd1 + Gd2;
Gff = -Gd/Gu;
bodemag(Gff,w);
grid;
LP = tf([2*pi*11.5] , [1 2*pi*11.5]);
Gff2 = Gff * LP * LP * LP * LP ;
bodemag(Gff2,w);
nyquist(Gff2,w);

```

```
grid;  
hsvd(Gff2);  
[Gff2s,Gff2ns]=stabsep(Gff2,'AbsTol',1e-5,'Offset',3);  
Gff2s=Gff2s*NF1*NF2  
hsvd(Gff2s);  
%nyquist(Gff2s,w);
```

Appendix A3 – Derivation of M, C and K Matrices for Elevation Axis

Solving the eqns θ_{pdd} ;

$$\begin{aligned}
 &4kb\theta m4 - 4kb\theta m5 + 4cb\theta m4_{\ddot{u}} - 4cb\theta m5_{\ddot{u}} - 2L^2 \cdot m5\theta m_{\ddot{u}} - 2L^2 \cdot m5\theta m_{\ddot{u}} - 2L^2 \cdot m5\theta m_{\ddot{u}} - 2L^2 \cdot m5\theta m_{\ddot{u}} - (L^2 \cdot m5 + 4I3) \cdot \theta m_{\ddot{u}} = 2 \cdot L \cdot m5Rg\theta p_{dd} \\
 &-4kb\theta m3 + 8kb\theta m4 - 4kb\theta m5 - 4cb\theta m4_{\dot{u}} + 8cb\theta m4_{\dot{u}} - 4cb\theta m5_{\dot{u}} + (2m4L^2 + 4m5L^2) \cdot \theta m_{\ddot{u}} + (2m4L^2 + 4m5L^2) \cdot \theta m_{\ddot{u}} + (2m4L^2 + 4m5L^2) \cdot \theta m_{\ddot{u}} + (4m5L^2 + 4I4 + m4L^2) \cdot \theta m_{\ddot{u}} + 2m5L^2 \cdot \theta m_{\ddot{u}} = -2 \cdot L \cdot Rg(m4 + 2m5) \cdot \theta p_{dd} \\
 &-4kb\theta m2 + 8kb\theta m3 - 4kb\theta m4 - 4cb\theta m2_{\dot{u}} + 8cb\theta m2_{\dot{u}} - 4cb\theta m3_{\dot{u}} + (2m3L^2 + 4m4L^2 + 4m5L^2) \cdot \theta m_{\ddot{u}} + (2m3L^2 + 4m4L^2 + 4m5L^2) \cdot \theta m_{\ddot{u}} + (m3L^2 + 4I3 + 4m4L^2 + 4m5L^2) \cdot \theta m_{\ddot{u}} + (2m4L^2 + 4m5L^2) \cdot \theta m_{\ddot{u}} + 2m5L^2 \cdot \theta m_{\ddot{u}} = -2 \cdot L \cdot Rg(m3 + 2m4 + 2m5) \cdot \theta p_{dd} \\
 &-4kb\theta m1 + 8kb\theta m2 - 4kb\theta m3 - 4cb\theta m1_{\dot{u}} + 8cb\theta m1_{\dot{u}} - 4cb\theta m2_{\dot{u}} + (2m2L^2 + 4m3L^2 + 4m4L^2 + 4m5L^2) \cdot \theta m_{\ddot{u}} + (m2L^2 + 4I2 + 4m3L^2 + 4m4L^2 + 4m5L^2) \cdot \theta m_{\ddot{u}} + (2m3L^2 + 4m4L^2 + 4m5L^2) \cdot \theta m_{\ddot{u}} + (2m4L^2 + 4m5L^2) \cdot \theta m_{\ddot{u}} + 2m5L^2 \cdot \theta m_{\ddot{u}} = -2 \cdot L \cdot Rg(m2 + 2m3 + 2m4 + 2m5) \cdot \theta p_{dd} \\
 &(2kd \cdot Yta^2 + 2kb) \cdot \theta m1 - 2kb\theta m2 + (2cb + 2cg) \cdot \theta m_{\dot{u}} - 2cb\theta m2_{\dot{u}} + (2m2L^2 + 2m4L^2 + 2m5L^2 + 2m3L^2 + 2m1\eta^2 + 2I1) \cdot \theta m_{\ddot{u}} + (m2L^2 + 2m4L^2 + 2m5L^2 + 2m3L^2) \cdot \theta m_{\ddot{u}} + (2m4L^2 + 2m5L^2 + m3L^2) \cdot \theta m_{\ddot{u}} + (2m5L^2 + m4L^2) \cdot \theta m_{\ddot{u}} + m5L^2 \cdot \theta m_{\ddot{u}} = -2(m2Rg \cdot L + m3Rg \cdot L + m4Rg \cdot L + m5Rg \cdot L - I_g - \eta \cdot m1Rg) \cdot \theta p_{dd} + 2cg \cdot \theta p_{\dot{d}} + 2kd \cdot Yta
 \end{aligned}$$

$$M_1 = \begin{bmatrix}
 & -2 \cdot L^2 \cdot m5 & & & \\
 & (2 \cdot m4 \cdot L^2 + 4 \cdot m5 \cdot L^2) & & & \\
 & (2 \cdot m3 \cdot L^2 + 4 \cdot m4 \cdot L^2 + 4 \cdot m5 \cdot L^2) & & & \\
 & (2 \cdot m2 \cdot L^2 + 4 \cdot m3 \cdot L^2 + 4 \cdot m4 \cdot L^2 + 4 \cdot m5 \cdot L^2) & & & \\
 (2 \cdot m2 \cdot L^2 + 2 \cdot m4 \cdot L^2 + 2 \cdot m5 \cdot L^2 + 2 \cdot m3 \cdot L^2 + 2 \cdot m1 \cdot \eta^2 + 2 \cdot I1) & (m2 \cdot L^2 + 2 \cdot m4 \cdot L^2 + 2 \cdot m5 \cdot L^2 + 2 \cdot m3 \cdot L^2) & (2 \cdot L^2 \cdot m5) & (-2 \cdot L^2 \cdot m5) & -(L^2 \cdot m5 + 4 \cdot I5)
 \end{bmatrix}$$

120

$$C_1 = \begin{bmatrix}
 0 & 0 & 0 & 4 \cdot cb & -4 \cdot cb \\
 0 & 0 & -4 \cdot cb & 8 \cdot cb & -4 \cdot cb \\
 0 & -4 \cdot cb & 8 \cdot cb & -4 \cdot cb & 0 \\
 -4 \cdot cb & 8 \cdot cb & -4 \cdot cb & 0 & 0 \\
 (2 \cdot cb + 2 \cdot cg) & -2 \cdot cb & 0 & 0 & 0
 \end{bmatrix}$$

$$K_1 = \begin{bmatrix}
 0 & 0 & 0 & 4 \cdot kb & -4 \cdot kb \\
 0 & 0 & -4 \cdot kb & 8 \cdot kb & -4 \cdot kb \\
 0 & -4 \cdot kb & 8 \cdot kb & -4 \cdot kb & 0 \\
 -4 \cdot kb & 8 \cdot kb & -4 \cdot kb & 0 & 0 \\
 (2 \cdot kd \cdot Yta^2 + 2 \cdot kb) & -2 \cdot kb & 0 & 0 & 0
 \end{bmatrix}$$

$$I_1 = \begin{bmatrix}
 0 & 2 \cdot L \cdot m5 \cdot Rg & 0 \\
 0 & -2 \cdot L \cdot Rg \cdot (m4 + 2 \cdot m5) & 0 \\
 0 & -2 \cdot L \cdot Rg \cdot (m3 + 2 \cdot m4 + 2 \cdot m5) & 0 \\
 0 & -2 \cdot L \cdot Rg \cdot (m2 + 2 \cdot m3 + 2 \cdot m4 + 2 \cdot m5) & 0 \\
 2 \cdot kd \cdot Yta & -2 \cdot (m2 \cdot Rg \cdot L + m3 \cdot Rg \cdot L + m4 \cdot Rg \cdot L + m5 \cdot Rg \cdot L - I_g - \eta \cdot m1 \cdot Rg) & 2 \cdot cg
 \end{bmatrix}$$

Appendix A4 – MATLAB® m-file for Elevation Axis


```

%*****
%*****ELEVATION AXIS 5-DOF
MODELING*****
%***BY: TURKER KARAYUMAK, METU MECHANICAL ENGINEERING*****
%*****

clear all;

%*****MODEL PARAMETERS*****
m1=2500;    %Mass of Gun Part 1 (kg) (Includes Gun Breech)
m2=125;     %Mass of Gun Part 2 (kg)
m3=150;     %Mass of Gun Part 3 (kg)
m4=125;     %Mass of Gun Part 4 (kg)
m5=100;     %Mass of Gun Part 5 (kg) (This is the Gun Muzzle)
L=1;        %Length of each gun part except Part 1 (m)
eta=0.5;    %Trunnion to CG of Gun Part 1 (m)
I1=1000;    %Inertia of Gun Part 1 (kg.m^2)
I2=9.5;     %Inertia of Gun Part 2 (kg.m^2)
I3=9.5;     %Inertia of Gun Part 3 (kg.m^2)
I4=9.5;     %Inertia of Gun Part 4 (kg.m^2)
I5=9.5;     %Inertia of Gun Part 5 (kg.m^2)
Ig=7000;    %Total Inertia of Gun (kg.m^2)
cd=10;      %Drive viscous friction (N*m*s/rad)
cg=9e4;     %Trunnion viscous friction (N*m*s/rad)
ctg=1e4;    %Turret to gun(m1) viscous friction (N*m*s/rad)
kd=5.3e6;   %Drive stiffness (N*m/rad)
cb=2e3;     %Gun parts joint viscous friction (N*m*s/rad) (Between
m1,m2,m3,m4,m5)
kb=4e6;     %Gun parts joint stiffnesses (N*m/rad) (Between m1,m2,m3,m4,m5)
Rg=0.9;     %Turret rotation center to Turret-Gun_m1 (trunnion) Joint
Distance
Yta=0.5;    %Trunnion to elevation drive distance (m)

```

```
%*****SYSTEM MATRICES*****
```

```
%Mass Matrix
```

```
M1=[
    -2*L^2*m5
    , -2*L^2*m5
    , -2*L^2*m5
    , -(4*I5+ L^2*m5)
    ,
    2*m4*L^2+4*m5*L^2
    , 2*m4*L^2+4*m5*L^2
    , 2*m4*L^2+4*m5*L^2
    ,
    4*m5*L^2+4*I4+m4*L^2
    , 2*m5*L^2
    ,
    2*m3*L^2+4*m4*L^2+4*m5*L^2
    , 2*m3*L^2+4*m4*L^2+4*m5*L^2
    , m3*L^2+4*I3+4*m4*L^2+4*m5*L^2
    ,
    2*m4*L^2+4*m5*L^2
    , 2*m5*L^2
    ,
    2*m2*L^2+4*m3*L^2+4*m4*L^2+4*m5*L^2
    , m2*L^2+4*I2+4*m3*L^2+4*m4*L^2+4*m5*L^2
    , 2*m3*L^2+4*m4*L^2+4*m5*L^2
    ,
    2*m4*L^2+4*m5*L^2
    , 2*m5*L^2
    ,
    2*m2*L^2+2*m4*L^2+2*m5*L^2+2*m3*L^2+2*m1*eta^2+2*I1
    , m2*L^2+2*m4*L^2+2*m5*L^2+2*m3*L^2
    , 2*m4*L^2+2*m5*L^2+m3*L^2
    ,
    2*m5*L^2+m4*L^2
    , m5*L^2
    ];
```

```
%Damping Matrix
```

```
C1=[0
    , 0
    , 0
    , 4*cb
    , -4*cb
    ;
    0
    , 0
    , -4*cb
    , 8*cb
    , -4*cb
    ;
    0
    , -4*cb
    , 8*cb
    , -4*cb
    , 0
    ;
    -4*cb
    , 8*cb
    , -4*cb
    , 0
    , 0
    ;
    2*cb+2*cg
    , -2*cb
    , 0
    , 0
    , 0
    ];
```

```
%Stiffness Matrix
```

```
K1=[0
    , 0
    , 0
    , 4*kb
    , -4*kb;
    0
    , 0
    , -4*kb
    , 8*kb
    , -4*kb;
    0
    , -4*kb
    , 8*kb
    , -4*kb
    , 0;
    -4*kb
    , 8*kb
    , -4*kb
    , 0
    , 0;
    2*kd*Yta^2+2*kb
    , -2*kb
    , 0
    , 0
    , 0];
```

```
%Inertia Matrix
```

```
I1=[0
    , 2*L*m5*Rg
    , 0
    ;
    0
    , -2*L*Rg*(m4+2*m5)
    , 0
    ;
    0
    , -2*L*Rg*(m3+2*m4+2*m5)
    , 0
    ;
    0
    , -2*L*Rg*(m2+2*m3+2*m4+2*m5)
    , 0
    ;
    2*kd*Yta
    , -2*(m2*Rg*L+m3*Rg*L+m4*Rg*L+m5*Rg*L-Ig-eta*m1*Rg)
    , 2*cg
    ];
```

```
%*****UNDAMPED FREE-VIBRATIONS NATURAL FREQUENCIES OF THE SYSTEM*****
```

```
eigenvalues=eig(inv(M1)*K1);
naturalfrequencies=(1/(2*pi))*sqrt(eigenvalues);
naturalfrequencies_sorted=sort(naturalfrequencies)
```

```

%*****STATE SPACE REPRESENTATION*****

%State Variables;
%x=[angpos_M1;angpos_M2;angpos_M3;angpos_M4;angpos_M5;
%   angvel_M1;angvel_M2;angvel_M3;angvel_M4;angvel_M5]
%u=[linposdrive ; angacc_hull_e1 ; angvel_hull_e1]

A=[(eye(5)*0) , eye(5) ;
    -inv(M1)*K1 , -inv(M1)*C1];

B=[0,0,0;0,0,0;0,0,0;0,0,0;0,0,0; -inv(M1)*I1];

C=eye(10);

D=[0,0,0;0,0,0;0,0,0;0,0,0;0,0,0;0,0,0;0,0,0;0,0,0;0,0,0;0,0,0;0,0,0;0,0,0];

%*****FREQUENCY RESPONSE *****
f=logspace(-1,2.5,5000);
w=2*pi*f;
t=0:0.001:2;

[m,p]=bode(A,B,C,D,1,w);
md=20*log10(m);

%*****FEEDFORWARD TRANSFER FUNCTION*****
Kp = 0.6989;
Ki = 2.5652;

[NUM1,DEN]=ss2tf(Ae1,Bel,Cel,Del,1);
Gu=tf(NUM1(6,:),DEN);
[NUM2,DEN]=ss2tf(Ae1,Bel,Cel,Del,2);
[NUM3,DEN]=ss2tf(Ae1,Bel,Cel,Del,3);
DER = tf([1 0],1);
Gd1= DER * tf(NUM2(6,:),DEN);
f=logspace(-1,2.5,5000);
w=2*pi*f;
Gd2= tf(NUM3(6,:),DEN);
Gd = Gd1 + Gd2;
Gff = -Gd/Gu;

```

```
bodemag(Gff,w);
grid;

LP = tf([2*pi*15] , [1 2*pi*15]);
Gff2 = Gff * LP
bodemag(Gff2,w);
nyquist(Gff2,w);
grid;

hsvd(Gff2);
[Gff2s,Gff2ns]=stabsep(Gff2,'AbsTol',1e-5,'Offset',0.001);
hsvd(Gff2s);
nyquist(Gff2s,w);
```

CURRICULUM VITAE

PERSONEL INFORMATION

Surname, Name: KARAYUMAK, Türker
Nationality: Turkish (TC)
Date and Place of Birth: 3 July 1977, İzmir
Marital Status: Married
Phone: +90 532 627 69 68
e-mail: turkerkarayumak@gmail.com

EDUCATION

Degree	Institution	Year of Graduation
MS	METU Mechanical Engineering	2002
BS	METU Mechanical Engineering	1999
High School	İzmir Atatürk Lisesi	1994

WORK EXPERIENCE

Year	Place	Enrollment
2010-Present	OTOKAR	Manager, Tank Electromechanical Systems Dpt.
2008-2010	FNSS	Senior Engineer, Weapon Systems Design
1999-2008	ASELSAN MGEO	Senior Engineer, Electro-Optic Systems Design

FOREIGN LANGUAGES

Advanced English

PUBLICATIONS

1. KARAYUMAK, T., “Leopard1A1 Tankı Termal Atış Kontrol Nisangah Sistemi” , ASELSAN Dergisi Temmuz Sayısı , Aselsan, Ankara, 2002.
2. KARAYUMAK, T., “İki Eksenli Jiroskobik Stabilizasyonlu Opto-mekanik Platform Tasarımı”, ANSYS Kullanıcılar Semineri, FİGES, Bursa, 2001.

HOBBIES

Riding Motorcycles, Building and Flying Radio Controlled Airplanes